Ion-Sensing Systems Based on Mesoporous Carbon: from Bulk Electrodes to Paper-Based Ion Sensors

A DISSERTATION
SUBMITTED TO THE FACULTY OF
UNIVERSITY OF MINNESOTA
BY

Jinbo Hu

IN PARTIAL FULFILLMENT OF THE REQUIREMENTS
FOR THE DEGREE OF
DOCTOR OF PHILOSOPHY

Advisors: Andreas Stein and Philippe Bühlmann

August 2017

Acknowledgements

I would like to express my sincere gratitude to the following individuals for their help, support, and tolerance throughout my entire career in graduate school:

It has been my great honor and privilege working under the co-guidance of my advisors Professors Andreas Stein and Philippe Bühlmann. Their passion for science inspired me and kept motivating me to pursue the truth, and their guidance helped me to improve my hard and soft skills on a continuous basis. They gave me the freedom and flexibility to explore the possibilities of what I can be, and helped me to establish a professional career. I came to the University of Minnesota 5 years ago for my interests in materials chemistry and electrochemistry. I have enjoyed my research during my graduate school, and it is great that I can still stay in the field after I graduate. I would not have gone this far without you.

I also would like to thank all the Stein and Buhlmann group members for their help and support throughout the years. Especially, Dr. Jesse Carey, Dr. Yuqiang Qian, Dr. Benjamin Wilson, Dr. Xu Zou, Dr. Maral Mousavi, Dr. Stephen Rudisill, Dr. Nicholas Petkovich, Yuan Fang and Adam Dittmer helped me to start my research from scratch during my first two years of graduate school. I also enjoyed working with Camille Malonzo, Evan Anderson, Siyao He, Nam Tran, Wenyang Zhao, Zhao Wang, Ellie Raethke, Xin Chen, Yao Zhang and Brian Spindler. I learned a lot from all of you.

Xue Zhen provided great support for my research on redox buffers. I hope we can co-publish a paper someday in the very near future.

I would like to acknowledge Professor Bohejin Tang for our collaboration on electrochemical energy-storage devices. It was my great pleasure to work with him, and his dedication and hard work always motivates me.

Dr. James Caney and Carl Schu from Medtronic not only sponsored my research project, but also opened a door for me. They helped me to get prepared for a professional industrial career.

Professors William Smyrl, Renee Frontiera, Aaron Massari, and Michelle Driessen served in my preliminary exam and final defense committees. Thank you for your help and advice for my thesis research.

Abstract

Potentiometric sensors, comprising ion-selective electrodes (ISEs) and reference electrodes, are a large subgroup of electrochemical ion sensors. In view of affordable and portable analytical devices, all-solid-state ISEs and reference electrodes, in which a solid contact is used as an ion-to-electron transducer, are highly desirable. Compared with conventional ISEs, all-solid-state ISEs offer comparable electrochemical performance with the distinct advantages of simple maintenance and miniaturization.

This dissertation focuses on the development of robust all-solid-state potentiometric ion-sensing systems. It starts with the investigation of colloid-imprinted mesoporous (CIM) carbon as a novel solid contact material. CIM carbon exhibits desirable properties as a solid contact material, including a low content of redox-active impurities and a high double layer capacitance. Therefore, sensors based on CIM carbon can be constructed with superior electrochemical performance, including excellent ionic response, reproducibility, signal stability, and resistance to common interfering agents. These outstanding characteristics make CIM carbon-based potentiometric sensors promising candidates for the next generation of commercial ion sensors.

To develop low-cost and simple ion sensors for point-of-care applications, this dissertation also involves the development of disposable ion-sensing platforms based on paper. The use of ISEs can be significantly simplified by embedding a conventional potentiometric cell into paper. Paper-based Cl^- and K^+ sensors are fabricated with highly reproducible and linear responses towards different concentrations of analyte ions in aqueous and biological samples. To further simplify the use of these paper-based ion

sensors, CIM carbon-based ISEs and reference electrodes can be integrated into the paper substrate, thus constructing all-solid-state paper-based ion-sensing platforms.

Finally, the dissertation explores the possibility of constructing robust calibration-free ion sensors by covalently attaching a redox buffer to CIM carbon. Click chemistry and amide coupling reactions are evaluated for the attachment, and the cobalt-based redox buffer can be attached to CIM carbon. It is found that the open circuit potential of modified CIM carbon films can be affected by the oxidation states of the redox buffer, but a higher redox buffer loading is required to achieve high electrode-to-electrode reproducibility. Possible approaches to achieving such high redox buffer loading are discussed at the end of this dissertation.

Table of Contents

List of Tables

Chapter 1

Chapter 2

Chapter 3

List of Figures

Chapter 1

Chapter 3

Chapter 4

Chapter 7

List of Abbreviations

°C	Degrees Celsius
3DOM	Three-dimensionally ordered macroporous
BET	Brunauer-Emmett-Teller
BJH	Barrett-Joyner-Halenda
$[C_8min^+][C_1C_1N^-]$	1-Methyl-3-octylimidazolium bis(trifluoromethylsulfonyl)imide
CIM	Colloidal imprinted mesoporous
CV	Cyclic voltammetry
DIPEA	*N*,*N*-Diisopropylethylamine
DMTMM	4-(4,6-Dimethoxy-1,3,5-triazin-2-yl)-4-methylmorpholinium chloride
EDC	1-Ethyl-3-(3-dimethylaminopropyl) carbodiimide
EIS	Electrochemical impedance spectroscopy
EMF	Electromotive force
F	Farad
FTIR	Fourier-transform infrared spectroscopy
g	Gram
h	Hour
HHCAE	Hydrophilic high-capacity anion exchange
HOBt	Hydroxybenzotriazole
ISE	Ion-selective electrode
ISM	Ion-selective membrane

L	Liter
LiTPFPB	Lithium tetrakis(pentafluorophenyl)borate
M	Molarity
mg	Milligram
min	Minute
mL	Milliliter
mV	Millivolt
NaTFPB	Sodium tetrakis[3,5-bis-(trifluoromethyl)phenyl]borate
nm	Nanometer
o-NPOE	*o*-nitrophenyl octyl ether
pA	picoampere
PEDOT	Poly(3,4-ethylenedioxythiophene)
POT	Poly(3-octylthiophene)
PSS	Poly(sodium 4-styrenesulfonate)
PVC	Poly(vinyl chloride)
SC-ISE	Solid-contact ion-selective electrode
SEM	Scanning electron microscopy
$TBAClO_4$	Tetrabutylammonium perchlorate
TCNQ	7,7,8,8-Tetracyanoquinodimethane
TCPP	Tetrakis(4-carboxyphenyl)porphyrin
$TEABF_4$	Tetraethylammonium tetrafluoroborate
TEM	Transmission electron microscopy

TGA	Thermogravimetric analysis
THF	Tetrahydrofuran
TTF	Tetrathiafulvalene
XPS	X-ray photoelectron spectroscopy

Chapter 1

Introduction to All-Solid-State Ion-Selective Electrodes and Reference Electrodes

Ion-selective electrodes (ISEs) are electrochemical ion sensors that convert the activity of a target ion into an electrical potential as the measurable signal. In potentiometry, they are coupled with reference electrodes and used under near-zero current conditions. Over the past half-century, ISEs have evolved into well-established, routine analytical tools, with sensors for more than 60 analytes, and they are widely used in various fields, including clinical analysis, environmental analysis, physiology, and process control.[1-7]

Conventional ISEs have several limitations that need to be overcome to meet the demand for portable analytical devices with small sample volumes, easy maintenance, simple operation, and low cost. These ISEs contain liquid contacts (typically referred to as inner filling solutions) that separate the sensing membrane from the inner reference element. As a result, they are sensitive to evaporation of these inner filling solutions and changes in the sample temperature and pressure. Moreover, osmotic pressure originating from differences in the ionic strength of samples and the inner filling solution result in net water transport into or out of the inner filling solution, which can lead to large volume changes and delamination of the sensing membrane.[8] Therefore, conventional ISEs have to be well maintained and used with care. Moreover, it is difficult to reduce the volume of the liquid contact to a value much lower than the milliliter level, which poses challenges for sensor miniaturization. Although micropipette-based microelectrodes with sensing areas less than 100 nm have been used for a long time,[9] their fabrication requires a delicate process, and they are fragile, which limits their application. Next-generation devices require robust, miniaturized ion-sensing systems that can be integrated with

electronic control, measuring, and data acquisition units for acquiring complex biological and chemical information. Thus, it is highly desirable to eliminate the cumbersome liquid contacts by replacing conventional electrodes with all-solid-state potentiometric sensors. In all-solid-state ISEs and reference electrodes, a solid contact is formed between the sensing membrane and an electron-conducting substrate to replace the liquid contact, serving as an ion-to-electron transducer. Note that all-solid-state ISEs are not to be confused with ISEs that comprise a solid-state ion-selective membrane, an expression that has historically been reserved for ion-selective membranes prepared from inorganic materials such as LaF_3 or Ag_2S.[10] In this chapter, discussions are limited to all-solid-state electrodes with polymeric sensing membranes. It has been more than four decades since the first all-solid-state electrode was proposed, and all-solid-state ISEs and reference electrodes are generally considered to be the future of potentiometric sensors. However, major challenges still remain.[11-13]

In 1970, Hirata and Date proposed an all-solid-state Cu^{2+} ISE that contained a Pt wire coated with a Cu_2S-impregnated silicone rubber sensing membrane.[14] This was followed by Cattrall et al., who used a Pt wire coated with a Ca^{2+} ionophore-doped polymeric membrane, thereby constructing the first coated-wire electrode comprising an ionophore.[15] The resulting Ca^{2+}-ISE is generally considered to be the ancestor of present-day ionophore-based all-solid-state ISEs. As Nikolskii and Materova summarized three decades ago, three conditions need to be fulfilled for stable and reliable response of all-solid-state ISEs: (1) reversible transitions from ionic to electronic conduction and vice

versa, (2) ideally nonpolarizable interfaces with high exchange current densities, and (3) absence of side reactions.[16]

Although the design of the coated-wire electrode was simple, it was not reliable due to the interrupted ion-to-electron transduction at the 'blocked' solid contact/membrane interface.[15] No charged species could transfer between the membrane and the metal contact, resulting in a purely capacitive interface to the metal wire. Because of the small interfacial contact area, coated-wire electrodes easily pick up noise. They also exhibit large signal drifts, which may be due to both residual currents passing through the membrane but also the formation of an aqueous layer. It was hypothesized based on the observation of O_2 interference that an O_2/H_2O half-cell can form at the metal/membrane interface,[17,18] but it is very likely that this O_2/H_2O half-cell is not reversible. Various solid-contact sensors with improved designs were proposed in the literature but many of them still do not match the performance of conventional electrodes, and quality control criteria for all-solid-state ISEs were not critically discussed until recently.[8,19] Yet, through persistent efforts made by the community, the performance of all-solid-state electrodes has been dramatically improved, with significant advances brought about by the introduction of novel solid-contact materials, the understanding of the transport and accumulation of water in membranes, the control of transmembrane ion fluxes, and the development of novel ion-sensing platforms. Also, complementary to zero-current potentiometry, a new family of all-solid-state ion sensors has emerged that takes advantage of dynamic electrochemical instrumental control techniques,[20] such as ion transfer voltammetry,[21,22] chronopotentiometry,[23,24] and constant potential

coulometry.[25-27] Regardless of the mode in which these all-solid-state sensors are operated, their electrochemical performance is highly dependent on the solid contact that is employed. Among all the solid contacts, conducting polymers and high-surface-area nanostructured materials are the most studied candidates for commercial all-solid-state potentiometric sensors and have been reviewed previously.[28,29]

This chapter provides an overview of how potentiometric all-solid-state ISEs and reference electrodes function and gives guidance on how to improve their performance. Also, it provides an overview of this dissertation. Section 1.1 describes the ion-to-electron transduction mechanism of all-solid-state ISEs and reference electrodes, with an emphasis on the interface between the solid contact and the sensing membrane. Section 1.2 discusses the design of high-performance, all-solid-state potentiometric sensors for specific applications, with a focus on improving the electrode reproducibility in order to achieve calibration-free sensors (Section 1.2.1), enhancing potential stability for accurate measurements (Section 1.2.2), and lowering detection limits for trace-level analysis (Section 1.2.3). Section 1.3 presents recent research on the design of simple and miniaturized potentiometric ion-sensing devices, highlighting disposable and paper-based ion sensors. The chapter ends with our own perspective of the field (Section 1.4), as well as an overview of this dissertation (Section 1.5). This chapter focuses primarily on the design of the solid contact and its impact on the performance of all-solid-state ISEs and reference electrodes. For those who are new to the field, reviews on potentiometric ion sensors[1-6] can serve as introductory reading material. Those interested in non-potentiometric, dynamic control techniques are referred to another recent review.[20]

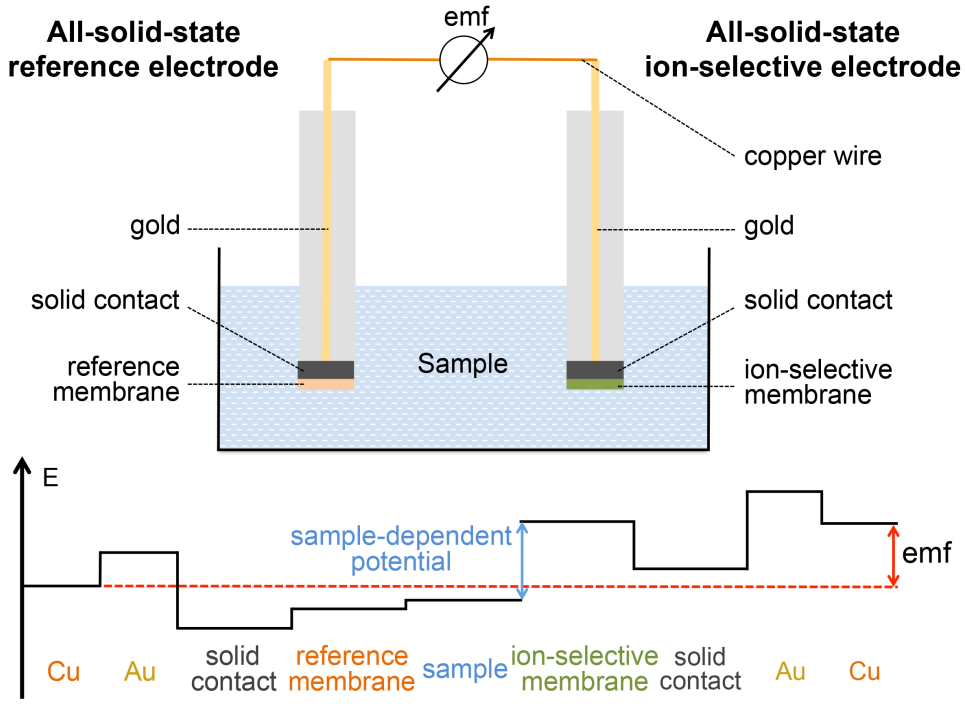

Figure 1.1 Schematic representation of a potentiometric cell containing an all-solid-state ISE and an all-solid-state reference electrode. The electrical potential profile within this cell is depicted, showing the interfacial potential difference at each interface. The measured potentiometric emf is the sum of all the phase boundary potentials.

1.1 Transduction Mechanism

Figure 1.1 represents a typical all-solid-state potentiometric cell that comprises an all-solid-state ISE, an all-solid-state reference electrode, and a high impedance voltmeter to ensure near-zero current conditions. The measured electromotive force (emf) is the difference in electrical potential between the connecting leads (e.g., Cu wires) of the ISE and of the reference electrode. As illustrated by the electrical potential profile in Figure 1.1, the measured emf is equal to the sum of all the interfacial potentials within the cell.

In an ideally currentless system, there are no potential drops through bulk phases since there is no Ohmic drop, and the only sample-dependent potential is the interfacial potential at the sample/ion-selective membrane interface.

1.1.1 Transduction Mechanism of All-Solid-State ISEs

For any ISE, the input signal is the activity of a specific ion and the output is an electrical potential. This part of the overall signal transduction occurs at the interface of the sample and the ISE membrane.[1,30,31] Behind that interface, i.e., within the ion-selective membrane, the charge carriers that are free to move are still ions. However, at some point between this membrane and the connecting lead occurs the second half of the overall signal transduction, i.e., the conversion of the charge carrier from ions to electrons. A conventional ISE usually contains a AgCl-coated Ag wire as inner reference electrode in contact with an inner filling solution that contains Cl^- at a fixed concentration (Figure 1.2a). Consequently, ion-to-electron transduction is achieved by the reversible redox reaction $AgCl(s) + e^- \rightleftarrows Ag(s) + Cl^-(aq)$, which defines the interfacial potential between the AgCl/Ag electrode and the inner filling solution ($\Delta\varphi_{a3}$). For the sample/ISE membrane and the ISE membrane/inner filling solution interfaces, the charge carrier is the target ion. In the case of ISEs with polymeric sensing membranes, the potential differences across the latter two interfaces ($\Delta\varphi_{a1}$ and $\Delta\varphi_{a2}$, respectively) are defined by the distribution of the target ion across two immiscible phases, which can be described quantitatively by the classical phase-boundary-potential model.[1,30,31]

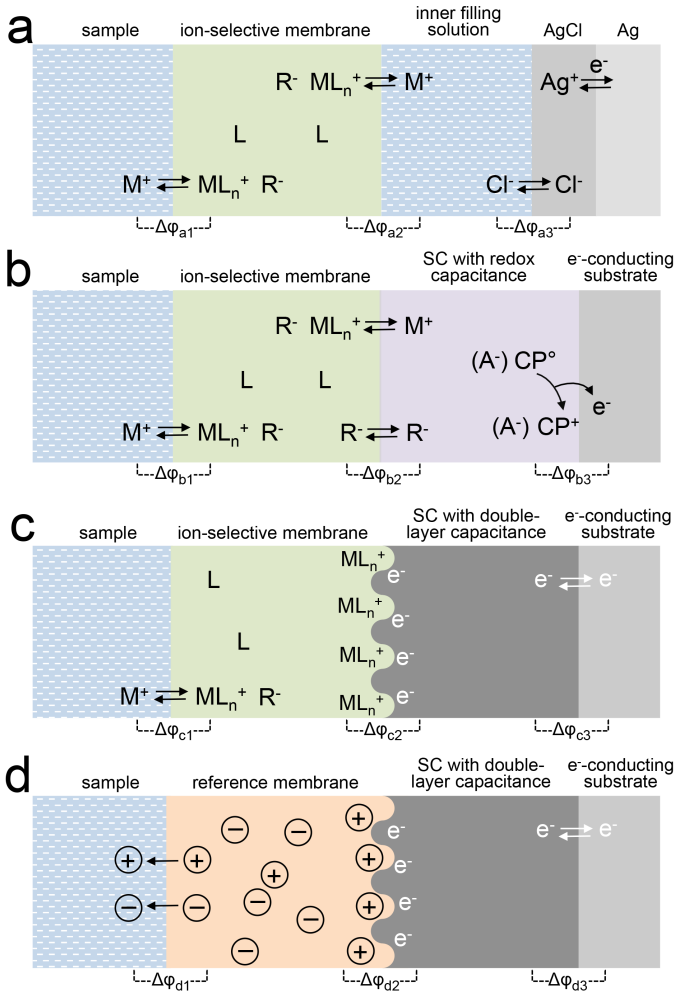

Figure 1.2 Schematic representation of all relevant interfaces within different types of ISEs with cation (M^+) selective membranes that contain an electrically neutral ionophore (L) and anionic sites (R^-): (a) a conventional ISE with an inner filling solution; (b) an all-solid-state ISE based on an anion (A^-, R^-) doped-conducting polymer (CP) solid contact (SC) with a high redox capacitance; (c) an all-solid-state ISE based on a high-surface-area SC exhibiting a high double layer capacitance; (d) an all-solid-state reference electrode with a high-surface-area SC and a reference membrane containing a pair of ions that leach into the sample.

1.1.1.1 Solid Contacts with a High Redox Capacitance

Figure 1.2b represents an all-solid-state ISE containing a conducting polymer as a solid contact with a high redox capacitance. Conducting polymers are effective ion-to-electron transducers because they are both electrically conductive and exhibit ionic conductivity through doping. They can be conveniently deposited on an electron-conducting substrate by electrochemical polymerization or drop-casting of a polymer solution, techniques that are both suitable for mass fabrication. Similarly as in the case of the internal reference of conventional ISEs, all-solid-state ISEs with a conducting polymer as solid contact convert the charge carrier from ions to electrons through the oxidation/reduction (doping/undoping) of the underlying conducting polymer. This type of redox reaction can be described by the following processes:

$$CP^{+}A^{-}_{\text{(solid contact)}} + M^{+}_{\text{(membrane)}} + e^{-} \rightleftarrows CP^{\circ}A^{-}M^{+}_{\text{(solid contact)}} \quad (1.1a)$$

$$CP^{+}R^{-}_{\text{(solid contact)}} + e^{-} \rightleftarrows CP^{\circ}_{\text{(solid contact)}} + R^{-}_{\text{(membrane)}} \quad (1.1b)$$

in which CP stands for the conducting polymer, and A^{-} refers to a doping ion (e.g., poly(sodium 4-styrenesulfonate) polyanion, PSS^{-}). M^{+} and R^{-} represent the analyte ion (e.g., K^{+}) and hydrophobic counter ion (e.g., a tetraphenylborate derivative), respectively, which may transfer across the interface between the ISE membrane and the conducting polymer film. The ratio of the contributions from the two reactions 1.1a and 1.1b may be quantified by the transference numbers of M^{+} and R^{-} and is related to their individual ion mobilities. For conducting polymers doped with a large immobile polyelectrolyte (e.g., PSS^{-}), the ion exchange at the ISE membrane/conducting polymer interface is dominated by cations (e.g., M^{+}, 1.1a), whereas small anion-doped conducting polymers

predominantly exchange anions (e.g., R^-, 1.1b). Consequently, the interfacial potential at the interface between the conducting polymer and the electron-conducting substrate ($\Delta\varphi_{b3}$) is controlled by the redox reactions 1.1a and 1.1b in the conducting polymer layer, whereas the potential difference across the interface of the ISE membrane and the conducting polymer ($\Delta\varphi_{b2}$) is determined by the ion distribution between these two phases. The overall observed capacitance of some conducting polymer-based all-solid-state ISEs, however, can be significantly lower than that of the conducting polymers themselves in the absence of the ISE membranes.[32,33] This phenomenon was systematically studied by Maksymiuk et al. using two types of poly(3,4-ethylenedioxythiophene) (PEDOT) membranes doped with bulky PSS^- ions that were immobilized in the PEDOT, as well as mobile Cl^- counter ions that can reversibly transfer into the contacting Cl^--ISE membrane. It was found that the reduced capacitance of the all-solid-state ISE can be attributed to the low amount of ions transferrable across the conducting polymer/ISE membrane interface, which may be ascribed to the low concentration of mobile ions in the conducting polymer or concentration polarization effects.[34] The ability of conducting polymers to be oxidized or reduced gives them redox buffer capacity, although the conducting polymers are not ideal redox buffers due to the continuum of redox potentials that they represent (see Section 1.2.1).

Among the many conducting polymer solid contacts that have been investigated, polypyrrole,[35] poly(3-octylthiophene) (POT),[36] polyaniline,[37] and PEDOT[32] are the most commonly used ones. On the one hand, polypyrrole, polyaniline, and PEDOT are typically stable in a highly oxidized (p-doped) state with a high redox capacitance and

electronic conductivity, but are electroactive within a broad range of potentials, as discussed in Section 1.2.1. As a result, they may participate in chemical reactions that cause drift of the emf response. For example, it was reported that a polyaniline layer is highly pH sensitive due to the partial conversion of its conducting emeraldine salt form to its non-conducting emeraldine base form.[38] This conversion can lead to inadequate long-term potential stability for polyaniline-based ISEs with sensing membranes permeable to H^+ and OH^-,[39] which has made polyaniline a less common conducting polymer used for all-solid-state ISEs and reference electrodes. On the other hand, POT is less subject to reactions with ambient species such as oxygen because it has a relatively high oxidation potential and is usually used in an undoped ion-free form. Therefore, POT films have a relatively low redox capacitance and electronic conductivity,[5] and ion-to-electron transduction at their interfaces occurs mainly through the electrical double layer that forms at the solid contact/membrane boundary, as discussed in Section 1.1.1.2. POT films can also be doped with anions through electropolymerization, which assures that some of the POT is in an oxidized form and enables reversible interfacial charge transfer.[21,40] A recent study of electropolymerized POT solid contacts using surface synchrotron radiation-X-ray photoelectron spectroscopy and near-edge X-ray absorption fine structure analysis showed structural evidence that the lipophilic anions of a plasticized poly(vinyl chloride) (PVC) ISE membrane penetrated only into the outermost surface layer (≤14 Å) of POT. This suggests that, in the case of the sensors investigated in that study, ion-to-electron transduction at the POT layer is a surface-confined process, and indicates that the thickness and the extent of ion diffusion within the conducting

polymer layer has only minimal effects on the performance of these all-solid-state ISEs.[41] The extent to which other ISE membrane matrixes may be more compatible with this and other underlying conducting polymers and, therefore, form less sharply defined membrane/conducting polymer interfaces with more mutual interpenetration is not clear yet.

Conducting polymers are not the only suitable redox-reaction-based transducers though. The redox properties needed for effective ion-to-electron transduction can also be provided by other electroactive species, such as lipophilic silver complexes,[42] redox-active self-assembled monolayers based on fullerene and tetrathiafulvalene (TTF),[43,44] ferrocene,[45] Prussian blue[46] and its analogues,[47] arenethiolate monolayer-protected gold nanoclusters,[48] lipophilic Co(II)/Co(III) salts,[49,50] 7,7,8,8-tetracyanoquinodimethane (TCNQ),[51,52] TTF with its radical salts,[53] as well as $LiFePO_4/FePO_4$ redox couple.[54] Generally, these redox-active ion-to-electron transducers transduce ionic signals to electrical signals through redox reactions of the type $Ox + e^- \rightleftarrows Red$. Devices with such transducer layers are discussed in the following sections.

1.1.1.2 Solid Contacts with a High Double Layer Capacitance

For all-solid-state ISEs without redox properties, ion-to-electron transduction is the result of the electrical double layer forming at the ISE membrane/solid contact interface (Figure 1.2c). This interface can be schematically described as an asymmetrical electrical capacitor, in which one side carries charge in the form of ions, i.e., cations and anions from the ion-selective membrane, and the other side is formed by electrical charge, i.e., electrons or holes in the solid contact.[55] Unlike in the case of conducting-polymer

solid contacts, the interfacial potential at the ISE membrane/solid contact interface ($\Delta\varphi_{c2}$) is neither defined by ion partitioning between two phases nor by a redox reaction. Instead, it relies on the quantity of charge in the electrical double layer. The experimental evidence for this double layer at the interface of a carbon nanotube solid contact and an ISE membrane containing sodium tetrakis[3,5-bis(trifluoromethyl)phenyl]borate (NaTFPB) was obtained using synchrotron radiation-X-ray photoelectron spectroscopy. Under electrode polarization conditions, considerable enrichment of $TFPB^-$, followed by Na^+, was observed at the back side of the ISE membrane contacting the carbon nanotube layer, supporting the hypothesis that a double layer is formed at the solid contact/ISE membrane interface.[56]

The ion-to-electron transduction through the interfacial electrical double layer is also true for coated-wire electrodes, in which a metal is used as the solid contact and is covered with an ISE membrane, without any intermediate transduction layer. Unfortunately, coated-wire electrodes suffer from erratic responses due to the eventual formation of an undesired aqueous layer between the membrane and the underlying metal. Moreover, signal drift can arise as the result of the purely capacitive 'blocked' nature and small contact area of the interface between the sensing membrane and the underlying metal. A coated-wire electrode can be easily polarized by the small but non-zero currents (i.e., pA or less) that are common in potentiometric measurements with routinely used voltmeters, which exhibit a finite input impedance and not the infinite input impedance of an ideal voltmeter (see also Section 1.2.2.2).

A straightforward approach to increase the double layer capacitance is to increase the interfacial contact area between the ISE membrane and the underlying solid contact without necessarily increasing the geometric projection of the solid contact. This strategy can be demonstrated by using porous materials. Porous carbons, such as porous graphite rods[57,58] and compressed charcoal,[59,60] were used in early works as solid contact materials, although no attempts were made to quantify the interfacial contact area or to relate the large contact area to response characteristics. In recent years, the importance of the large interfacial areas was recognized and, consequently, various nanostructured carbon materials with well-controlled structures and tunable surfaces have been employed as novel solid contacts, such as three-dimensionally ordered macroporous (3DOM) carbon (Figure 1.3a),[61] carbon nanotubes (Figure 1.3b),[62] fullerene,[63,64] graphene (Figure 1.3c),[65-68] colloid-imprinted mesoporous (CIM) carbon (Figure 1.3d),[69] and porous carbon spheres.[70] These carbon materials are chemically stable under potentiometric conditions and exhibit high specific surface areas due to their unique nanostructures. Besides their use for potentiometric ion sensing, porous materials with high surface areas have also been widely studied for other electrochemical applications, such as biosensing, energy conversion, and energy storage.[71,72]

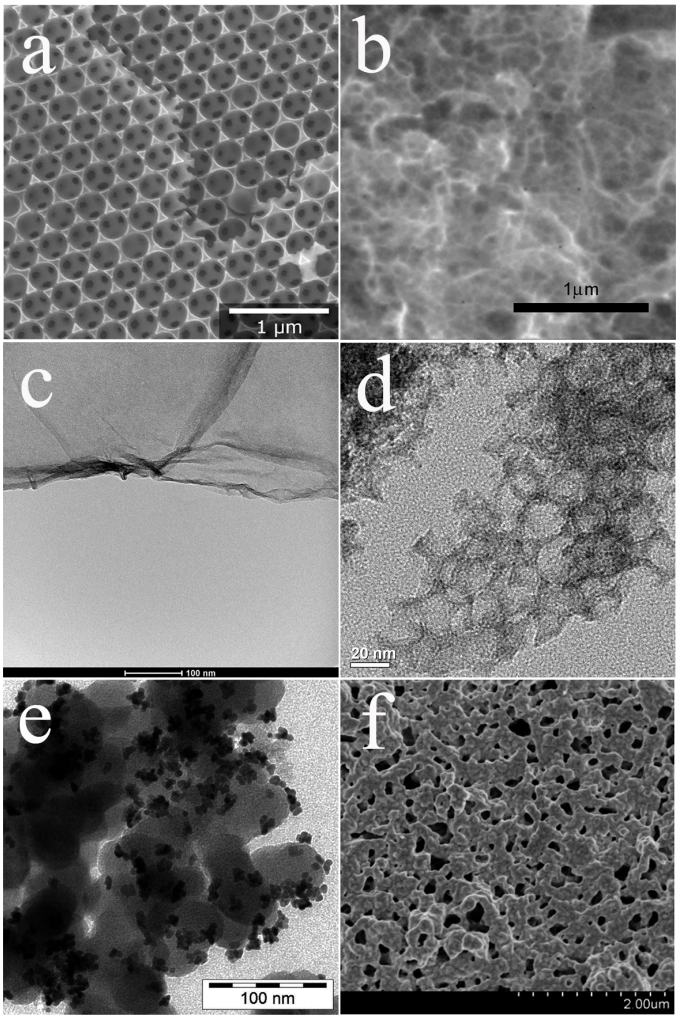

Figure 1.3 Electron micrographs of solid contact materials that can be used to form large contact areas between an electronically conducting solid contact and the ion sensing membrane, resulting in high double layer capacitances: (a) 3DOM carbon, (b) single-walled carbon nanotubes, (c) graphene oxide, (d) CIM carbon, (e) platinum nanoparticles supported on carbon black, and (f) nanoporous gold film. Adapted with permission from ref. 73 (a), ref. 62 (b), ref. 66 (c), ref. 69 (d), ref. 74 (e), ref. 75 (f), © 2008, 2010, 2012, 2013, 2014 American Chemical Society.

To maximize the contact area between the sensing membrane and the carbon, solutions of the membrane components are usually drop-cast onto the carbon layer for maximum penetration. This results in a bicontinuous composite material that exhibits both ionic and electrical conductivity, with ions moving in the ion-selective membrane phase and electrons travelling through the carbon framework. Effective ion-to-electron transduction has been demonstrated not only at high-surface-area carbon materials but also for nanostructured noble metals, such as gold nanoparticles,[76] platinum nanoparticles supported on carbon black (Figure 1.3e),[74] nanoporous gold films (Figure 1.3f),[75] as well as nanocomposites containing graphene loaded with platinum nanoparticles.[77]

1.1.2 Transduction Mechanism of All-Solid-State Reference Electrodes

In potentiometric measurements, reference electrodes are equally as important as ISEs. Their purpose is to provide stable and reproducible sample-independent electrical potentials. Nowadays, a conventional reference electrode usually contains a Ag/AgCl half cell and contacts samples through a concentrated aqueous salt solution (referred to as salt bridge), although in simplified devices the chloride-containing reference solution into which the AgCl-coated silver wire is inserted serves itself as the salt bridge. The liquid junction potential at the interface between the salt bridge and the sample is ideally dominated by the high concentration of ions in the salt bridge and is, therefore, sample-independent.[78,79] To keep liquid junction potentials not only sample independent but also small, an equitransferrent salt is typically used as bridge electrolyte, which comprises a cation and an anion with nearly the same ion mobility.

Similar to all-solid-state ISEs, all-solid-state reference electrodes do not rely on a liquid contact to an internal reference element and instead rely on a solid contact layer sandwiched in between a hydrophobic reference membrane and an underlying electron-conducting substrate. The operation principle of all-solid-state reference electrodes is somewhat different from that of their ISE counterparts. As illustrated in Figure 1.2d, polymeric reference membranes are typically loaded with ions that slowly but continuously leach into the sample. Ideally, the interfacial potential at the membrane/sample interface ($\Delta\varphi_{d1}$) only depends on the local distribution of the doping ions across these two immiscible phases and is not affected by the sample. Reference membranes have been doped with various salts, including polyionic salts,[80] salts with varying lipophilicities,[81-83] and ionic liquids.[84] A reference membrane can contain an inert electrolyte such as tetraalkylammonium tetrakis(4-chlorophenyl)borate with intermediate lipophilicity,[80] which was demonstrated with polypyrrole- and PEDOT(PSS)-based reference electrodes[81] as well as reference electrodes with carbon solid contacts such as carbon nanotubes[85,86] and graphene.[87] Also, reference membranes loaded with ionic liquids were applied in all-solid-state reference electrodes with PEDOT,[88] 3DOM carbon,[89] CIM carbon,[90] and lipophilic Co(II)/Co(III) salts[91] to form the solid contact. It should be noted that the formulation of a reference membrane is as important as the choice of the solid contact, and the optimum composition of the reference membrane should be considered with respect to particular applications. The interfacial potential at the membrane/solid contact interface ($\Delta\varphi_{d2}$) is ideally not affected by the samples but is governed by redox reactions involving a conducting polymer or other redox-active

transducers, or is stabilized by the electrical double layer at the interface of high-surface-area solid contacts. Readers interested in all-solid-state reference electrodes are also referred to a recent book.[92]

1.2 Performance Criteria for the Design of All-Solid-State Potentiometric Sensors

1.2.1 *E*° Reproducibility

Conventional ISEs have to be recalibrated frequently, which requires a supply of calibrating solutions and either automation or trained personnel to carry out the calibration protocols. To avoid such obstacles, calibration-free sensors with high device-to-device reproducibility are highly desirable, in particular for portable point-of-care devices and remotely operated environmental sensing. In this dissertation, reproducibility is discussed with a view to the repeatability of the standard potential, *E*° (i.e., the calibration curve intercept of the calibration curve), for multiple electrodes, rather than variations in the calibration slope, which is expected to be very close to the theoretical value for reliable devices. Different applications require different measuring accuracies. For example, according to the U.S. Code of Federal Regulations,[93] in clinical laboratories the acceptable measuring error for Na^+ is ±4 mM, which corresponds to a variation in the electrode potential of approximately 0.7 mV. Therefore, assuming either negligible electrode drifts or single use devices, no Na^+-ISE calibration would be needed for clinical measurements if for a range of different electrodes the variation of *E*° were less than 0.7 mV. A type of electrode that provides this reproducibility of *E*° and potential stability could be referred to as calibration-free. It should be noted that a well-defined ion-to-

electron transduction is essential but does not guarantee good $E°$ reproducibility. Since the electrical potential and, therefore, the $E°$ of an ISE is affected by all interfacial potential differences within the electrochemical cell (as illustrated by Figure 1.1), not only the interface of the sample and the sensing membrane but also all other interfacial potentials have to be controlled well to ensure that variations in $E°$ remain small.

As mentioned in Section 1.1.1.1, conducting polymers affect $E°$ in two ways. Ideally, the redox potential of the conducting polymer layer defines the interfacial potential at the conducting polymer/electron-conducting substrate interface, and the distribution of ions affects the potential drop across the membrane/conducting polymer interface (Figure 1.2b). However, unlike redox-active species of low molecular weight with well-defined redox potentials, a conducting polymer film usually exhibits a continuum of redox potentials that can be affected by variations in crystallinity of the conducting polymer film,[94] slowness of conformational changes following redox reactions,[95] changes in the glass transition temperature that depend on the doping level,[96] formation of intermolecular bonds between neighboring chains,[97] the ability of counterions to penetrate the conducting polymer film,[41] and the dependence of the film morphology on the fabrication process.[98] Consequently, it is a challenge to control the $E°$ of devices that comprise a conducting polymer film to the level that a highly reproducible all-solid-state electrode is obtained. It was reported that all-solid-state ISEs employing well-defined polyaniline nanoparticles (mean particle size 8 nm) together with silicone rubber sensing membranes showed good $E°$ reproducibility, but the reproducibility of $E°$ was not explicitly discussed.[99]

Only a few approaches were reported to control the $E°$ of all-solid-state ISEs based on conducting polymers. Bobacka et al. reported a method of adjusting the $E°$ values of PEDOT(PSS)-based ISEs after device fabrication by application of a potential or current.[100] Similarly, $E°$ values can be adjusted by short-circuiting these ISEs with a reference electrode immersed into the same solution as the ISEs.[101] After three days, the potential values of multiple equally treated electrodes were reported to approach each other. Improved reproducibility could be achieved by short circuiting for an ever longer time period, but it would be time-consuming due to the reduced driving force towards the end of the process. When the short-circuiting was performed between two identically prepared ISEs, the electrode potentials became nearly equal overnight. However, the $E°$ values of these electrodes started to drift again after current was no longer allowed to flow, which could be explained by spontaneous redox reactions of the conducting polymer. Improved potential stability and $E°$ reproducibility were achieved by pre-polarizing the conducting polymer to its stable equilibrium state before the application of the ISE membrane. For a demonstration, polypyrrole films were doped with a highly hydrophobic anion perfluorooctane sulfonate and polarized to a pre-determined equilibrium potential at which the polypyrrole films exhibited the highest potential stability. After the application of K^+-ISE membranes, the resulting all-solid-state K^+-ISEs demonstrated a high $E°$ reproducibility with a standard deviation of 0.7 mV (n=4) as well as a low $E°$ drift of 69 μV/h over 46 days. However, larger electrode $E°$ variations were observed for a larger batch of electrodes fabricated using the same method. This may be improved by using microfabricated substrate electrodes and clean-room conditions.[102]

As an alternative to the conducting polymer approach, the interfacial potential across the interface to an underlying electron-conducting substrate can be controlled by use of a well-defined redox buffer that contains both the oxidized and reduced forms of a redox couple. In the same way as a pH buffer resists pH changes when small quantities of acids or bases are added into a solution, a redox buffer guarantees highly reproducible potentials and resists changes in the electrical potential caused by redox-active interferences. The electrical potential of a redox buffer is determined by its standard redox potential and the ratio of the oxidized and reduced species of the redox couple, as predicted by the Nernst equation[103]:

$$E = E^{\circ'} + \frac{RT}{nF} \ln \frac{a_{ox}}{a_{red}} \tag{1.2}$$

where E is the electrical potential of the redox buffer, E°' is the standard potential of the redox couple, R is the ideal gas constant, F is the Faraday constant, T is the temperature, n is the number of moles of electrons transferred in the redox reaction, and a_{ox} and a_{red} are the activities of the oxidized and reduced species of the redox couple, respectively. Redox buffers consisting of cobalt(II/III) tris(1,10-phenanthroline) or of the more hydrophobic cations cobalt(II/III) tris(4,4'-dinonyl-2,2'-bipyridyl) were doped as tetrakis(pentafluorophenyl)borate ($TPFPB^-$) salts into ionophore-free ion-exchange membranes[49] and ionophore-doped membranes,[50] respectively. The E° values of the resulting all-solid-state electrodes correlated well with the ratios of the Co(II) and Co(III) species, as predicted by the Nernst equation, confirming the effectiveness of these compounds as redox buffers. Importantly, E° values were reproducible with a standard deviation less than 1 mV. The challenge of approach to calibration-free electrodes is the

gradual change of $E°$ caused by the transfer of the redox-active species from the sensing membrane into the sample in exchange for ionophore-facilitated analyte ions entering the sensing membrane. The covalent attachment of the redox-active species to a polymer or to inorganic membrane components is being investigated as a solution to this problem.[104]

Few other solid contacts that contain both the oxidized and reduced forms of a redox couple were reported. Ionophore complexes of Ag^+ were doped into a sensing membrane in contact with a Ag° epoxy substrate, forming a $Ag^{+/\circ}$ redox couple to enhance the electrode reproducibility.[42] However, the extension of this approach appears to be limited to Ag^+-ISEs. Doping of ISE membranes with a small amount of a Ag^+ complex along with an ionophore for another analyte ion is conceivable for the preparation of ISEs for other ions, but the amount of Ag^+ in these sensing membranes can be depleted by ion-exchange with analyte ions when these electrodes are used in solutions free of Ag^+. In another report, redox-active self-assembled monolayers whose redox potential was controlled by an applied current were used to improve the electrode potential stability,[44] but a precise control of the ratio of the oxidized and reduced species was difficult, and the redox buffer capacity was evidently limited by the comparatively small redox buffer capacity of the monolayer on a planar substrate. In another approach, ISE membranes that contained arenethiolate monolayer-protected gold nanoclusters were prepared, with equimolar amounts of nanoclusters with two charge states differing only by one electron (i.e., nanoclusters° and nanoclusters$^+$). This approach was reported to yield $E°$ values with a standard deviation of less than 1 mV.[48] The fabrication of ISEs of this type is rather complex and may not be suitable for mass fabrication. Recently,

standard deviations of $E°$ less than 1 mV were also reported for all-solid-state ISEs comprising membranes doped with TTF or its radical salt $TTF^+NO_3^-$ as ion-to-electron transducers.[53] Although the authors did not intentionally prepare transduction layers that contained both TTF and TTF^+, it is possible that the high $E°$ reproducibility originated from the presence of a TTF/TTF^+ redox buffer, since the electrodes with a TTF^+ layer were obtained by electrochemical oxidation of electrodes membranes doped with TTF.

Very recently, intercalation compounds were reported by Schuhmann et al. as a new family of solid contact materials exhibiting high $E°$ reproducibility. $LiFePO_4$ is a well-studied cathode material in Li^+-ion batteries that can reversibly intercalate and deintercalate Li^+ ions upon the electrochemical reduction and oxidation of its Fe(II/III) center, with very well defined redox potential and large redox capacity. When $LiFePO_4$ was coated with a Li^+-ISE membrane, the interfacial potential at the solid contact/ISE membrane was well controlled by the $LiFePO_4/FePO_4$ redox couple with a standard deviation of the electrode $E°$ of 1.4 mV.[54] Following this principle, the same research group utilized Prussian blue analogues (i.e., $M_xT_y[Fe(CN)_6]_z$, where M is the primary ion and T is a transition metal center) as solid contacts to develop all-solid-state ISEs for K^+, Na^+ and Ca^{2+} detection. The $E°$ variations of these electrodes were generally good and in the range of 1.0 – 3.0 mV.[47] Unlike most solid contact materials that can be coupled with various ISE membranes for sensing different ions, the match of a specific intercalation compound for each individual primary ion is required for sensors based on this approach to ensure a well-defined and reversible interface between the solid contact and the ISE membrane.

For carbon-based solid contacts without well-defined redox-active species, the interfacial potentials at the membrane/solid contact interface ($\Delta\varphi_{c2}$) and solid contact/electron-conducting substrate interface ($\Delta\varphi_{c3}$) are affected by redox-active impurities within the system, thus influencing the $E°$ reproducibility. For example, it was shown by acid-base titrations and cyclic voltammetry that CIM carbon[69] contains a much lower amount of oxygen-based surface functionalities than 3DOM carbon,[73] which is consistent with the better $E°$ reproducibility of CIM carbon-based electrodes. The standard deviation of $E°$ of CIM carbon-based ISEs was 7.3 mV while this value was 27 mV for ISEs with a 3DOM carbon solid contact. The $E°$ reproducibility of such electrodes can be significantly improved by adding a high-capacity redox buffer into the system. For instance, doping of an ISE membrane with a lipophilic Co(II)/Co(III) redox buffer salt in combination with a CIM carbon solid contact improved the $E°$ reproducibility.[69] Due to the effect of the redox buffer, the standard deviations of $E°$ was reduced to 1 mV. In another work, a hybrid transducer layer comprising graphene, a silver substrate, and the lipophilic silver tetrakis[3,5-bis(trifluoromethyl)phenyl]borate was developed.[105] This resulted also in a standard deviation of $E°$ of approximately less than 1 mV.

Besides the solid contact itself, the selection of the electron-conducting substrate can also affect the interface between the solid contact and the electron-conducting substrate. Recently, Lindner et al. studied the equilibration times of all-solid-state ISEs with the same PEDOT(PSS) transduction layer and ion-selective membrane composition but different electron-conducting substrates (i.e., glassy carbon, Au, and Pt). When these

all-solid-state ISEs were exposed to an aqueous solution for the first time, electrodes built on glassy carbon and Au substrates had much shorter equilibration times than electrodes with a Pt substrate.[106] A follow-up study by the same group revealed that these different electron-conducting substrates affect electrode equilibration times by causing different degrees of oxidation of the electropolymerized PEDOT(PSS) solid contacts that were otherwise prepared under the same conditions. Those PEDOT(PSS) films contained different PSS^- doping levels that can lead to different extents of hydrophobicity, thus influencing sensor equilibration times. This effect is more noticable when the film thickness is less than 2 μm.[107] In another study, electrodes with Au substrates were reported to exhibit a higher $E°$ reproducibility than otherwise identical electrodes with glassy carbon substrates.[49] This difference can be attributed to the surface chemistry of the underlying electron-conducting substrate, which is affected by the intrinsic substrate properties as well as the fabrication process. Therefore, when designing all-solid-state electrodes, careful consideration should be given to the selection of the electron-conducting substrate, as commonly used underlying substrates (i.e., glassy carbon, Au, and Pt) cannot be used equivalently.

1.2.2 Stability of the EMF Response

For any analytical device, a stable signal is a prerequisite for a reliable measurement. The stability of the emf response of an all-solid-state ISE or reference electrode can be characterized by the level of potential drift that is unrelated to changes in the ionic composition of the sample. On the one hand, the potential drift of an electrode (observed as a drift of $E°$) is related to non-idealities of the sensor, such as slow

equilibrium processes and polarizable interfaces. On the other hand, interferents such as light, O_2, and CO_2 can cause all-solid-state electrodes with inadequate transducers to respond seemingly erratically. In this section, we discuss aspects to consider when trying to improve the potential stability of all-solid-state potentiometric electrodes.

1.2.2.1 Trans-Membrane Transport and Accumulation of Water

Although it was reported earlier that water can be taken up into ISE membranes,[108,109] it was only in 2000 that Pretsch and co-workers showed that the unintentional accumulation of a thin layer of water at the ISE membrane/solid contact interface affects the electrode potential in a predictable way long before the ISE membrane detaches from the underlying metal substrate.[110] In the literature, this thin layer of water is usually referred to as aqueous layer, water layer or water film. All-solid-state electrodes with such an aqueous layer suffer from potential drifts, sensitivity to osmolality changes, and ultimately mechanical failure due to membrane delamination. For a particular interface between a PVC sensing membrane and a silicon wafer substrate, the thickness of this aqueous layer was determined to be 100 ± 10 Å,[111] showing that the volume of this unintended inner filling solution can be extremely small. Importantly, the composition of this aqueous layer is sample-dependent since both primary and interfering ions can diffuse through the ISE membrane and, eventually, into the aqueous layer. Because of the strong interactions between ionophores and primary ions, replacing interfering ions in this layer by primary ions takes much longer than the reverse.

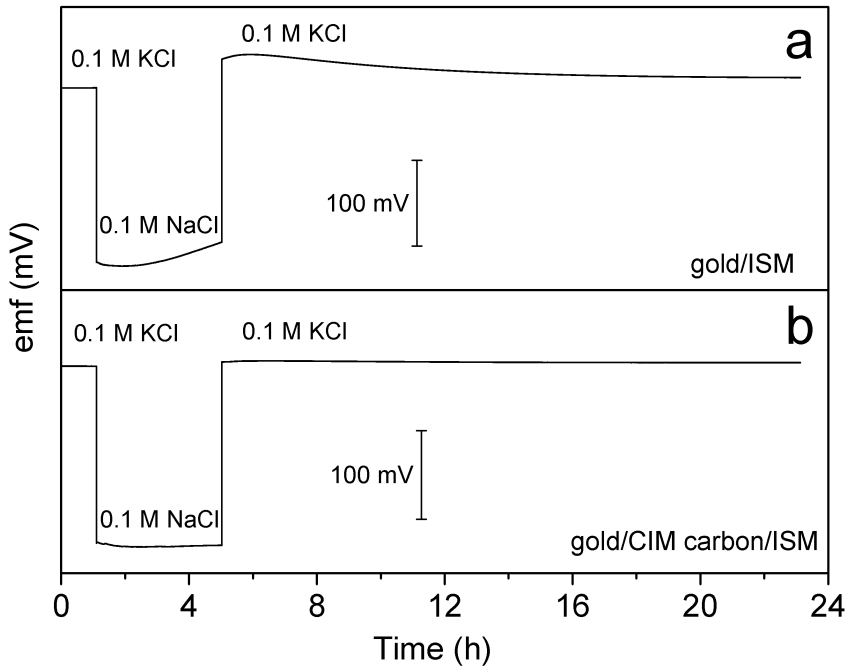

Figure 1.4 Aqueous layer tests of (a) a coated-wire electrode with a K^+-selective membrane (ISM) on a gold electrode, and (b) an all-solid-state ISE with a CIM carbon intermediate layer. The electrodes were immersed in a 0.1 M KCl solution for 24 h prior to measurement. At t = 1.15 h, the 0.1 M KCl solution was changed to a 0.1 M NaCl interfering ion solution, and at t = 5.06 h, the 0.1 M NaCl solution was changed back to a 0.1 M KCl solution.

As shown in Figure 1.4, cation-selective electrodes that are conditioned sequentially in concentrated solutions of the primary and interfering ions for several hours exhibit a positive potential drift upon changing from primary to the interfering ion, and a negative drift is observed when the sample is changed back to a primary ion solution.[110] This asymmetry enables simple testing protocols to confirm the presence of an aqueous layer. As Lindner and Gyurcsányi emphasized, electrodes that contain thick

membranes with low water diffusion coefficients should be tested over extended periods of time, and highly discriminated ions are not suited for such a test because they do not enter the membrane to a sufficiently large extent.[8]

The first step to impede the formation of a detrimental aqueous layer is to use a sensing membrane fabricated from a polymer matrix that absorbs only small amounts of water. The uptake of water into and diffusion within ISE membranes based on poly(acrylates),[112] silicone rubber,[112] and PVC[113] were studied using attenuated total reflectance Fourier transform infrared spectroscopy (ATR-FTIR). It was found that the diffusion coefficient of water in poly(acrylate) membranes was approximately one order of magnitude lower than in plasticized PVC and silicone rubber-based membranes, while the water diffusion coefficients for PVC and silicone rubber membranes were almost the same. However, at "infinitely" long times, the water uptake into poly(acrylate) membranes was higher than for PVC membranes, while the silicone rubber membranes exhibited the lowest water uptake.[112] Coulometric Karl Fischer titrations showed that water uptake is also affected by the electrolyte solutions to which the electrodes are exposed for conditioning.[114] Water transport was also studied using a holographic approach, revealing that the diffusion of water vapor through a poly(acrylate) membrane can proceed with little condensation within the membrane. This process is driven by the vapor pressure differences across the membrane, rather than by osmotic pressure [115]. Since all sensing membranes take up water to some extent, choosing a solid contact with a high hydrophobicity is the next important step to avoid water accumulation. For example, it was shown that a poly(methyl methacrylate)–poly(decyl methacrylate) ISE

membrane was susceptible to the pooling of water, with micrometer sized droplets forming at the interface of the ISE membrane and a gold substrate, while addition of a POT layer in between the ISE and the gold contact successfully eliminated aqueous layer formation.[116,117] In another study, a silicone rubber-based ISE membrane was combined with a POT solid contact. Due to the very low water content, equilibrium was quickly reached, with excellent initial potential stability. When unconditioned electrodes were allowed to contact the conditioning solution for the first time, a potential drift of 4 mV was observed during the first 4 h, and the electrode potential remained stable during the subsequent 20 h of testing.[118] A similarly stable initial potential was observed with a plasticized PVC K^+-ISE membrane coupled with a pre-polarized hydrophobic polyazulene solid contact that exhibited a water contact angle of 98 ± 11°. After the first contact with aqueous solution, the potential drift of all-solid-state ISEs based on polyazulene was only 0.1 mV/h within 49.5 h, which is 5 times lower than that of POT-based electrodes.[119] For oxidized conducting polymers doped with ions to compensate the positive charges, an excess of salt trapped in the membrane during polymerization can also contribute to the formation of an aqueous layer, which was demonstrated with a polypyrrole solid contact electropolymerized in the presence of $K_4Fe(CN)_6$. When the excess salt of $K_4Fe(CN)_6$ in the polypyrrole film was removed by thorough washing, the observed aqueous layer was effectively suppressed.[120]

Because of the hydrophobic nature of carbon, the formation of an aqueous layer seems not to be a problem for electrodes based on carbon solid contacts with conventional PVC sensing membranes. However, it should be noted that an aqueous layer

can still form if a significant amount of hydrophilic functional groups (e.g., hydroxyl groups) is present on the surface of the carbon contact. For example, all-solid-state ISEs with 3DOM carbon solid contacts do not suffer from the formation of an aqueous layer due to the hydrophobic nature of the 3DOM carbon surface.[61] However, when 3DOM carbon was oxidized using concentrated nitric acid, ketone, phenol, lactone and carboxylic acid surface functionalities are formed on the carbon surface, and an aqueous layer was observed.[73]

1.2.2.2 Potential Stability under Constant Ambient Conditions

Beyond the slow ionic equilibrium induced by formation of an aqueous layer, drifts in sensor response can also arise from electrode polarization in a constant measuring environment. Ideally, a solid contact should have a nonpolarizable interface with a high exchange current density that is not influenced by the very small input current of the measuring amplifier.[16] However, in practice all solid contacts can be polarized to some extent. When a polarizable electrode reaches steady state equilibrium in a constant ambient environment, it exhibits the same potential as a capacitor that is charged galvanostatically:

$$E = E_0 + i\,(R + t/C) \tag{1.3}$$

where E is the electrode potential, i is the current, R is the bulk resistance of the electrode, t is the time, and C is the electrode capacitance at low frequencies. Therefore, the time dependence of the electrode potential ($\Delta E/\Delta t$) is related to the electrode capacitance as well as the applied current:

$$\text{Potential drift} = \Delta E/\Delta t = i/C \tag{1.4}$$

It can be seen from equation (1.4) that a sufficiently large electrode capacitance is necessary for a satisfactory potential stability, although all-solid-state electrodes are usually operated under potentiometric near-zero current conditions in which the residual current is extremely small (i.e., pA or less). This is achieved by use of voltmeters with a high input impedance (as large as 10^{13} to 10^{15} Ω). To further stabilize the electrode potential by means of the electrode design, solid contacts with a high redox or double layer capacitance are highly desired. For example, potential drifts of 200 to 500 μV/h were observed with all-solid-state electrodes comprising single-walled carbon nanotubes[121,122] or nanoporous gold films[75] as solid contacts, and approximately 10–50 μV/h for electrodes with 3DOM carbon,[61,89] graphene,[65,66] arenethiolate monolayer-protected gold nanoclusters,[48] TCNQ,[52] porous carbon spheres,[70] polypyrrole doped with hexacyanoferrate,[123] and lipophilic multi-walled carbon nanotubes.[124] Benefiting from the large interfacial area between the solid contact and the sensing membrane, excellent potential stabilities with drifts less than 10 μV/h were reported for electrodes based on CIM carbon[69,90] and platinum nanoparticles supported on carbon black.[74] A stable signal is of great importance for those applications in which continuous monitoring of an analyte over an extended time period is needed. Besides the polarization of the solid contact/sensing membrane interface, mechanical failure and membrane-related processes can also contribute to potential drifts. For example, a gradual decrease in adhesion between the sensing membrane and the solid contact was observed upon extended exposure of all-solid-state electrodes to aqueous solutions,[125] and leaching or

decomposition of membrane components can lead to the deterioration of a sensor's response, as discussed in detail elsewhere.[8]

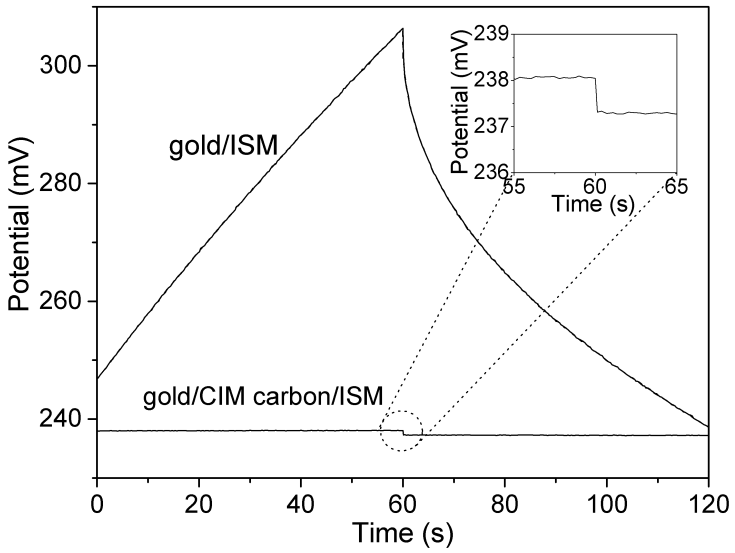

Figure 1.5 Potential stability evaluated by chronopotentiometry of a coated-wire electrode with a PVC-based sensing membrane on a gold substrate (top) and a CIM carbon-based all-solid-state ISE (bottom). Constant currents of +1 nA ($t \leq 60$ s) and –1 nA ($t > 60$ s) were applied to the electrodes while the emf was monitored. An expanded view that shows the Ohmic drop of the CIM carbon-based ISE at the current reversal point is shown in the inset. Reprinted with permission from ref. 69, © 2014 American Chemical Society

For those applications in which long-term monitoring is not needed, or when the electrodes are frequently calibrated, a small signal drift can be tolerated. Assuming an acceptable potential drift of 1 mV/h and a potentiometric residual current of 1 pA in a moderately accurate measurement, it can be calculated from equation (1.4) that a minimal electrode capacitance of 3.6 μF is required. Actual electrode capacitances can be

determined with chronopotentiometry. As suggested by Bobacka,[32] an electrode can be polarized with a few nA (usually 1 nA) of direct current while the electrode potential is recorded. The bulk resistance of the electrode can be calculated from the Ohmic drop (*iR*) when the current is reversed (Figure 1.5). This approach has become a standard method to evaluate potential stabilities of all-solid-state electrodes. Examples of potential drifts for applied currents of 1 nA and the resulting electrode capacitances for different solid contact materials are summarized in Table 1.1.

Table 1.1 ***Electrode Capacitance Measured by Chronopotentiometry and Continuous Potential Drifts of All-Solid-State ISEs***

solid contact	emf drift with 1 nA applied (μV/s)	capacitance (μF)	emf drift (μV/h)	ref.
PEDOT(PSS)[a]	4.9	204	-	32
TCNQ[a]	6.5	154	9.2	52
gold nanoclusters[a]	8.5	118	10.1	48
TTF[a]	16.5	61	-	53
Pt nanoparticles on carbon black[b]	0.6	1666	6.3	74
CIM carbon[b]	1.0	1000	1.3	69
3DOM carbon[b]	1.6[c]	625[c]	11.7	61
graphene[b]	12.8	78	12.6	65
carbon nanotubes[b]	17.0	60	-	62

[a] Solid contact with high redox capacitance.
[b] Solid contact with high double layer capacitance.
[c] Unpublished results.

1.2.2.3 Interferences from Light, O_2, and CO_2

It is well known that some conducting polymers are photosensitive organic semiconductors that can convert light into electrical energy; because of this, they are widely used in the photovoltaic industry. Not surprisingly, light sensitivity is a concern for some conducting polymer-based all-solid-state electrodes. Lindfors systematically compared the effects of light on the potential stability of conducting polymer films (i.e., polypyrrole, PEDOT, polyaniline, and POT) deposited on glassy carbon electrodes. It was found that except for POT, these conducting polymers exhibited no significant response towards illumination with room light. However, when these conducting polymers were exposed to more intensive light, only the polyaniline film retained a relatively stable potential.[126] The excellent light resistance of polyaniline was later confirmed for an all-solid-state ISE with a silicone rubber sensing membrane and a transducer layer containing polyaniline nanoparticles deposited on glassy carbon or gold electrodes.[99] In the case of electrodes comprising highly photosensitive conducting polymers, light interference may be avoided by protecting the photosensitive material from light, as this is similarly the case for Ag/AgCl internal reference electrodes protected by a conventional ISE body. For all-solid-state electrodes with other transducers, such as carbon and redox-active species without a suitable band gap, potentiometric responses are not affected by light.

O_2, CO_2, and other small neutral molecules can readily diffuse through a sensing membrane, reaching the solid contact and causing seemingly erratic responses if the all-solid-state electrode is not adequately designed. The effect of O_2 was observed in early

reports of coated-wire electrodes, and it was hypothesized that an O_2/H_2O half-cell is formed at the metal/PVC interface.[17,18] It is very likely that this O_2/H_2O half-cell is not reversible and thus its half-cell potential is not predictable. The potentiometric response of conducting polymers can be affected by the presence of O_2 due to the oxidation of the conducting polymer, and possibly the formation of charge-transfer complexes between the two species.[127] It was reported that PEDOT is less sensitive to O_2 than polypyrrole, whose potential changed by as much as 25 mV upon exposure to dissolved O_2 for 1 h.[128] Such undesired potential changes can be eliminated by use of a redox buffer with adequate buffer capacity, as demonstrated in all-solid-state electrodes with redox-active self-assembled monolayers,[44] arenethiolate monolayer-protected gold nanoclusters,[48] and lipophilic Co(II)/Co(III) salts.[49,50,91] For carbon-based solid contacts, a clean surface without redox-active impurities is highly desirable.

The interference of CO_2 is usually considered to be a strong indicator of the presence of an aqueous layer between the solid contact and the sensing membrane, since CO_2 can reach the (unbuffered) aqueous layer and alter its pH.[8] Sensitivity towards CO_2 can also be induced by interactions of CO_2 with surface functionalities on the solid contact, even in the absence of an aqueous layer. For example, while there is no evidence for an aqueous layer in the case of 3DOM and CIM carbon due to the hydrophobic nature of their surfaces, 3DOM carbon-based ISEs were subject to a potential drift of 11.8 mV/h upon CO_2 exposure[61] while ISEs based on CIM carbon were not affected by CO_2.[69] The superior CO_2 resistance of the CIM carbon can be attributed to the low amount of surface

functional groups on CIM carbon. As long as there is no aqueous layer and the ambient CO_2 concentration is constant, some CO_2 sensitivity may be acceptable, though.

1.2.3 The Lower Detection Limit

Until the late 1990, most ISEs could only detect sample concentrations down to micromolar levels, which strongly limited their application in situations in which trace-level measurements are required. The realization of Pretsch et al. that the lower detection limit of conventional ISEs is often determined by transmembrane ion fluxes from the inner filling solution into the sample quickly led to the lowering of detection limits down to picomolar levels by minimizing such ion fluxes.[129] Although all-solid-state ISEs do not contain inner filling solutions as large reservoirs of the primary ions, their lower detection limits are still similar to those of conventional ISEs. This is explained by primary ions that can leach from the sensing membrane into the sample, as it was observed by atomic absorption spectrometric measurements.[130]

The first effort to lower the detection limits of all-solid-state ISEs was based on the use of a solid contact consisting of a conducting polymer doped with a primary ion-complexing agent to reduce the contamination of the membrane/sample interface with primary ions. Michalska et al. reported that the incorporation of ethylenediaminetetraacetate into a poly(3-methylthiophene) transducer layer induces a super-Nernstian response for Ca^{2+} activities lower than 10^{-5} M, and that the lifetime of the electrodes was less than ten days, possibly because this hydrophilic complexing agent eventually leaches into the sample.[131] A more robust system with a lifetime of more than six weeks was reported subsequently, using a polypyrrole solid contact doped with the

Ca^{2+} complexing ligand Tiron that enables nanomolar detection of Ca^{2+}.[132] For a conventional ISE, primary ion fluxes can be driven backwards through the membrane into the inner filling solution by the application of a galvanostatic current.[133] This approach was also demonstrated with all-solid-state ISEs, taking advantage of the redox properties of conducting polymers. When an anodic current was applied to a polypyrrole film, polypyrrole was oxidized, accompanied by transport of the primary ion Cl^- from the sensing membrane into the polypyrrole film. Therefore, it reduced the loss of Cl^- into the sample and lowered the detection limit for chloride by two orders of magnitude.[134] However this method is difficult to use in routine analysis because the optimal current depends on the sample composition and the previous history of the membrane. It was shown by theoretical studies that the traditional steady-state treatment is invalid in this regard, and that the current- and concentration-driven ion fluxes depend on each other, making it difficult to achieve reliable elimination of ion fluxes.[135,136] Since the undesirable aqueous layer can serve as a reservoir of primary ions, it should be avoided for trace-level measurements. As discussed in Section 1.2.2.1, the hydrophobic polymer matrix poly(methyl methacrylate)–poly(decyl methacrylate) with low water diffusivity can be combined with a lipophilic POT solid contact to suppress water-layer formation.[116,117] This strategy can also be used to achieve low detection limits. Trace-level detection was shown for Ag^+, Pb^{2+}, Ca^{2+}, K^+, and I^-, with detection limits from the submicromolar to the subnanomolar range.[137,138] Recently, the same combination of sensing membrane and transducer layer was deposited onto a filter paper modified with single-walled carbon nanotubes, and the resulting paper-strip ISEs exhibited nanomolar

detection limits for Cd^{2+}, Ag^{+}, and K^{+}.[139] At these impressively low concentration levels, interfering ions strongly compete with primary ions to generate the potentiometric response, and detection limits are often determined by equilibrium selectivity.[1,140] One approach to enhance selectivities and to achieve low detection limits is to use fluorous sensing membranes with noncoordinating and weak solvating properties.[141,142] Highly selective all-solid-state ISEs were developed with fluorous sensing matrixes and 3DOM carbon solid contacts for the trace-level detection of Ag^{+},[143] and perfluorinated anionic surfactants in the environment.[144] Both types of sensors exhibited subnanomolar detection limits.

No matter what solid contacts are employed, proper conditioning protocols are crucial for low detection limits. Usually, electrodes are conditioned in two steps, starting from a higher primary ion concentration such as 1 mM or 1 μM to replace the counterions originally present in the freshly prepared sensing membrane with analyte ions, which is then followed by a second step of conditioning of the sensing membranes in an analyte solution of much lower concentration, such as 1 μM or 1 nM. Although time-consuming, this is an effective and probably the most robust approach to achieve low detection limits for adequate all-solid-state ISEs with conventional PVC sensing membranes, as first demonstrated with a polypyrrole solid contact for Pb^{2+} detection,[120] and recently successfully applied to 3DOM carbon-based ISEs for K^{+} and Ag^{+},[145] POT derivative-based solid-contact ISEs for Cd^{2+},[146] and electrodes with PEDOT(PSS) contacts for Pb^{2+} measurements.[147] Radu et al. proposed a pretreatment protocol that involves conditioning of PEDOT-based ISEs in a solution of the ionophore in a mixed solvent consisting of

tetrahydrofuran and water. It was suggested that during this conditioning process, primary ions poisoning the membrane/sample interface are transported into the membrane together with the lipophilic ionophore, thus minimizing ion fluxes from the membrane into the sample. The required conditioning time was reported to be reduced to approximately 1 h, and the detection limit for CO_3^{2-} was lowered by four orders of magnitude to 5 ppt.[148] The practical application of this approach may be limited by the solubility of lipophilic ionophores in the conditioning solution.

1.3 Novel Sensor Designs

Over the past three decades, the interest in the development of simple and portable analytical devices has continued to grow due to the high demand for point-of-care and in-field testing applications, especially for the emerging market of developing countries. All-solid-state ISEs and reference electrodes are advantageous over their conventional counterparts because they are miniaturizable and can be compatible with scalable fabrication techniques (e.g., screen-printing). Therefore, they have been widely employed in the designs of miniaturized ion-sensing devices, such as microelectrodes[149] and electronic tongues.[150,151] In this section, we present recent trends of this rapidly growing field by highlighting strip-type potentiometric sensors and paper-based ion-sensing devices developed in the past few years.

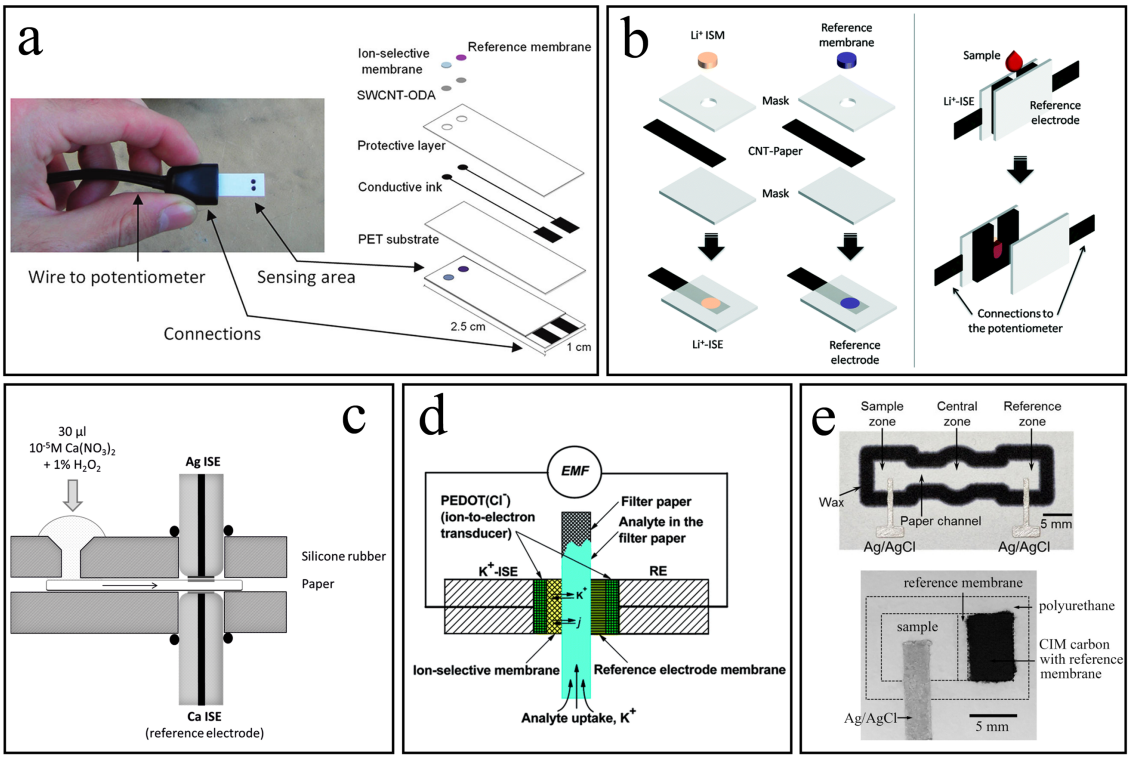

Figure 1.6 Design of miniaturized potentiometric devices with integrated all-solid-state electrodes: (a) planar strip cell with measuring and reference electrode based on screen-printed carbon nanotubes; (b) device based on conductive paper coated with carbon nanotubes for blood Li^+ detection; (c) device utilizing paper-based microfluidic sampling with coated-wire Ag^+-ISE and pseudo-reference Ca^{2+}-ISE (d) device with paper-based microfluidic sampling with an ISE and reference electrode based on PEDOT; (e) disposable paper-based Cl^- sensing devices with stencil-printed Ag/AgCl electrodes as Cl^--ISEs. Reference half cells comprise a Ag/AgCl electrode (d, upper image) or an ionic liquid doped polymeric membrane on CIM carbon (d, lower image). Reprinted with permission from ref. 152 (a), ref. 90 and ref. 153 (e), © 2011, 2014, 2015 American Chemical Society; from ref. 154 (b), ref. 155 (d), © 2014, The Royal Society of Chemistry; from ref. 156 (c), © 2012, Wiley-VCH.

Strip-type potentiometric sensors known as Ektachem slides were available for K^+ analysis in the early 1980s,[157] and have recently been adapted for the construction of miniaturized ion sensors. Rius et al. developed a strip-type potentiometric cell on a polyethylene terephthalate substrate, with a carbon nanotube-based all-solid-state ISE and a reference electrode fabricated by screen-printing (Figure 1.6a).[86,152] This cell was successfully used for K^+ analysis in saliva and beverage samples. To reduce cost and increase flexibility, paper was employed as a substrate to mechanically support the solid contact for the construction of strip-type cells. Conductive papers based on carbon nanotubes[158,159] and graphene[87] were reported, and the resulting electrochemical cells exhibited comparable performance to their bulk counterparts. Using a cell assembled from a separate strip-type ISE and reference electrode (Figure 1.6b), Li^+ levels in whole blood can be measured with a sample volume of 50 μL.[154] Furthermore, carbon nanotube-based conductive paper was combined with a POT solid contact and a poly(methyl methacrylate)–poly(decyl methacrylate) sensing membrane to achieve nanomolar detection limits for Cd^{2+}, Ag^+, and K^+.[139]

Besides mechanically supporting solid contacts, paper can also be used for microfluidic sampling in simple and affordable analytical devices, because it can transport fluids by capillary forces.[160] This concept was first applied to potentiometric sensors in a paper-based bioassay, where the Ag^+ generated in the system was detected by a coated-wire Ag^+-ISE coupled with a Ca^{2+}-ISE as a pseudo-reference (Figure 1.6c).[156] Following the same principle, paper was used as a disposable sampling tool to transport sample solutions to the sensing area of ion-sensing devices with a bulk PEDOT-

based all-solid-state ISE and a reference electrode (Figure 1.6d)[155] as well as commercial solid-state membrane ISEs.[161] Eventually, when paper functions as both the mechanical support and the microfluidic sampling tool, single-use ion-sensing platforms can be constructed with very low cost. Figure 1.6e presents two simple potentiometric Cl^- ion-sensing devices based on paper, which comprise a stencil-printed Ag/AgCl electrode serving as a solid-state Cl^--selective electrode and contain the sample by a hydrophobic barrier either based on printed wax (Figure 1.6e, upper device)[153] or polyurethane (Figure 1.6e, lower device).[90] For the upper device, the reference system was provided by a conventional Ag/AgCl electrode coupled with 1 M KCl reference electrolyte. The reference electrolyte can be eliminated by the integration of a miniaturized CIM carbon-based reference electrode, as shown in the lower device. Neither of the two devices requires any pretreatment (i.e., conditioning), and both of them require sample volumes as low as 10 μL. Simple and affordable paper-based ion-sensing devices have also been developed with coulometric,[162] chronopotentiometric,[163] and colorimetric techniques,[164] which opens up new opportunities for miniaturized ion sensing.

1.4 Conclusions

Over the past decade and a-half, all-solid-state potentiometric sensors have become promising candidates for the construction of ion-sensing instrumentation with high portability, simplicity of use, affordability, and flexibility. Signal stability has been improved and detection limits were lowered through persistent research efforts in the development of new solid contact materials, effective approaches to enhance reproducibility, and the better control of the ion-to-electron transduction, water uptake,

and transmembrane ion fluxes. Milestones include, but are not limited to, the understanding of the effects of water-layer formation (2000),[110] the first measurements with subnanomolar detection limit (2004),[137] the introduction of nanostructured carbon materials as solid contacts (2007/8),[61,62] and the development of well-defined redox buffers as inner reference (2013).[49]

Looking beyond, exciting opportunities await. Calibration-free and pretreatment-free all-solid-state electrodes are still at an early age of development. Methods for the accurate control of cell potentials (i.e., E^{o}) and robust redox buffers with a high buffer capacity are needed for highly reproducible potentiometric responses, which are essential for calibration-free single-use ion sensors and long term monitoring with a minimal recalibration frequency. The development of new solid contact materials and the optimization of current systems are still of interest. The combination of redox and double-layer capacitance within the same solid contact has been realized with nanostructured conducting polymers (i.e., 3DOM PEDOT(PSS))[165] and nanocomposites (e.g., graphene and polyaniline).[166] All-solid-state electrodes with both high reproducibility and signal stability will benefit from both redox properties and high contacting areas. Affordable solid contact materials suitable for mass production and mass fabrication are still needed for commercial devices. Eventually, all-solid-state potentiometric sensors will likely replace conventional electrodes and be integrated into modern analytical devices, providing advantages of low cost, ease of operation, and small sample volumes.

1.5 Dissertation Overview

The goal of this dissertation research was to develop robust all-solid-state potentiometric ion-sensing systems with high electrode stability and reproducibility. The dissertation involves fundamental inquiries on further understanding the ion-to-electron transduction mechanism of all-solid-state potentiometric ion sensors, revealing the specific properties that an adequate solid contact should exhibit, and seeking approaches to generate stable and reproducible sensor performance. Depending on specific targeted applications, the ion-sensing system can contain robust all-solid-state ISEs and reference electrodes as bulk electrodes that are used for routine and long-term measurements, or the proposed ion-sensing system can be a simple and affordable paper-based platform with miniaturized high-performance all-solid-state electrodes integrated. The goal can be divided into three specific objectives as follows:

(1) Development of a novel solid contact material

At the time when this thesis work started (i.e., fall 2012), no solid contact material had been reported in literature that exhibited both a high interfacial capacitance to reduce the sensor drift to lower than 10 μV/h, as well as a clean material surface that is essential to achieve a highly reproducible E° with a standard deviation less than 1 mV. Although all-solid-state ISEs and reference electrodes based on 3DOM carbon demonstrated high potential stability benefiting from the high surface area from the macropores,[61,89] its monolithic nature poses challenges for sensor miniaturization and mass production. Also, 3DOM carbon contains large amounts of redox-active surface functionalities, which strongly affects the electrode $E°$ reproducibility. To address these issues, CIM carbon is

proposed as a novel solid contact material. CIM carbon consists of accessible and interconnected mesopores that can be infiltrated by a sensing membrane, providing large interfacial contact area with high double-layer capacitance. Also, the carbon precursor of CIM carbon is a synthetic high-purity hydrocarbon material, so that CIM carbon is expected to exhibit very low amount of redox-active surface impurities. Furthermore, CIM carbon is prepared in a flexible powder form, which is favorable in terms of sensor fabrication and miniaturization.

Based on the above hypothesis, Chapter 2 presents a detailed discussion of the structural features, electrochemical properties, and surface chemistry of CIM carbon, together with its evaluation as a solid contact material in all-solid-state ISEs. The results demonstrate that CIM carbon is an excellent ion-to-electron transducer to construct all-solid-state ISEs, especially for long-term measurements. Chapter 3 discussses the use of CIM carbon in all-solid-state reference electrodes, and explores the possibility of sensor miniaturization by intergrating CIM carbon-based reference electrodes into paper-based ion-sensing platforms.

(2) Development of simple and affordable ion-sensing platforms

With the ever-growing demand for in-field and point-of-care testing applications, paper-based analytical devices have attracted enormous attention due to their ability to combine simplicity, affordability, scalability and flexibility. Previous paper-based ion-sensing devices are based on potentiometry,[153,158] coulometry,[162] chronopotentiometry,[163] and colorimetry,[164] with paper serving either as a substrate to mechanically support the solid contact or a microfluidic sampling tool. Although these devices can be used for

measuring various ions in aqueous solutions, they usually require cumbersome preparation protocols prior to measurements, such as sensor assembly, membrane conditioning, and sensor calibration. Also, the demonstration of sensor performance of these devices in biological samples is rare.

With the motivation of developing a pretreatment-free device, Chapter 4 discusses the design and evaluation of a planar paper-based ion-sensing platform with a conventional ISE and reference electrode embedded into the paper substrate. The device relies on a symmetrical design with each interfacial potential well-defined, so that the sensor response can be theoretically predicted and the resulting sensor is calibration-free. Besides aqueous solutions, the proposed ion-sensing platform also functions in undiluted blood serum samples with high selectivity and reproducibility. To further simplify the use of the device, Chapter 5 explores the opportunity of integrating CIM carbon-based all-solid-state ISEs and reference electrodes onto the paper substrate to construct a pretreatment-free all-solid-state ion-sensing device.

(3) Development of an all-solid-state redox buffer

As discussed in Section 1.2.1, a robust redox buffer is of vital importance for the development of calibration-free potentiometric ion sensors with high E° reproducibility. Current state-of-the-art redox buffers are based on hydrophobic cobalt(II/III) salts that are doped in the sensing membrane. Although proof-of-concept calibration-free ion sensing was demonstrated, the redox buffer can leach out of the sensing membrane over time, thus leading to undesired large potential drifts and deteriorated E° reproducibility.[50] To

construct robust calibration-free all-solid-state ion sensors that can be used for long-term measurements, the loss of the redox buffer must be prevented.

One approach to address this issue is to graft the redox buffer onto the solid contact through covalent linkage. CIM carbon is considered as a good solid contact material in this regard. It consists of accessible and interconnected mesopore structure with large surface area onto which the redox buffer can be anchored. More importantly, CIM carbon exhibits low amounts of redox-active impurities on the surface, so that the grafted redox buffer can function with minimal redox interference arising from the redox-active surface impurities. By covalently attaching the redox buffer onto the surface of CIM carbon, the interfacial potential at the solid contact/sensing membrane interface can be well-controlled, leading to high $E°$ reproducibility of the resulting all-solid-state ISEs and reference electrodes.

Based on the aforementioned assumptions, Chapter 6 presents the evaluation of two approaches to covalently attach the cobalt-based redox buffer on the surface of CIM carbon. CIM carbon is first modified with azide or amine surface functional groups as anchoring points, and then the cobalt complexes are attached to the surface through click chemistry or amide coupling reactions. The CIM carbon surface chemistry, reactivity and the resulting surface coverage of the cobalt complexes are discussed in detail.

This dissertation ends with Chapter 7, which summarizes the state of the art of this thesis and identifies the author's view on the exciting opportunities ahead for the continuation of this research direction.

Chapter 2

Ion-Selective Electrodes with Colloid-Imprinted Mesoporous Carbon as Solid Contact

Reproduced with permission from "Ion-Selective Electrodes with Colloid-Imprinted Mesoporous Carbon as Solid Contact" by Hu, J.; Zou, X. U.; Stein, A.; and Bühlmann, P. in *Anal. Chem.* **2014**, *86*, 7111-7118.

Parts of this chapter relate to U.S. patent application (14/716564) entitled "Ion-Selective Electrodes and Reference Electrodes with a Solid Contact Having Mesoporous Carbon" by Hu, J.; Stein, A.; and Bühlmann, P. filed on 26 May 2015.

Xu Zou contributed to this chapter by synthesizing the cobalt-based redox buffer.

2.1 Introduction

Ion-selective electrodes (ISEs) are widely used in various application fields, including clinical analysis, process control, and environmental monitoring.[1-3,5,30] To achieve sensor miniaturization, small sample volumes, easy maintenance, and scalability for mass production, solid-contact ion-selective electrodes (SC-ISEs), in which a solid contact is used as the ion-to-electron transducer, have attracted much attention.[5,8,11,12]

The first proposed SC-ISE, the coated-wire electrode, was extremely simple but unreliable due to the ill-defined interfacial potential between the ion-selective membrane (ISM) and the underlying conducting metal.[15] To stabilize this interfacial potential, intermediate layers consisting of conducting polymers with high redox capacitance, such as derivatives of polypyrrole,[35] polythiophene,[36] and polyaniline,[37] were introduced. Some of these sensors have shown interference from gases[128] or are affected by the build-up of an unintended water layer between the ISM and the solid contact.[110] More importantly, conducting polymer films do not have a well-defined redox potential but instead exhibit a continuum of redox potentials (which manifests itself, e.g., by broad, scan rate independent peaks in cyclic voltammograms).[97] There are several causes for this energetic inhomogeneity, including the coexistence of crystalline and amorphous regions,[94] slow conformational changes as the result of oxidation or reduction (often referred to as redox transformations, the slowness of which manifests itself in hysteresis),[95,167] changes in the glass transition temperature as a result of doping,[96] the formation of intermolecular bonds between neighboring chains,[97] and the dependence of the film morphology on the method of film fabrication.[98,168] Moreover, the penetrability

of counterions and, concomitantly, the film capacitance depend on the counterion size,[169] and, likely, the local polymer morphology. Consequently, it is difficult to obtain high device-to-device reproducibility and to minimize long-term drift resulting from reactions of the conducting polymer with ambient redox-active species such as oxygen.

More recently, nanostructured carbon materials such as three-dimensionally ordered macroporous (3DOM) carbon,[61,73] carbon nanotubes,[55,62] fullerene,[63] and graphene[65-67] have gained the attention of electrochemists due to their intrinsic hydrophobicity and electric conductivity. SC-ISEs based on these carbon materials have exhibited few problems with water layer formation and interference by O_2, CO_2, or light. Among the sensors with one of these carbon materials as an interlayer, the 3DOM carbon-based SC-ISEs have shown the most favorable long-term potential stability, which can be explained by the high capacitance of the interface between this carbon material and the ISM.

3DOM carbon consists of a glassy carbon skeleton with interconnected macropores that can be infiltrated with the ISM to form a bicontinuous structure, in which electrons are conducted through the carbon framework while ions move through the infused ISM. Its large interfacial contact area and high capacitance lead to excellent long-term stability of 3DOM carbon-based SC-ISEs, with a drift as low as 11.7 μV/h.[61,73] With these sensors, a subnanomolar detection limit of Ag^+ [145] and trace-level detection of perfluorinated surfactants in lake water[144] have been achieved. However, 3DOM carbon prepared from resorcinol-formaldehyde precursors contains significant amounts of redox-active surface functional groups[73] that can affect the reproducibility of the calibration

curve intercept, E^o. As a consequence, SC-ISEs that use 3DOM carbon still require calibration. Moreover, the monolithic nature of 3DOM carbon as used in the past is problematic in view of mass production of sensors.

To address issues of E^o reproducibility and with the ultimate goal to prepare calibration-free SC-ISEs, we report here the investigation of colloid-imprinted mesoporous (CIM) carbon as a new solid contact material. Similar to 3DOM carbon, CIM carbon exhibits open and interconnected pores that can form a bicontinuous carbon and pore space. It can be synthesized by employing a colloidal imprinting method, in which colloidal silica is used as the template and mesophase pitch as the carbon precursor.[170] Both of these starting materials are inexpensive and commercially available, and the synthesis can be easily scaled up. The mesopore size and pore volume of CIM carbon can be tuned by the size of the colloidal silica particles, usually ranging from approximately 10 to 50 nm depending on the source of colloidal silica.[171] Due to its pore texture, CIM carbon exhibits a higher capacitance than 3DOM carbon. In addition, the high purity carbon precursor for CIM carbon, i.e., the mesophase pitch, introduces fewer redox-active surface functional groups. While pitch materials obtained from coal tar or petroleum products have mixed compositions and are difficult to purify, the type of mesophase pitch used here as precursor for the preparation of CIM carbon is a fully synthetic material prepared by condensation of an aromatic hydrocarbon, accounting for its exceptional purity and low oxygen content.[172] Moreover, unlike monolithic 3DOM carbon, CIM carbon is prepared in powder form and can be made into thin films for mass production and fabrication. CIM carbon has been used as a template for zeolite

synthesis[173] and as a stationary phase for reversed-phase liquid chromatography,[174] but its utilization as a solid contact material for ISEs is novel.

Herein, we report the use of CIM carbon with 24-nm diameter mesopores as a new solid contact material. Benefiting from the aforementioned characteristics, CIM carbon-based SC-ISEs exhibit excellent Nernstian response and potential stability. No water layer or interferences by light, O_2, or CO_2 are observed. When combined with a redox buffer layer provided by the tetrakis(pentafluorophenyl)borate ($TPFPB^-$) salts of cobalt(II) and cobalt(III) tris(4,4'-dinonyl-2,2'-bipyridyl) ($[Co(C_9,C_9\text{-bipy})_3]^{2+/3+}$),[50] SC-ISEs can be fabricated with a standard deviation of E° as low as 0.7 mV. This suggests that for many applications these sensors can be used without prior calibration.

2.2 Experimental

Materials. Reagents were obtained from the following sources: mesophase pitch from Mitsubishi Gas Chemicals (Tokyo, Japan), Ludox AS-40 colloidal silica, sodium ethoxide solution (21 wt % in ethanol), bromocresol green/methyl red (mixed indicator solution in methanol), tetraethylammonium tetrafluoroborate ($TEABF_4$), and valinomycin from Sigma-Aldrich (St. Louis, MO), *o*-nitrophenyl octyl ether (*o*-NPOE), and high molecular weight poly(vinyl chloride) (PVC) from Fluka (Buchs, Switzerland), sodium tetrakis[3,5-bis-(trifluoromethyl)phenyl]borate (NaTFPB) from Dojindo (Kumamoto, Japan), and lithium tetrakis(pentafluorophenyl)borate (LiTPFPB) ethyl etherate from Boulder Scientific (Boulder, CO). All chemicals were used as received without further purification. Deionized water was purified to a resistivity of 18.2 MΩ/cm with a Milli-Q PLUS reagent-grade water system (Millipore, Bedford, MA). The redox couple

consisting of $[Co(II)(C_9,C_9\text{-bipy})_3](TPFPB)_2$ and $[Co(III)(C_9,C_9\text{-bipy})_3](TPFPB)_3$ was synthesized as reported.[50]

CIM Carbon Synthesis. The CIM carbon was synthesized using a modification of a previously reported route.[170] A mass of 5 g of mesophase pitch was manually ground and dispersed in 100 mL of an ethanol/water mixture (~60:40 volume ratio) at 50 °C. Under vigorous stirring, 100 mL of Ludox AS-40 colloidal silica suspension was added gradually into the flask, and the resulting mixture was stirred overnight at 50 °C. The resulting mixture was transferred to an open plastic beaker, stirred, and kept at 50 °C overnight to allow solvent evaporation. The obtained pitch–silica composites were then transferred into a porcelain combustion boat and heated under a N_2 flow (0.5 L/min) with a heating ramp of 5 °C/min to 400 °C, at which temperature it was kept for 2 h. The subsequent carbonization at 900 °C for 2 h in a N_2 atmosphere converted the pitch–silica composites to carbon–silica composites. To remove the silica spheres, the carbon–silica composites were then soaked in 6 M KOH aqueous solution and kept for 48 h at 180 °C in a Teflon-lined steel autoclave. The obtained CIM carbon was filtered and washed with copious amounts of water until the pH was 7. Before use, the CIM carbon was pyrolyzed under a 5% H_2, 95% N_2 flow (0.6 L/min) at 900 °C for 5 h to reduce absorbed moisture and functional groups on the carbon surface with preservation of mesopores.[175]

Electrode Fabrication. The 2 mm diameter gold disk electrodes (gold disks embedded into a cylindrical plastic body, CH Instruments, Austin, TX) were polished over polishing cloths with aqueous dispersions of alumina (0.3 and 0.05 μm, Buehler, Lake Bluff, IL). They were cleaned by ultrasonication in water and ethanol, and dried

with a flow of argon. CIM carbon powder was manually ground for 5 min. The CIM carbon suspension was prepared by ultrasonicating 47.5 mg of CIM carbon and 2.5 mg of PVC as binder in 1 mL of freshly distilled tetrahydrofuran (THF) for 30 min. An amount of 30 μL of the CIM carbon suspension was dropcast onto gold electrodes and left to dry, forming CIM carbon films with a thickness of approximately 200 μm.

Precursor solutions for valinomycin-doped K^+-ISMs were prepared by dissolving in 1 mL of freshly distilled THF 66 mg of PVC as polymer matrix, 132 mg of *o*-NPOE as plasticizer, 2.0 mg of valinomycin as ionophore, and 1.2 mg of NaTFPB (75 mol % with respect to the ionophore) to provide for ionic sites. Solutions for K^+-ISMs doped with the redox couple were prepared by dissolving in 1 mL freshly distilled THF 66 mg of PVC, 132 mg of *o*-NPOE, 2.0 mg of valinomycin, 0.6 mg of LiTPFPB ethyl etherate (46 mol % with respect to the ionophore) to provide for anionic sites, and 1.4 mmol/kg each of $[Co(II)(C_9,C_9\text{-bipy})_3](TPFPB)_2$ and $[Co(III)(C_9,C_9\text{-bipy})_3](TPFPB)_3$.

To form ISMs with a thickness of approximately 100 μm, two portions of one of the above solutions (20 μL, followed by 30 μL) were dropcast onto the CIM carbon layer on a gold disk electrode. As a precaution to avoid the possible delamination of the ISMs and CIM carbon films from the gold electrodes, the coated electrodes were mounted into cylindrical bodies custom-made from the Dupont™ Delrin® acetal resin. A screw cap at the opposite end of the electrode allowed to gently press the ISM with the CIM carbon film onto the electrode (see Figure 2.1 and Figure 2.3). (Use of gold disk electrodes embedded into or printed onto a PVC compatible polymer, rather than the commercial gold disk electrodes as used here, would make the cylindrical bodies unnecessary.) Prior

to measurements, the electrodes with the redox couple were conditioned in a 1.0 mM KCl solution for 1 h, and those without the redox couple for 24 h. The short conditioning time of the electrode membranes containing the redox couple minimized the loss of redox couple species by leaching into the aqueous solution, as discussed in ref. [50].

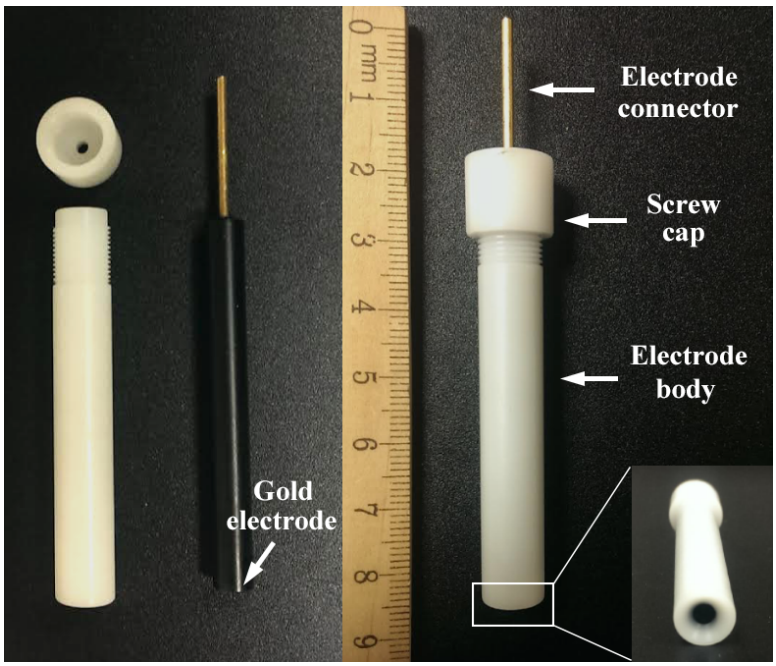

Figure 2.1 Photograph of a disassembled (left) and assembled (right) electrode setup including a gold electrode, a custom-made cylindrical electrode body, and a screw cap. The inset is a bottom view of the assembled electrode showing the ISE membrane with the CIM carbon film.

CIM Carbon Characterization. Acid–base titrations to determine surface functional groups were performed according to a previously reported procedure.[73,176] C, H, N elemental analyses were performed by Atlantic Microlab (Norcross, GA). Transmission electron microscopy (TEM) was carried out with a Technai T12

microscope (FEI, Hillsboro, OR) operating at 120 kV with emission currents ranging from 7 to 12 μA. Nitrogen-sorption measurements were performed on an Autosorb iQ_2 gas sorption analyzer (Quantachrome, Boynton Beach, FL), with samples outgassed at 1 mTorr at 200 °C for 12 h before measurements. Specific surface areas were calculated by the Brunauer–Emmett–Teller (BET) method, and the pore sizes and volumes were estimated from the pore size distribution curves obtained from the adsorption branches of the isotherms using the Barrett–Joyner–Halenda (BJH) method.

Potentiometric Measurements. Electrode potentials were measured with an EMF 16 potentiometer (input impedance 10 TΩ) controlled by EMF Suite 1.03 software (Lawson Labs, Malvern, PA). A double-junction type external reference electrode (DX200, Mettler Toledo, Switzerland; 3.0 M KCl saturated with AgCl as inner filling solution and 1.0 M LiOAc as bridge electrolyte) was used. Activity coefficients were calculated according to a two-parameter Debye-Hückel approximation,[177] and all emf values were corrected for liquid-junction potentials with the Henderson equation.[10]

Capacitance Measurements. A three-electrode setup was used for measurements of the capacitance of CIM carbon. A gold electrode with a CIM carbon film was used as the working electrode, a Pt wire as the counter electrode, and a Ag wire in $AgNO_3$/acetonitrile as a nonaqueous reference electrode. To ensure complete wetting of CIM carbon, 0.1 M $TEABF_4$ in propylene carbonate was used as the nonaqueous electrolyte. The electrolyte solution was purged with argon for 15 min prior to each measurement.

For cyclic voltammetry experiments, a potential window of 0.6 V centered at 0.0 V with a scan rate of 0.5 mV/s was used. The capacitance was calculated by averaging the absolute value of the two current values at 0.0 V. This average current was then divided by the scan rate and the mass of the CIM carbon to give a specific capacitance value in F/g.

Electrochemical impedance spectroscopy (EIS) experiments were carried out on a Solartron 1255B frequency response analyzer with an SI 1287 electrochemical interface (Farnborough, Hampshire, U.K.) controlled by ZPlot software, and the data was fit using ZView software (Scribner Associates, Southern Pines, NC). The frequency range was 1 MHz to 0.01 Hz, with an ac amplitude of 10 mV versus the open circuit potential.

For chronopotentiometry experiments involving a CIM carbon film on a gold electrode, a constant current of 0.1 mA was applied to the working electrode until an upper potential limit of 1.0 V was reached, at which time an equal but opposite current was applied to discharge the device until a lower potential limit of 0.0 V was reached. The specific capacitance in F/g was calculated by dividing the applied current by the mass of the CIM carbon and by the slope of the discharge curve in a potential versus time graph.

For chronopotentiometry measurements with CIM carbon-based ISEs, a gold electrode coated with CIM carbon and an ISM without a redox couple was used as the working electrode, a 1 mM KCl solution was used as aqueous electrolyte, and an aqueous double-junction Ag/AgCl electrode (with a 1.0 M LiOAc bridge electrolyte and AgCl-saturated 3.0 M KCl inner reference electrolyte) and a Pt wire served as the reference and

counter electrodes, respectively. A constant current of +1 nA was applied to the ISE for 60 s, followed by a reverse current of the same magnitude for the same length of time.[32] The capacitance of the electrode was calculated by using the constant current divided by slope of the discharge curve in a potential versus time graph.

2.3 Results and Discussion

2.3.1 Structure of CIM Carbon

The CIM carbon prepared in this work consisted of remarkably uniform mesopores of about 24 nm (Figure 2.2 and Table 2.1) due to the monodispersity of the colloidal silica particles that were used to template the pores.[170] As Figure 2.3 shows, these mesopores are highly interconnected but randomly distributed, which is different from the periodic nature of 3DOM carbon. After manual grinding for 5 min, CIM carbon particles have irregular shapes with average sizes of approximately 15 μm. When used in a SC-ISE, these particles are bound together by the PVC binder as well as the plasticized ISM.

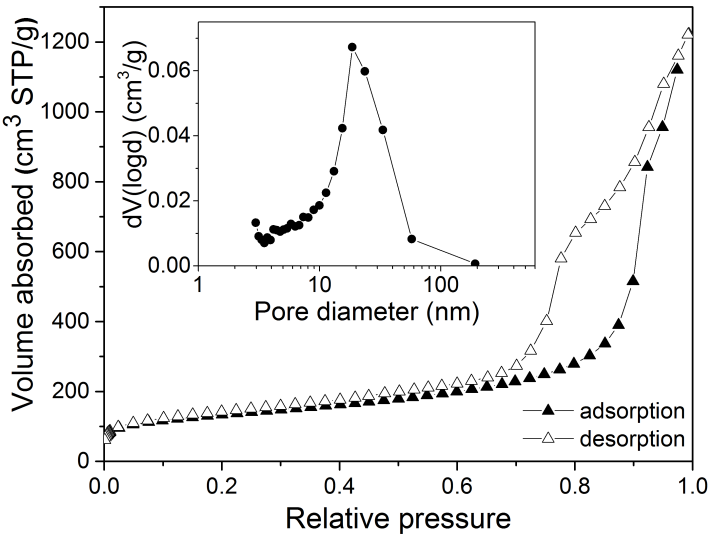

Figure 2.2 Nitrogen sorption isotherm of CIM carbon and the corresponding BJH pore size distribution shown in the inset.

Table 2.1 ***Textural Data of CIM Carbon and 3DOM Carbon***

	BET surface area (m^2/g)	mesopore surface area (m^2/g)	micropore surface area (m^2/g)	mesopore volume (cm^3/g)	micropore volume (cm^3/g)	average pore diameter (nm)
CIM carbon	442	321	117	1.65	0.07	23.7
3DOM carbon[73]	247	25	192	0.03	0.09	1.8

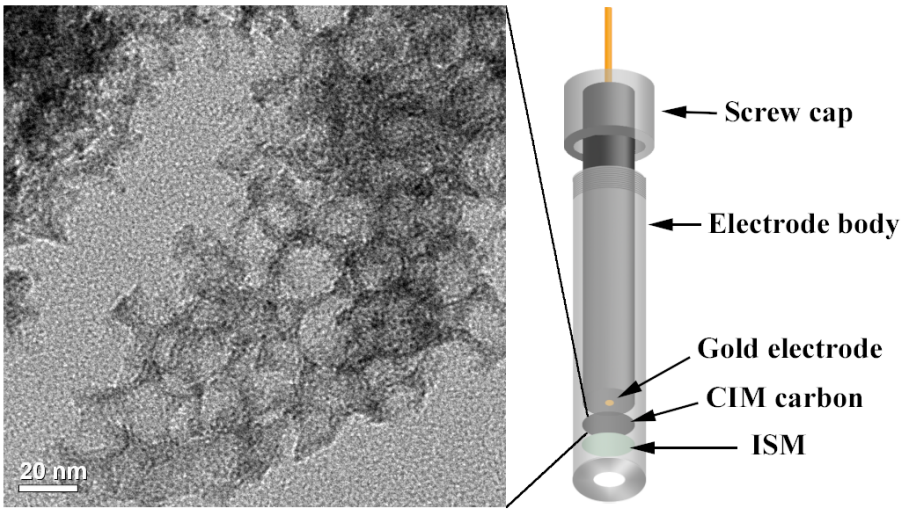

Figure 2.3 Schematic diagram of a CIM carbon-based SC-ISE with a TEM image showing the interconnected mesopores of CIM carbon. CIM carbon is used as an intermediate layer between the gold electrode and ISM.

2.3.2 Purity and Surface Functionality of CIM Carbon

CIM carbon exhibits higher purity and fewer surface functional groups than 3DOM carbon because its carbon precursor, the mesophase pitch used here, is a polyaromatic resin produced by catalytic synthesis from naphthalene, comprising only carbon and hydrogen.[172] In comparison, the resorcinol-formaldehyde precursor of 3DOM carbon contains a considerable amount of oxygen, which can introduce oxygen-based impurities. As shown in Table 2.2, the oxygen content of CIM carbon is 0.43 wt %, i.e., 1.7 wt % lower than that of 3DOM carbon synthesized from resorcinol–formaldehyde. The surface functionality of CIM carbon was characterized by acid–base titrations with four different bases, as previously reported.[73,176] In contrast to 3DOM carbon (see Table 2.3), no phenol functional groups are detected, and the ketone content is cut in half. We

assume that the residual trace amount of oxygen in CIM carbon arises from the KOH hydrothermal treatment used to remove the silica template as well as from small amounts of unremoved silica.

Table 2.2 ***Elemental Analysis Data for CIM Carbon and 3DOM Carbon*** [a]

	C (wt %)	H (wt %)	O (wt %)	N (wt %)
CIM carbon	96.02	0.46	0.43	0.00
3DOM carbon[73]	92.95	0.27	2.13	0.00

[a] All elemental analysis values are ±0.3% according to Atlantic Microlab.

Table 2.3 ***Concentration of Functional Groups on the Surface of CIM Carbon and 3DOM Carbon***

	ketone (mmol/g)	phenol (mmol/g)	lactone and lactol (mmol/g)	carboxylic acid [a] (mmol/g)
CIM carbon	0.17	0.00	0.00	0.00
3DOM carbon[73]	0.34	0.27	0.00	0.00

[a] The titration method cannot distinguish between carboxylic acid and anhydride functional groups, which may also be present.

2.3.3 Capacitance of CIM Carbon

Mesoporous carbon materials are well known for their high double-layer capacitance due to their large surface areas and highly accessible mesopores.[178] In this study, three electrochemical techniques, i.e., cyclic voltammetry (CV), chronopotentiometry, and electrochemical impedance spectroscopy (EIS) were used to determine the specific capacitance of the CIM carbon. For all the measurements, a gold electrode with a CIM carbon film was used as the working electrode, with 0.1 M $TEABF_4$ in propylene carbonate as the electrolyte solution that effectively wets CIM carbon.

In the CV measurement obtained with a scan rate of 0.5 mV/s, a symmetrical curve without Faradaic currents, typical for capacitive behavior, is observed (Figure 2.4a). The absence of Faradaic currents demonstrates the low amount of redox-active surface functional groups on the CIM carbon. For chronopotentiometry, a constant current of +0.1 mA was applied to the working electrode until the potential reached +1.0 V, and then a current of –0.1 mA was applied until the potential reached 0.0 V. Except for the immediate voltage drop after current reversal, the chronopotentiogram appears symmetrical with respect to charging and discharging (Figure 2.4b). For the EIS data (Figure 2.4c), the capacitance of CIM carbon can be represented by the impedance of the electrode at low frequencies ranging from 1 to 0.01 Hz. This data can be fitted with a constant phase element (CPE1 in Figure 2.4c) with a capacitance of 27 mF and a phase value of 0.94, representing capacitive behavior. The specific capacitance of CIM carbon is obtained by dividing the absolute capacitance of the working electrode by the mass of

CIM carbon. Those values are summarized and compared with the corresponding values for 3DOM carbon in Table 2.4. It is very likely that the different values determined with these electrochemical techniques are affected by the different magnitudes of current passing through the working electrode, which can affect the rate of ion transport across the interconnected mesopores of CIM carbon.[179]

Table 2.4 ***Specific Capacitance of CIM and 3DOM Carbon as Measured by Different Methods***

	CV [a] (F/g)	chronopotentiometry[b] (F/g)	EIS (F/g)
CIM carbon	31.3	40.7	20.5
3DOM carbon[73]	3.9	2.3	1.8

[a] Scan rate 0.5 mV/s. [b] Current 0.1 mA.

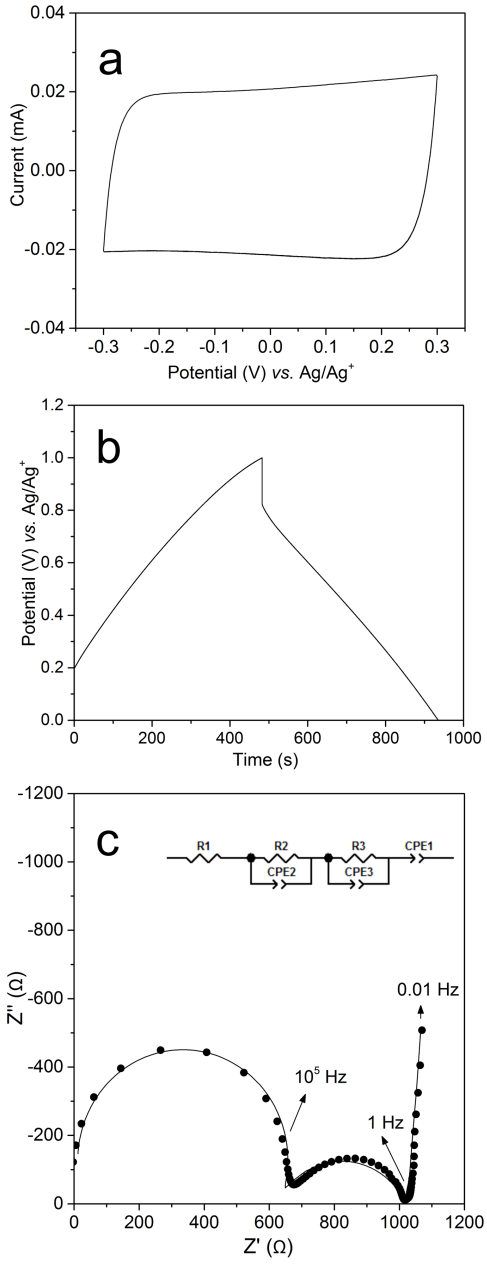

Figure 2.4 Capacitance measurements of a gold/CIM carbon electrode using 0.1 M $TEABF_4$ as the nonaqueous electrolyte. (a) CV with a scan rate of 0.5 mV/s. (b) Chronopotentiometry with a constant current of 0.1 mA. (c) EIS; the actual data is shown as the solid circles, and the solid line represents the data fit. The proposed equivalent circuit is shown in the inset.

Due to the occurrence of redox reactions in the CV and chronopotentiometry experiments for 3DOM carbon,[73] specific capacitance values determined by EIS are more suitable for comparison. This data shows that CIM carbon has a specific capacitance of 20.5 F/g, which is 11 times higher than that for 3DOM carbon. The large capacitance of CIM carbon is due to its interconnected mesopores with average diameters of 24 nm that are accessible to the electrolyte, whereas less accessible micropores of 1.8 nm in average diameter contribute to most of the surface area of 3DOM carbon (see Table 2.1). From nitrogen-sorption data (Figure 2.1), the mesopore surface area of CIM carbon was determined to be 321 m^2/g, which is nearly 13 times that of 3DOM carbon. This ratio is in good agreement with the observed specific capacitance values for these two carbon materials.

2.3.4 Ionic Response

The ionic response of the CIM carbon-based SC-ISEs was measured by successive dilution of a 0.1 M KCl solution while monitoring the emf. For comparison, three different electrode assemblies were used, i.e., a gold electrode with an ISM (gold/ISM), a gold electrode with a CIM carbon intermediate layer and an ISM (gold/CIM carbon/ISM), and a gold electrode with a CIM carbon layer and an ISM doped with the redox couple of $[Co(II)(C_9,C_9\text{-bipy})_3](TPFPB)_2$ and $[Co(III)(C_9,C_9\text{-bipy})_3](TPFPB)_3$ (gold/CIM carbon/ISM with redox couple). The corresponding calibration curves and other potentiometric K^+ response characteristics of these electrodes are shown in Figure 2.5 and summarized in Table 2.5.

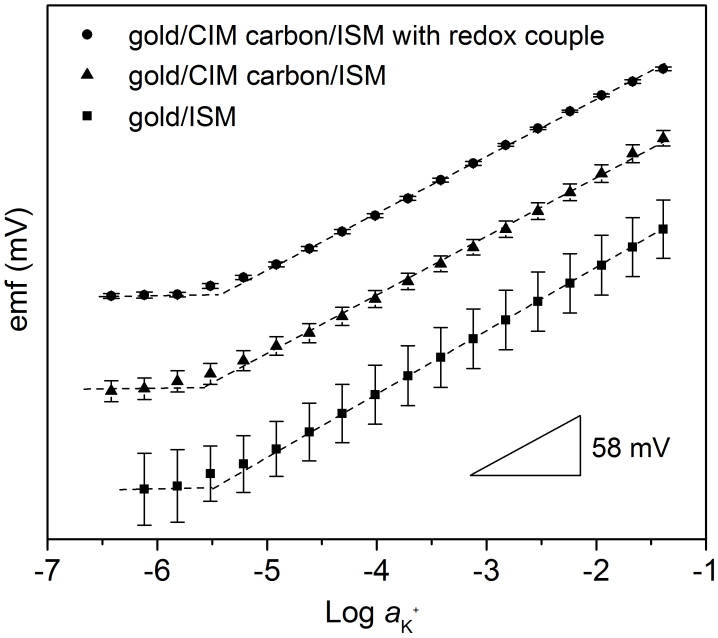

Figure 2.5 Potentiometric K^+ response curves of SC-ISEs with different electrode configurations, i.e., a gold/CIM carbon/ISM with redox couple, a gold/CIM carbon/ISM, and a gold/ISM electrode. For clarity, response curves have been shifted vertically.

Table 2.5 ***Potentiometric K^+ Responses of Different Electrode Assemblies***

electrode type	slope (mV/decade) [a]	$E°$ (mV) [a]	detection limit (M)	linear range (M)
gold/CIM carbon/ISM with redox couple	57.3 ± 0.5	237.5 ± 0.7	$10^{-5.4}$	$10^{-5.0}$ – $10^{-1.0}$
gold/CIM carbon/ISM	59.5 ± 0.6	58.8 ± 7.3	$10^{-5.6}$	$10^{-5.2}$ – $10^{-1.0}$
gold/ISM	64.0 ± 1.4	466.6 ± 32.2	$10^{-5.5}$	$10^{-5.2}$ – $10^{-1.0}$

[a] Average and standard deviation of slopes and $E°$ values determined individually for 6 different electrodes of each type of electrode. $E°$ values refer to the potential of the ISE cell obtained by extrapolation of the linear section of the emf response to the K^+ activity of 1.0 M.

Since there is no ion- and electron-conducting intermediate layer for the gold/ISM interface, the corresponding electrodes behaved quite poorly, as expected for coated wire electrodes. The reproducibility of the emf of these electrodes can be represented by the standard deviation of $E°$, which is as large as 32.2 mV due to the ill-defined interfacial potential. The slightly larger than Nernstian slope of 64.0 mV/decade is likely an artifact from the instability of $E°$. When CIM carbon is used as an intermediate layer between the gold electrode and the ISM, a Nernstian response with a slope of 59.5 mV/decade in the range from $10^{-5.2}$ to $10^{-1.0}$ M is observed. This response is consistent with a high stability of the interfacial potential of the solid contact and can be attributed to the ability of the CIM carbon to combine ionic and electronic conduction when the interconnected mesopores are filled with the ionophore-doped solvent polymeric sensing phase. The detection limit of these sensors is $10^{-5.6}$ M, and might be further improved by using reagents of higher purity and more dilute conditioning and starting solutions.[145] Since no internal reference is present, the standard deviation of $E°$ of these electrodes is 7.3 mV. The best results were obtained after the introduction of the redox couple as an internal reference standard since the interfacial potential between the CIM carbon and the ISM is well controlled by the redox couple.[49,50] With a standard deviation of $E°$ as low as 0.7 mV, these SC-ISEs may be used for some applications without calibration. We assume that the low amount of redox active impurities on the surface of CIM carbon is of particular importance for the proper functioning of the redox couple so that the interfacial potential between the CIM carbon and the ISM is controlled by the redox couple rather than redox active impurities.

2.3.5 Water Layer Test

The formation of an unintentional thin water layer between the ISM and the solid contact is a common problem for SC-ISEs when these electrodes are exposed to aqueous solutions for long periods of time. The presence of this water layer can be tested with a method proposed by Pretsch et al. and is indicated by a positive potential drift when changing from a primary cation solution to a solution of a (discriminated) interfering cation, and a negative potential drift when changing back to the primary cation solution.[110]

In this experiment, the gold/CIM carbon/ISM electrodes were initially conditioned in a 0.1 M KCl solution for 24 h. At t = 1.03 h, the 0.1 M KCl solution was replaced by a 0.1 M NaCl solution, and an immediate potential drop of 176 mV was observed, confirming a high selectivity for K^+ over Na^+. At t = 3.23 h, the return to the 0.1 M KCl solution resulted in an immediate potential increase back to the original value (Figure 2.6). During these processes, no potential drift was observed, indicating that no water layer had formed in the CIM carbon-based SC-ISEs. The absence of a water layer can be attributed to the highly hydrophobic surface of CIM carbon.

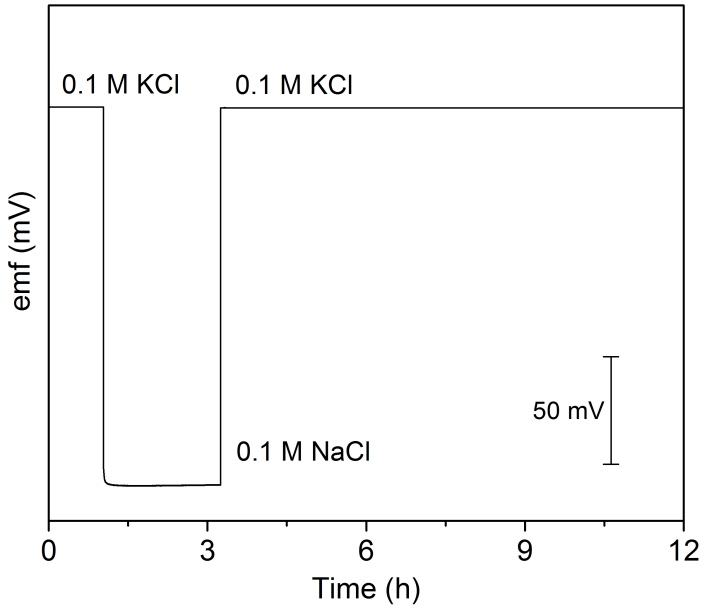

Figure 2.6 Water layer test for a gold/CIM carbon/ISM electrode. The electrode was immersed in a 0.1 M KCl solution for 24 h prior to the measurement. At t = 1.03 h, the 0.1 M KCl solution was changed to a 0.1 M NaCl solution, and at t = 3.25 h, the 0.1 M NaCl solution was changed back to a 0.1 M KCl solution.

2.3.6 Effects of Light, Oxygen, and Carbon Dioxide

Light, O_2, and CO_2 have been reported to cause interference for several SC-ISEs, especially for SC-ISEs with an interlayer of a conducting polymer.[128] A SC-ISE can be photosensitive if the solid contact is an organic semiconductor with a suitable band gap. In addition, O_2 and CO_2 can diffuse across the ISM to reach the solid contact and cause interference. Specifically, O_2 can affect the phase boundary potential by forming an irreversible O_2 half-cell when redox active species are present, and CO_2 can alter the local pH when a water layer exists between the solid contact and the ISM.[8,17]

In this study, the effect of light on the CIM carbon-based SC-ISEs was investigated by continuously recording the emf of gold/CIM carbon/ISM electrodes in a 1 mM KCl solution while turning on/off the ambient light. Effects of O_2 or CO_2 were tested by bubbling these gases through the solution, followed by purging with Ar to remove O_2 or CO_2. As illustrated in Figure 2.7, when the sensors were exposed to light, O_2, or CO_2, no significant effect was recorded. The excellent resistance to these interferents relies on the low extent of surface functionality and the high hydrophobicity of the surface of CIM carbon.

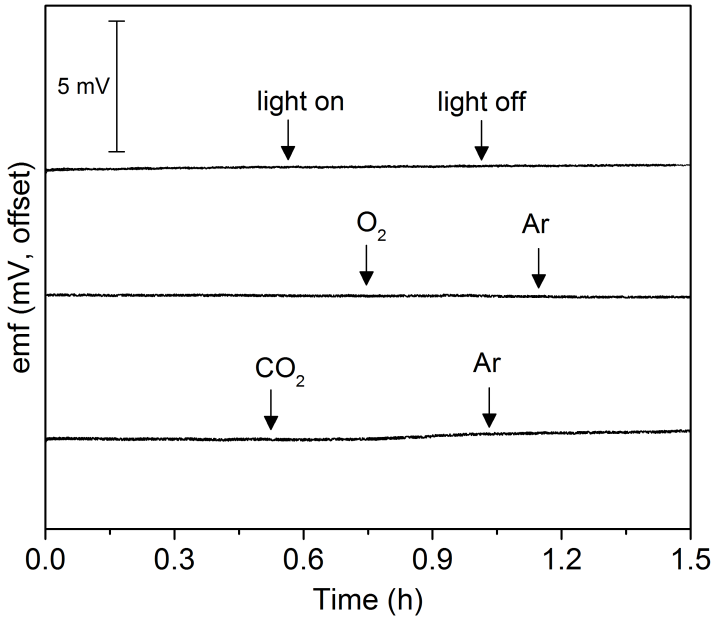

Figure 2.7 Effects of light (top), O_2 (middle), and CO_2 (bottom) on the potential stability of gold/CIM carbon/ISM electrodes immersed in 1 mM KCl solution. For clarity, the emf responses of these electrodes have been shifted vertically.

2.3.7 Potential Stability

The potential stability of gold/CIM carbon/ISM electrodes without redox couple was evaluated by chronopotentiometry[32] by applying consecutively current pulses of +1 nA and –1 nA for 60 each while recording the potential. For comparison, gold/ISM electrodes without CIM carbon were also tested. As shown in Figure 2.8, the gold/ISM electrodes are subject to potential drifts up to 0.9 mV/s because of the ill-defined phase boundary potential and low capacitance. When CIM carbon is used as the intermediate layer between the gold electrode and the ISM, the potential drift is significantly reduced to 1.0 ± 0.2 μV/s (n=3), with an Ohmic drop of 0.36 mV. The capacitance of the electrode is calculated to be 1.0 mF, with a total resistance of 0.36 MΩ. Due to the high double-layer capacitance resulting from the interconnected mesopores of CIM carbon, gold/CIM carbon/ISM electrodes exhibit a higher capacitance than other SC-ISEs with valinomycin-doped membranes, such as the electrodes previously studied with interlayers of poly(3,4-ethylenedioxythiophene) (300 μF),[32] carbon black with platinum nanoparticles (217 μF),[74] graphene (83 μF),[67] and carbon nanotubes (60 μF).[62]

Although chronopotentiometry shows on a short timescale a very good potential stability with a relatively large applied current (in comparison to the residual current in potentiometry), other factors such as a gradual decrease in adhesion between the ISM and the substrate[125] might also lead to the deterioration of the electrode response on a longer timescale. Therefore, continuous tests of gold/CIM carbon/ISM electrodes without redox couple were performed for 70 h in 1 mM KCl solution at a constant temperature of 25 °C using temperature-controlled samples. These experiments showed an emf drift of 1.3 ±

0.3 μV/h (n=3) for gold/CIM carbon/ISM electrodes (Figure 2.9), making these electrodes the most stable SC-ISEs reported so far. We propose that the high double-layer capacitance of CIM carbon contributes to this superior electrochemical performance.

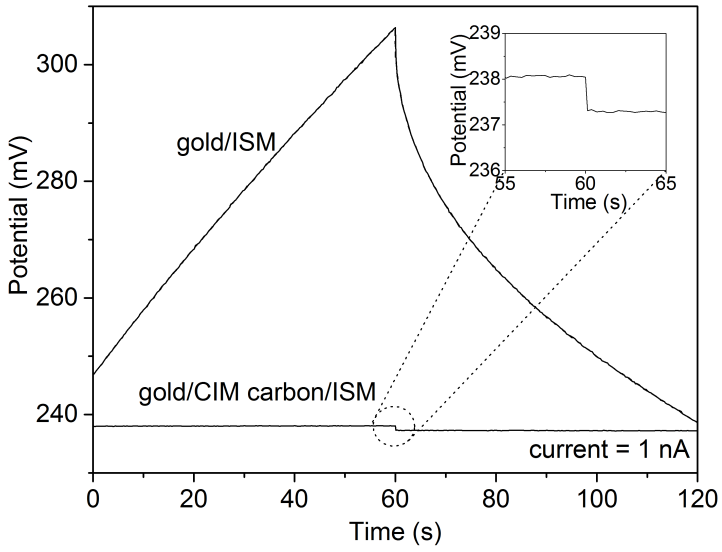

Figure 2.8 Potential stability of gold/ISM (top) and gold/CIM carbon/ISM (bottom) electrodes under constant currents of ±1 nA in 1 mM KCl solution. An expanded view showing the Ohmic drop of the gold/CIM carbon/ISM electrode at the current reversal point is shown in the inset.

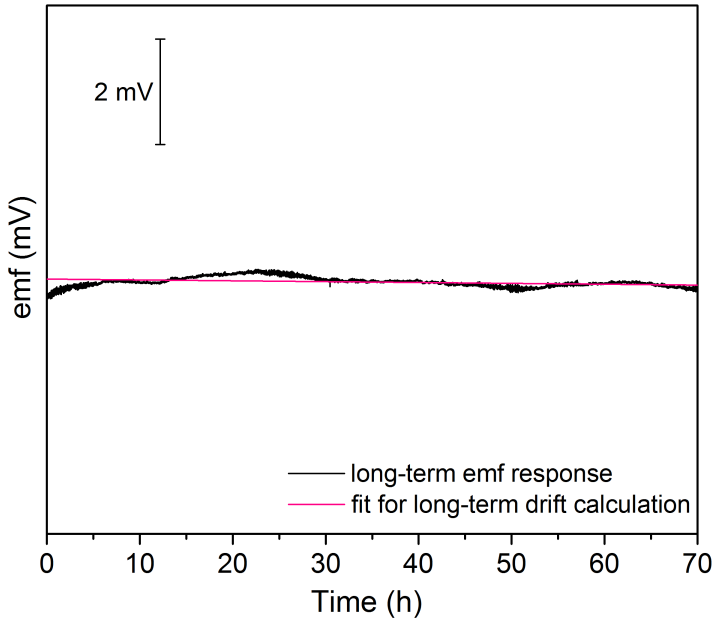

Figure 2.9 Potentiometric emf stability of a gold/CIM carbon/ISM electrode measured in a 1 mM KCl solution at a constant temperature of 25 °C. The emf response of the electrode is shown as the black line, and the red line is the linear fit of the raw data used for the long-term drift calculation.

2.4 Conclusions

This work has demonstrated that CIM carbon can be used as a novel solid contact material to construct SC-ISEs. Sensors with a CIM carbon interlayer exhibit good Nernstian responses with excellent resistance to interference by light, O_2, and CO_2 and no indication for the formation of a water layer. Due to the bicontinuous mesopore structure and large double-layer capacitance of CIM carbon, outstanding potential stability is achieved under conditions where either a large current is present or continuous potentiometric measurements are conducted (at least in tests up to 70 h). When a redox couple is incorporated into the ISM, SC-ISEs can be constructed with a standard

deviation of $E°$ as low as 0.7 mV, which suggests the use for calibration free applications. A challenge for ongoing work lies in the development of even more hydrophobic redox couples that will make it possible to perform long-term experiments with ISEs with CIM carbon solid contacts that exhibit the same excellent long-term stability possible with CIM carbon solid contacts and the $E°$ reproducibility provided by redox buffers. Compared to other solid contact materials, CIM carbon is cheaper and easier to prepare and process, which makes it more suitable for scale-up than 3DOM carbon. These outstanding characteristics make CIM carbon-based SC-ISEs promising candidates for the next generation of commercial ISEs.

2.5 Acknowledgements

This research was supported by the University of Minnesota Initiative for Renewable Energy and the Environment (IREE). Portions of this work were carried out in the University of Minnesota Characterization Facility, which receives partial support from the NSF through the MRSEC, ERC, MRI, and NNIN programs. We thank Stephen Rudisill for taking the TEM image of CIM carbon.

Chapter 3

All-Solid-State Reference Electrodes Based on Colloid-Imprinted Mesoporous Carbon and Their Application in Disposable Paper-Based Potentiometric Sensing Devices

Parts of this chapter relate to U.S. patent application (14/716564) entitled "Ion-Selective Electrodes and Reference Electrodes with a Solid Contact Having Mesoporous Carbon" by Hu, J.; Stein, A.; and Bühlmann, P. filed on 26 May 2015.

Kieu Ho and Xu Zou contributed to this chapter by providing help with the experiments and synthesizing the cobalt-based redox buffer, respectively.

3.1 Introduction

Ion-selective electrodes (ISEs) are widely used in clinical analysis, process control, and environmental monitoring.[1,3-5,30] In view of the need for affordable and portable analytical devices for small sample volumes, miniaturizable all-solid-state ISEs are highly desirable but are only meaningful if the reference electrode is also miniaturized. While the development of all-solid-state ISEs represents a highly active research field,[5,8,180] much less work has been performed to develop all-solid-state reference electrodes,[12] even though the accuracy of potentiometric measurements relies equally on both the reference and measurement half cell.

Conventional reference electrodes are typically Ag/AgCl or Hg/Hg_2Cl_2 half cells and are connected to the sample through a salt bridge. The latter usually contains an aqueous solution of an equitransferent salt that minimizes the liquid junction potential at the interface of the bridge electrolyte and the sample.[78] Although very stable and reliable, such reference electrodes exhibit disadvantages owing to the presence of the salt bridge, such as the need for frequent maintenance, a large size, and the mutual contamination of the bridge electrolyte and sample.[181,182]

A recent example that demonstrates the difficulty of integrating conventional reference electrodes into affordable and disposable sensing devices is that of the paper-based ion sensors that were recently developed for the analysis of Cl^-, K^+, Na^+, and Ca^{2+}.[153] Different from other paper-based potentiometric sensors where paper was used either as a substrate to mechanically support the solid contact[86,87,152,154] or as a microfluidic sampling tool,[155] wax-imprinted paper used in this design served as a

substrate to support the electrodes, the reference electrolyte, and the sample. Although highly miniaturized, these ion sensors still employed a conventional reference system that contained a stencil-printed Ag/AgCl electrode coupled with a KCl solution as reference electrolyte.[153] This conventional reference system requires the manual application of the reference electrolyte and, therefore, still relies on transport and storage of supply reagents. This demonstrates the need for replacing conventional designs.

One of the key components of an all-solid-state reference electrode is a hydrophobic reference membrane attached to an electronically conducting solid contact, thus resembling the setup of an all-solid-state ISE. The reference membranes are usually doped with ions that can leach into the samples on a slow but continuous basis so that the phase boundary potentials at the reference membrane/sample interfaces are sample-independent and defined by the interfacial distribution of the doping ions. Several ions have been doped into reference membranes, including polyions,[183] ionic liquids,[84,88,184] lipophilic and hydrophilic salts.[81,82,185] At the reference membrane/solid contact interface, the interfacial potential can be stabilized by employing various solid contacts that are also used in all-solid-state ISEs. The most common solid contacts include conducting polymers[5,35,81,185,186] and nanostructured carbon materials, such as three-dimensionally ordered macroporous (3DOM) carbon,[61,89] carbon nanotubes,[62,85,86] and graphene.[65,87] Several miniaturized potentiometric cells into which an all-solid-state ISE and reference electrode are integrated have been proposed.[87,152,154,155]

The electrochemical performance of these all-solid-state reference systems is highly dependent on the solid contact between the reference membrane and the

underlying electron conductor. We demonstrated previously that a highly capacitive interface between the ISE membrane and the solid contact provides for a high potential stability of all-solid-state ISEs,[61] and we have shown that the same is also true for reference electrodes with a reference membrane/solid contact interface.[89] In particular, 3DOM carbon-based reference electrodes were found to exhibit a potential drift as low as 42 μV/h over 26 days, which is very favorable in terms of continuous long-term use.[89] However, in regard to device-to-device reproducibility, it is a disadvantage that the 3DOM carbon derived from resorcinol and formaldehyde contains some redox-active surface functional groups that can affect the reproducibility of the calibration curve intercept, E^o.[73] Moreover, the monolithic nature of 3DOM carbon is not optimal for mass production and integration into miniaturized potentiometric sensing devices.

To address these issues, we report here the use of colloid-imprinted mesoporous (CIM) carbon as a solid contact to construct all-solid-state reference electrodes. CIM carbon was recently introduced as a solid contact material to fabricate all-solid-state ISEs.[69] It consists of open and interconnected mesopores that can be filled with a polymeric sensing phase to provide a bicontinuous arrangement of carbon and polymer phases.[170] It has a very high level of purity because it is prepared from a pure hydrocarbon mesophase-pitch precursor. The use of CIM carbon combined with the hydrophobic redox buffer consisting of cobalt(II) and cobalt(III) tris(4,4'-dinonyl-2,2'-bipyridyl) ($[Co(C_9,C_9\text{-bipy})_3]^{2+/3+}$) has enabled the construction of all-solid-state ISEs with a standard deviation of E^o as low as 0.7 mV. [69] Benefiting from the high double-layer capacitance provided by its interconnected mesopores, the emf drift of these all-

solid-state ISEs is 1.3 μV/h over 70 h. Moreover, the synthesis of CIM carbon can be easily scaled up, and CIM carbon is prepared in powder form and, therefore, can be made into thin films, suspensions, or potentially carbon inks for production and fabrication on an industrial level.

Herein, we use CIM carbon with 24 nm diameter mesopores to fabricate all-solid-state reference electrodes. The reference membranes are doped with the ionic liquid 1-methyl-3-octylimidazolium bis(trifluoromethylsulfonyl)imide ($[C_8min^+][C_1C_1N^-]$) to define the potential at the reference membrane/sample interface,[84] as well as a hydrophobic redox buffer consisting of $[Co(II)(C_9,C_9\text{-bipy})_3](TPFPB)_2$ and $[Co(III)(C_9,C_9\text{-bipy})_3](TPFPB)_3$ to define the potential at the CIM carbon/reference membrane interface.[50] Benefiting from the high capacitance of the interface between the CIM carbon and the reference membrane, outstanding potential stability is observed, with a potential drift as low as 1.7 μV/h over 110 h, making CIM carbon-based reference electrodes the most stable all-solid-state reference electrodes reported so far. To demonstrate their compatibility with miniaturized potentiometric systems, CIM carbon-based reference electrodes are integrated into disposable paper-based Cl^- sensing devices to replace the conventional Ag/AgCl reference electrodes, eliminating the reference electrolyte and the associated liquid junction potentials.

3.2 Experimental

Materials. Reagents were obtained from the following sources: mesophase pitch from Mitsubishi Gas Chemicals (Tokyo, Japan), Ludox AS-40 colloidal silica from Sigma-Aldrich (St. Louis, MO), *o*-nitrophenyl octyl ether (*o*-NPOE) and high molecular

weight poly(vinyl chloride) (PVC) from Fluka (Buchs, Switzerland), ionic liquid $[C_8min^+][C_1C_1N^-]$ from IOLITEC (Tuscaloosa, AL), Tecoflex SG-80A polyurethane from Thermedic Polymer Products (Woburn, MA), and AGCL-675 Ag/AgCl ink from Conductive Compounds (Hudson, NH). All chemicals were used as received without further purification. Deionized water was purified to a resistivity of 18.2 MΩ/cm with a Milli-Q PLUS reagent-grade water system (Millipore, Bedford, MA). CIM carbon and the redox couple consisting of $[Co(II)(C_9,C_9\text{-bipy})_3](TPFPB)_2$ and $[Co(III)(C_9,C_9\text{-bipy})_3](TPFPB)_3$ were prepared as previously reported.[50,69,170]

Electrode Fabrication. The 2 mm diameter gold disk electrodes (CH Instruments, Austin, TX) were polished over polishing cloths with aqueous dispersions of alumina (0.3 and 0.05 μm, Buehler, Lake Bluff, IL). They were cleaned by ultrasonication in water and ethanol and dried with a flow of argon. CIM carbon powder was manually ground for 5 min using a pestle. The CIM carbon suspension was prepared by ultrasonicating 47.5 mg of CIM carbon and 2.5 mg of PVC as binder in 1 mL of freshly distilled tetrahydrofuran (THF) for 30 min. An amount of 30 μL of the CIM carbon suspension was drop-cast onto the gold electrodes and left to dry, forming CIM carbon films with a thickness of approximately 200 μm.

Precursor solutions for reference membranes were prepared by dissolving in 2 mL of freshly distilled THF 60 mg the ionic liquid $[C_8min^+][C_1C_1N^-]$, 120 mg of PVC as polymeric matrix, and 120 mg of *o*-NPOE as plasticizer, as described by Zhang et al.[89] Moreover, 1.4 mmol/kg each of $[Co(II)(C_9,C_9\text{-bipy})_3](TPFPB)_2$ and $[Co(III)(C_9,C_9\text{-}$

bipy)$_3$](TPFPB)$_3$ was added to this solutions as an internal reference. The precursor solutions were stirred for 2 h to ensure complete dissolution.

To form reference membranes with a thickness of approximately 100 μm, two portions of the precursor solutions (20 μL, followed by 30 μL after 1 min) were drop-cast onto the CIM carbon layer on a gold electrode. The coated electrode was then mounted into a cylindrical body with a screw cap at the opposite end, as previously reported (see Figure 2.1 and Figure 2.3 in Chapter 2).[69] Prior to measurements, these electrodes were conditioned in a 1.0 mM NaCl solution for 1 h.[50]

Fabrication of Paper-Based Cl^- Sensing Devices. Paper-based sample zones and microfluidic channels were defined by patterning polyurethane lines that penetrated through the whole thickness of ashless filter papers (Whatman Grade 589/2 white ribbon). Approximately 2.5 g of polyurethane was dissolved in 40 mL of THF, and this solution was then applied to both sides of the paper using a capillary, forming polyurethane lines approximately 2 mm in width. The Ag/AgCl electrodes were patterned on paper by stencil printing. A hand-cut Frisket Film (low tack, Grafix, Maple Heights, OH) was used as the stencil and Ag/AgCl ink was applied to the openings of the stencil using a rubber brush, followed by a curing process at 100 ºC for 15 min.

To form 2-mm wide reference membranes, a 5 μL microcapillary was used to apply the precursor solution onto paper. To ensure the full penetration of the membrane components through the entire thickness of the paper, the precursor solution was applied on both sides of the paper 4 times with a 1 min time interval between applications to allow THF to evaporate. A CIM carbon-reference membrane suspension was prepared by

ultrasonicating for 30 min 60 mg of CIM carbon in 1 mL of the solution containing the reference membrane components. The resulting suspension was then applied onto paper using a capillary to form a homogenous mixture of CIM carbon and reference membrane, with an effort to maximize the contact area between this homogenous mixture and the reference membrane, which was applied separately.

Potentiometric Measurements. Electrode potentials were measured with an EMF 16 potentiometer (input impedance 10 TΩ) controlled by EMF Suite 1.03 software (Lawson Labs, Malvern, PA). To test the electrochemical performance of the CIM carbon-based all-solid-state reference electrodes, a conventional double-junction external reference electrode (DX200, Mettler Toledo, Switzerland; 3.0 M KCl saturated with AgCl as inner filling solution and 1.0 M LiOAc as bridge electrolyte) was used. To test the response of paper-based Cl^- sensing devices, two copper alligator clips were used to connect the Ag/AgCl and CIM carbon electrodes to a potentiometer. All of the paper-based Cl^- sensing devices were used without preconditioning, i.e., without exposure of the Ag/AgCl electrode and the reference membrane to aqueous solutions prior to measurements. Activity coefficients were calculated according to a two-parameter Debye-Hückel approximation.[177]

3.3 Results and Discussion

3.3.1 Ionic Response of CIM Carbon-Based Reference Electrodes

A good reference electrode should not respond to any sample species. To test whether this was also true for all-solid-state reference electrodes consisting of a gold

electrode coated with a CIM carbon layer and a reference membrane doped with the hydrophobic redox buffer $[Co(C_9,C_9\text{-bipy})_3]^{2+/3+}$ and the ionic liquid $[C_8min^+][C_1C_1N^-]$, the ionic responses of such electrodes were measured against a conventional double-junction reference electrode. The resulting emf responses are shown in Figure 3.1. Overall, the obtained calibration curve intercept, E^o, is -120.6 ± 3.7 mV for 3 electrodes, and for a given electrode, the E^o is -120.8 ± 8.0 mV in 6 electrolytes. For each electrolyte, there is only a very small emf response of the CIM carbon-based reference electrodes in the concentration range from 10^{-7} M to 10^{-1} M, demonstrating the low potential variability of CIM carbon-based reference electrodes to ions with different charges and hydrophilicities. The change in emf over the entire range of activities is 1.9 ± 0.8 mV/decade for NH_4^+, 1.1 ± 0.6 mV/decade for K^+, 0.9 ± 0.5 mV/decade for Na^+, 0.9 ± 0.6 mV/decade for Li^+, 1.1 ± 1.0 mV/decade for Mg^{2+}, and 0.5 ± 0.3 mV/decade for Ca^{2+} (n=3). This low dependence of the emf on the concentrations of ions is consistent with the phase boundary potential at the reference membrane/sample interface being defined by partitioning of the ionic liquid between the hydrophobic reference membrane phase and the aqueous sample phase. Unlike in the case of an ISE membrane, transfer of sample ions into the reference membrane is not occurring to an extent that it affects the phase boundary potential.

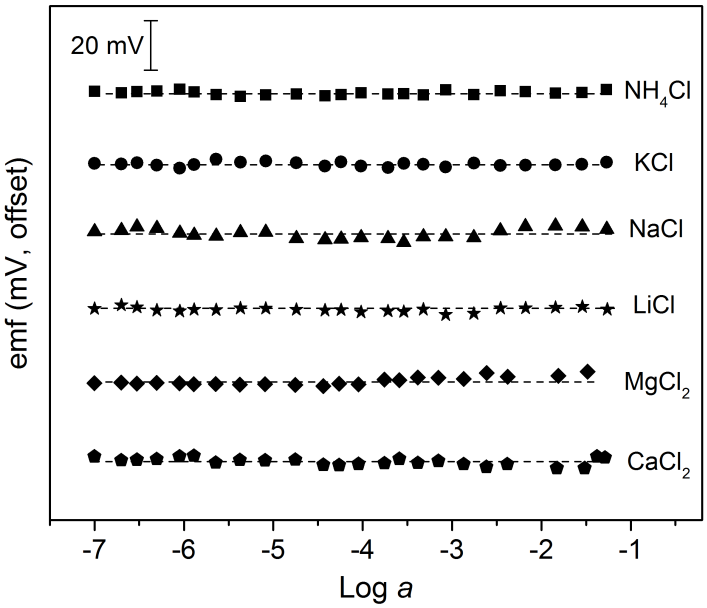

Figure 3.1 Potentiometric responses of gold/CIM carbon/reference membrane electrodes in aqueous solutions of NH_4Cl, KCl, NaCl, LiCl, $MgCl_2$, and $CaCl_2$ in the concentration range from 10^{-7} M to 10^{-1} M. The responses were measured by addition of aliquots of concentrated salt solutions under continuous stirring. The response curves have been shifted vertically for clarity.

3.3.2 Use of CIM Carbon-Based Reference Electrodes to Measure Cl^- Responses of a Ag/AgCl ISE

To assess the suitability and reproducibility of CIM carbon-based reference electrodes in ion-selective potentiometry, Cl^- measurements were performed with a AgCl-coated Ag wire as the ISE and two different reference electrode assemblies (i.e., gold/CIM carbon/reference membrane with or without redox couple). For comparison, a conventional double-junction reference electrode was also employed. The Cl^- responses were measured by successive dilution of a 0.1 M NaCl solution while monitoring the

emf. The corresponding potentiometric Cl^- response characteristics are shown in Figure 3.2 and summarized in Table 3.1.

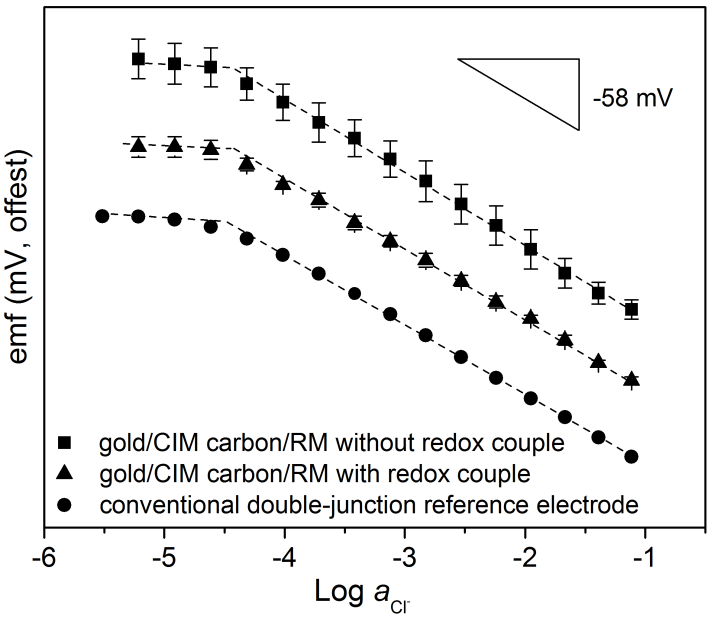

Figure 3.2 Potentiometric responses to Cl^- of a Ag/AgCl ISE against reference electrodes with different electrode configurations, i.e., gold/CIM carbon/reference membrane (RM) without redox couple, gold/CIM carbon/reference membrane with redox couple, and a commercial double-junction reference electrode. The response curves have been shifted vertically for clarity.

As Table 3.1 shows, CIM carbon-based reference electrodes both with and without the hydrophobic redox couple yield Nernstian responses (i.e., -55.5 ± 1.0 mV/decade with a reference membrane with the redox couple and -57.7 ± 2.3 mV/decade when no redox couple was used), with values that are within error indistinguishable from the response slope obtained with a conventional double-junction reference electrode (i.e.,

-55.9 mV/decade). The detection limits obtained from these different reference electrodes were all approximately $10^{-4.4}$ M. These values are close to the intrinsic detection limit for Cl^- using a Ag/AgCl ISE (i.e., $10^{-4.9}$ M), which is determined by the solubility of AgCl.

Table 3.1 ***Potentiometric Cl^- Responses of a Ag/AgCl ISE* vs. *Reference Electrode Assemblies with a Reference Membrane (RM) or a Conventional Double Junction*** [a]

reference electrode	slope (mV/decade)	$E°$ (mV)	detection limit (M)
gold/CIM carbon/RM without redox couple	-57.7 ± 2.3	122.9 ± 12.9	$10^{-4.4}$
gold/CIM carbon/RM with redox couple	-55.5 ± 1.0	82.8 ± 2.8	$10^{-4.4}$
conventional double-junction	-55.9	-12.1	$10^{-4.5}$

[a] Means and standard deviations for five separate measurements with one Ag/AgCl ISE and five different reference electrodes. The $E°$ values were obtained by extrapolation of the linear section of the emf response to a Cl^- activity of 1.0 M.

Since there is no internal reference for the gold/CIM carbon/reference membrane electrodes without redox couple, the standard deviation of $E°$ (12.9 mV) is relatively large. This value is comparable to what has been observed in the past for many solid contact ISEs and is not necessarily problematic if devices are properly calibrated, but it is unsuitable for calibration-free measurements with disposable miniaturized sensing devices. The poor electrode-to-electrode repeatability can be significantly improved by

doping the reference membrane with the hydrophobic redox couple $[Co(C_9,C_9\text{-bipy})_3]^{2+/3+}$, reducing the standard deviation of E^o to 2.8 mV.

3.3.3 Effects of Light, Oxygen, and Carbon Dioxide

Light, O_2, and CO_2 have been reported to interfere with the response of some all-solid-state ISEs,[12] and the possibility of such interferences should also be considered for all-solid-state reference electrodes. Generally, photosensitivity can be observed with conducting polymer and semiconductor solid contacts that have a suitable band gap.[8] Interference caused by CO_2 can be attributed to changes in the pH of a water layer formed at the solid contact-membrane interface,[110] and O_2 can interfere by forming an irreversible O_2 half-cell at the surface of the underlying electron conductor or by oxidizing functional groups on organic conductors.[128]

The effect of light on gold/CIM carbon/reference membrane electrodes was investigated by continuously recording their emf values versus a conventional double-junction electrode while switching off and on the fluorescent tube lights in the laboratory. The effects of O_2 or CO_2 were tested by bubbling these gases into 1.0 mM NaCl sample solutions, followed by purging with Ar to remove those gases again. As shown in the top two traces of Figure 3.3, no significant effects of light and O_2 were observed. While the insensitivity to light is due to the absence of a band gap of CIM carbon in the visible range, the excellent resistance to O_2 can be attributed to the low amounts of redox-active impurities and the absence of functional groups on the surface of CIM carbon.

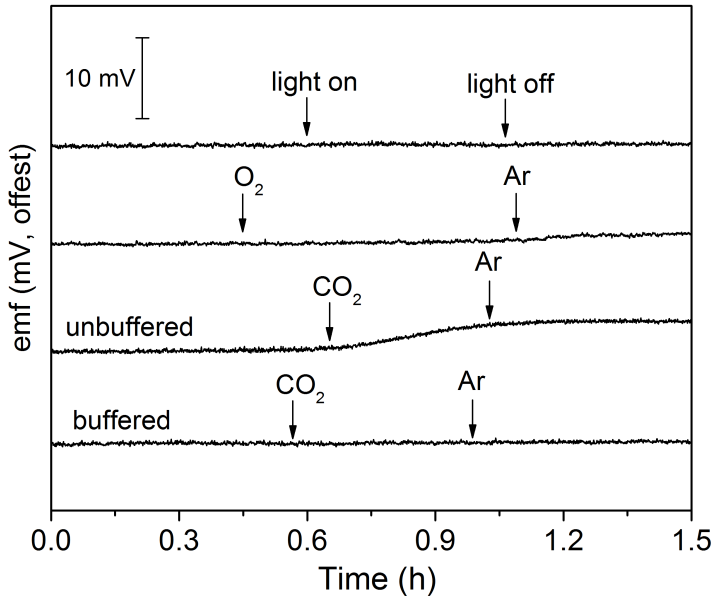

Figure 3.3 Effects of light, O_2, and CO_2 on the potential stability of gold/CIM carbon/reference membrane electrodes. The effect of CO_2 was studied both in an unbuffered 1.0 mM NaCl solution and a 0.1 M phosphate buffer solution (pH 7.5). The response curves have been shifted vertically for clarity.

When CIM carbon-based reference electrodes were exposed to CO_2 in an unbuffered solution, however, a potential drift of 9.5 mV/h is observed (Figure 3.3, 3rd trace from the top). This drift can be attributed to a decrease of the solution pH, promoting the co-ion extraction of H^+ and the ionic liquid anion, $[C_1C_1N^-]$ into the reference membrane. This affects the phase boundary potential at the reference membrane–sample interface, as we have reported previously.[89] This effect, combined with fluctuations in the stir rate, may have affected the noise level of the data shown in Figure 3.1. To eliminate this effect and make it possible to study the influence of CO_2 on the CIM carbon–reference membrane interface, a phosphate buffer (pH = 7.5) was used,

stabilizing the pH of the sample solution. As shown in the bottom trace of Figure 3.3, no significant effect of CO_2 is observed with this pH buffered sample system, demonstrating the excellent resistance of the CIM carbon–reference membrane interface to CO_2. Use of an ionic liquid that is less subject to protonation would enable the construction of CIM carbon-based reference electrodes with resistance to CO_2 in pH unbuffered solutions.

3.3.4 Long-Term Potential Stability

Potential stability is another important aspect for all-solid-state ISEs and reference electrodes, especially when they are used to continuously monitor the concentration of an analyte over an extended period of time. In this study, the potential stability of CIM carbon-based reference electrodes was assessed by monitoring the potentials of these references electrodes continuously for 110 h in a 1.0 mM NaCl solution at a constant temperature of 25 ºC (Figure 3.4). To avoid leaching of the redox couple from the reference membrane into the sample as a cause of potential drifts, gold/CIM carbon/reference membrane electrodes without redox couple were used. Due to the large double-layer capacitance of the CIM carbon layer, the potential drift of these reference electrodes was as low as 1.7 ± 1.2 μV/h (n = 3), which is on the same level as for CIM carbon-based ISEs (i.e., 1.3 ± 0.3 μV/h).[69] For measurements that require long-term potential stability with high E^{o} reproducibility, a more hydrophobic redox couple or a redox couple covalently attached to the polymer backbone could be employed.

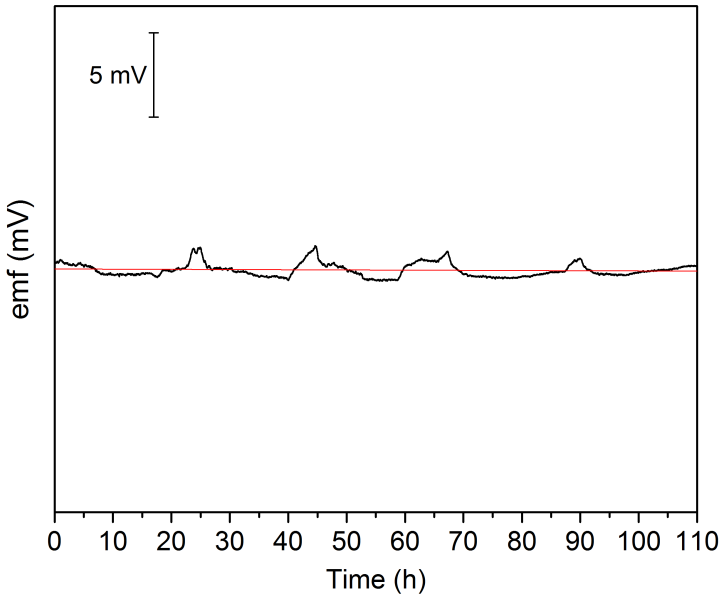

Figure 3.4 Potential stability of a gold/CIM carbon/RM electrode without redox couple, measured in a 1 mM NaCl solution at a constant temperature of 25 °C. The emf response of the electrode is shown as the black line, and the red line is the linear fit of the raw data used for the emf drift calculation.

3.3.5 Design of Disposable Paper-Based Potentiometric Cl^- Sensing Devices

Because they combine affordability, scalability, simplicity, and flexibility, paper-based analytical devices have recently attracted much attention.[187-189] In particular, miniaturized potentiometric Cl^- sensing devices were fabricated on wax-printed paper, with two stencil-printed Ag/AgCl electrodes serving as the ISE and the reference electrode. These devices resembled the one shown in Figure 3.5a but had a wax rather than a polyurethane barrier to contain aqueous solutions. For measurements, one droplet each of the sample and a reference electrolyte solution had to be applied onto the paper close to the corresponding electrodes, resulting in spontaneous wicking of the two liquids

into the central contacting area to complete the electric circuit.[153] While these Cl^- sensing devices have the advantage of being simple to use, they are subject to sample dependent liquid junction potentials at the sample/reference electrolyte interface and require the manual application of not only the sample but also a reference electrolyte solution.

To further simplify these paper-based potentiometric sensing devices and improve their accuracy, CIM carbon-based reference electrodes were used in this work to replace the conventional Ag/AgCl reference electrodes. Three designs were tested in a step-by-step approach to the final device. To start, a design similar to the one used for the previously reported paper-based Cl^- sensing devices, i.e., with two stencil-printed Ag/AgCl electrodes, was used (Figure 3.5a). However, instead of printed wax,[153] polyurethane was used to form the hydrophobic barriers that define the microfluidic channels. Polyurethane was chosen not only because it is inexpensive, readily commercially available, and can be inkjet-printed for mass fabrication,[190] but also because its use avoids the melting process that is required to fabricate wax-printed paper devices.[153,191] In a second step, to eliminate the liquid junction potentials at the sample/reference electrolyte interface, a reference membrane was integrated into the central zone of the device, as shown in Figure 3.5b. Finally, a CIM carbon-reference membrane reference system was used to replace the conventional Ag/AgCl reference electrode (Figure 3.5c).

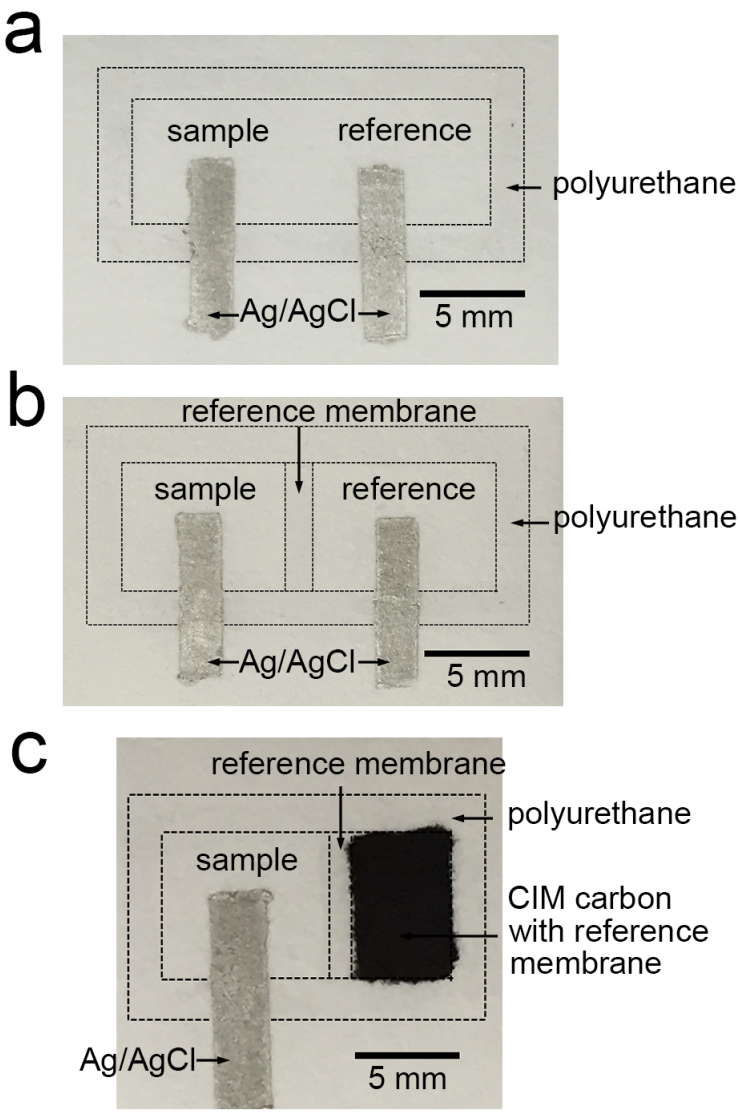

Figure 3.5 Photographs of paper-based potentiometric Cl^- sensing devices with different designs. (a) Device with a Ag/AgCl ISE and a Ag/AgCl reference electrode. (b) Device with a Ag/AgCl ISE and a reference electrode with a reference membrane. (c) Device containing a Ag/AgCl ISE and a CIM carbon-based reference electrode with a reference membrane.

3.3.6 Use of a Reference Membrane to Eliminate Liquid Junction Potentials in Paper-Based Potentiometric Cl^- Sensing Devices

To assess the effectiveness of reference membranes to eliminate the liquid junction potentials in paper-based potentiometric Cl^- sensing devices, Cl^- measurements were performed using a 1.0 M LiCl reference electrolyte and sample solutions containing different LiCl concentrations. LiCl was chosen here on purpose because of the large difference in the ionic mobilities of Li^+ and Cl^-, which results in liquid junction potentials as large as tens of millivolts. This offered the advantage that pinholes through the paper-supported reference membrane, which would have compromised the intended use of the reference membranes, would have been readily recognized by the occurrence of large liquid junction potentials within such pinholes.

As shown in the lower trace of Figure 3.6 (open circles), the Cl^- sensing devices without reference membranes (as shown in Figure 3.5a) exhibit a sub-Nernstian response with a slope of -38.8 ± 1.3 mV/decade, while their counterparts with reference membranes (Figure 3.5b) yielded a Nernstian response with a slope of -57.1 ± 1.5 mV/decade in the range from $10^{-1.0}$ to $10^{-3.5}$ M (solid circles). The inferior response slope of the Cl^- sensing devices without reference membranes could be improved by mathematically correcting liquid junction potentials using the Henderson equation, as illustrated in the top trace in Figure 3.6 (crossed circles).[10] The corrected response slope of -57.0 ± 1.3 mV/decade matches with the results for the devices with reference membranes, which demonstrates that the behavior of the system is well understood.

However, corrections of liquid junction potentials are not readily possible for real samples with complex and unknown compositions.[192]

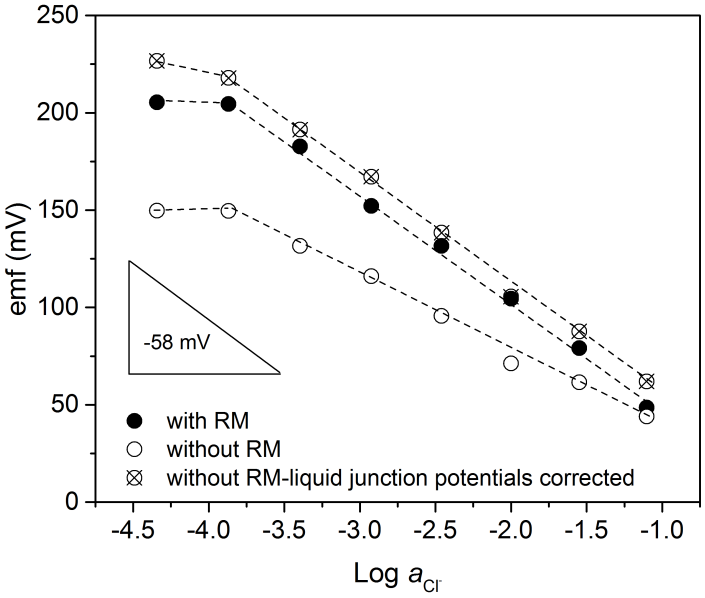

Figure 3.6 Comparison of the response to LiCl of paper-based potentiometric Cl^- sensing devices with and without reference membranes (RMs). The open and crossed circles represent the emf of the paper-based potentiometric Cl^- sensing device without a reference membrane before (open circles) and after (crossed circles) subtraction of the calculated liquid junction potential. The solid circles represent the emf of the paper-based potentiometric Cl^- sensing device with a reference membrane without any mathematical manipulation. Photographs of the two types of devices are shown on the top right.

3.3.7 Integration of a CIM Carbon–Reference Membrane Reference System into Paper-Based Potentiometric Cl^- Sensing Devices

The use of these disposable paper-based Cl^- sensing devices can be further simplified by employing an all-solid-state CIM carbon-based reference electrode to replace the conventional Ag/AgCl reference electrode, eliminating the reference electrolyte (Figure 3.5c). To test their electrochemical performance, 10 μL aliquots of sample solution containing different concentrations of NaCl were applied to the area around the Ag/AgCl ISE. The resulting Cl^- response curve is shown in Figure 3.7. In this potentiometric cell, all phase boundary potentials are well defined. Specifically, the phase boundary potential between the sample and Ag/AgCl is defined by the redox reaction $AgCl(s) + e^- \rightleftarrows Ag(s) + Cl^-(aq)$, the phase boundary potential at the sample/reference membrane interface is defined by the ionic liquid, and the phase boundary potential at the reference membrane/CIM carbon interface is defined by the redox couple. As a result, these paper-based Cl^- sensing devices exhibit a highly reproducible Nernstian response with a slope of -59.8 ± 0.9 mV/decade and a $E°$ of 19.8 ± 2.1 mV over the range from $10^{-1.0}$ to $10^{-3.5}$ M. This demonstrates that CIM carbon-based reference systems can be successfully integrated into miniaturized potentiometric systems based on paper.

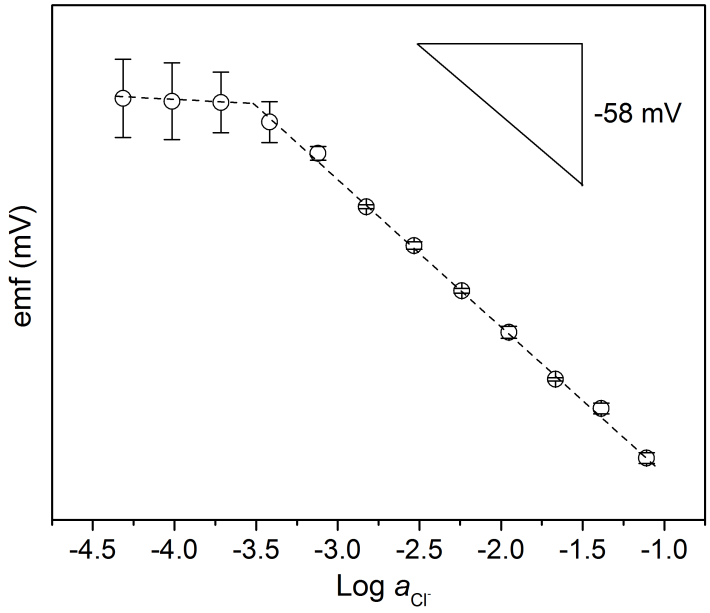

Figure 3.7 Potentiometric Cl^- response curve of paper-based potentiometric Cl^- sensing devices containing a Ag/AgCl ISE and a CIM carbon-based reference electrode with a reference membrane. A photograph of the device is shown on the bottom left. The average and standard deviation of each data point is based on measurements with three individual devices.

3.4 Conclusions

This work has demonstrated that CIM carbon can be used as a solid contact material to fabricate all-solid-state reference electrodes. This permits the construction of high-performance all-solid-state potentiometric ISEs and reference electrodes with the same type of solid contact, polymer matrix, fabrication process, and electrode configuration. CIM carbon-based reference electrodes exhibit a very low dependence of the half-cell potential in solutions of various electrolytes with concentrations in a wide range. Due to the low amounts of redox-active impurities on the surface of CIM carbon,

phase boundary potentials at the membrane/CIM carbon interfaces can be defined well by the $[Co(C_9,C_9\text{-bipy})_3]^{2+/3+}$ redox couple, permitting a high electrode-to-electrode reproducibility of E^o. The interconnected mesopores of CIM carbon offer the added advantage of a high double-layer capacitance, resulting in potential drifts as low as 1.7 μV/h and making these electrodes the most stable all-solid-state reference electrodes reported so far.

We also demonstrated that the CIM carbon-based reference system can be integrated into a disposable paper-based potentiometric Cl^- sensing device, replacing the conventional Ag/AgCl reference electrode, eliminating the need for reference electrolyte, and eliminating liquid junction potentials. These miniaturized Cl^- sensing devices with CIM carbon-based reference systems are inexpensive, easy to handle, and offer very reproducible Cl^- measurements with sample volumes as low as 10 μL. Ongoing research involves the development of paper-based potentiometric sensing devices for other ions employing the same CIM carbon-based reference system, and the development of even more hydrophobic redox buffers to extend the calibration-free character of these devices to long term measurements.

3.5 Acknowledgements

This research was supported by the University of Minnesota Initiative for Renewable Energy and the Environment (IREE). The authors are grateful to United Sciences LLC for providing the ionic liquid. J. H. appreciates the Krogh family for support with a Lester C. and Joan M. Krogh Fellowship in Chemistry. K. T. H. thanks the ACS Project SEED Program for a summer research fellowship for high school students.

Chapter 4

A Disposable Planar Paper-Based Potentiometric Ion-Sensing Platform

4.1 Introduction

Ion sensing is an important topic in various fields, such as clinical and environmental analysis.[1,4,5,180] As often introduced in general chemistry courses, selective and quantitative ion sensing can be achieved with a potentiometric cell that comprises an ion-selective electrode (ISE), a reference electrode, and a voltmeter as a readout tool. It has been estimated that each year over a billion measurements with ISEs are performed globally in clinical laboratories alone.[1] Besides detection of analytes with low (e.g., K^+, Na^+, Cl^-) and high valence charges (e.g., heparin),[193] biosensing of proteins[194] and detection of electrically neutral species have been achieved with ISEs.[195]

With the growing demand for point-of-care and in-field testing, paper has recently attracted much attention as a simple, affordable, flexible, and scalable substrate for microfluidic assays.[160,187,189,196,197] While paper-based colorimetric sensors offer the advantage of simple data interpretation, detection with electrochemical techniques is insensitive to color interferences and generally more quantitative.[188,198] Existing paper-based ion sensors rely on various techniques, including potentiometry,[139,153,156,158] coulometry,[162] chronopotentiometry,[163] and colorimetry.[164] Paper was used in these devices either as a microfluidic sampling tool, or a substrate to mechanically support the sensing components. Strip-type ISEs known as Ektachem slides were available in the 1980s,[157] and were recently adapted with a paper substrate to support carbon nanotubes or conducting polymer as solid contacts.[139,158] Although miniaturizable, these devices need cumbersome electrode conditioning and individual calibration. A more integrated device, reported by Whitesides et al., utilizes a reusable ISE membrane placed between two

disposable wax-imprinted paper substrates.[153] With different ISE membranes, various clinically relevant ions can be detected. However, the ISE membranes have to be well conditioned, and the devices have to be carefully assembled and calibrated, which may impede their practical use.

With the motivation of developing a simple and pretreatment-free device, we herein report a disposable planar paper-based ion-sensing platform with a potentiometric cell embedded into paper. In contrast to strip-type or other ion sensors that have to be calibrated individually, devices based on this highly integrated platform are suitable for single use and do not require any pretreatment or assembly. By design, each interfacial potential within these cells is well defined, so that their responses can be theoretically predicted, and highly reproducible measurements are achieved. For a demonstration of clinical applications, ion sensors were fabricated and successfully used for Cl^- and K^+ sensing in biological samples with a small sample volume of 20 μL. By using specific sensing membranes, this platform can potentially be adapted for detecting other ions that are currently measured with a conventional ISE setup. The fabrication of these planar devices can be readily scaled up by printing, and their integration into complex paper-based devices for complete analysis is conceivable too.

4.2 Experimental

Materials. Reagents were obtained from the following sources: Fumion® FAA-3 ionomer anion exchanger from FuMA-Tech GmbH (Bietigheim-Bissingen, Germany), the ionic liquid 1-methyl-3-octylimidazolium bis(trifluoromethylsulfonyl)imide $[C_8min^+][C_1C_1N^-]$ from IoLiTec (Tuscaloosa, AL, USA), *o*-nitrophenyl octyl ether (*o*-

NPOE), high molecular weight poly(vinyl chloride) (PVC), and tetradodecylammonium tetrakis(4-chlorophenyl)borate (ETH 500) from Fluka (Buchs, Switzerland), anhydrous tetrahydrofuran (THF), valinomycin, and potassium tetrakis(4-chlorophenyl)borate from Sigma-Aldrich (St. Louis, MO, USA), Tecoflex SG-80A polyurethane from Thermedic Polymer Products (Woburn, MA, USA), AGCL-675 Ag/AgCl ink from Conductive Compounds (Hudson, NH, USA), and Autonorm™ freeze-dried blood serum from SERO (Stasjonsveien, Norway). All chemicals were used as received without further purification. Deionized water was purified to a resistivity of 18.2 MΩ/cm with a Milli-Q PLUS reagent-grade water system (Millipore, Bedford, MA, USA).

Precursor Solutions of Sensing Membranes and Reference Membranes. Fumion® FAA-3 ionomer anion exchanger was used to prepare the hydrophilic high-capacity anion exchange (HHCAE) membranes and was obtained in the Br^- form. To exchange the Br^- counter ions with Cl^-, the anion exchanger was conditioned sequentially in aqueous solutions of 1 M KCl for 1 day and 1 mM KCl for 2 days. Then, the Cl^--loaded Fumion® FAA-3 ionomer was dried at 70 ºC overnight. Precursor solutions for the fabrication of the HHCAE membrane were prepared by dissolving 150 mg of Cl^--loaded Fumion® FAA-3 ionomer in 2 mL of methanol. Prior to use, the resulting solution was allowed to pass through a 5 μm syringe filter.

Precursor solutions for the deposition of K^+-selective membranes were prepared by dissolving 5.0 mg of valinomycin as ionophore, 1.7 mg of potassium tetrakis(4-chlorophenyl)borate (75 mol% with respect to the ionophore) as ionic sites, 50 mg of ETH 500 as inert electrolyte, 66 mg of PVC as polymer matrix, and 132 mg of *o*-NPOE

as plasticizer in 1 mL of anhydrous THF.

Precursor solutions for reference membranes were prepared by dissolving 60 mg of the ionic liquid [C_8min^+][$C_1C_1N^-$], 120 mg of PVC as polymeric matrix, and 120 mg of *o*-NPOE as plasticizer in 2 mL of anhydrous THF, as previously reported.[89,90]

Fabrication of Sensors Based on a Paper-based Ion-Sensing Platform. Paper-based sample zones and microfluidic channels were defined by patterning polyurethane lines that penetrated the whole thickness of filter paper (Whatman Grade 589/2 white ribbon for Cl^- sensors and Whatman Grade 2 for K^+ sensors) pieces. When choosing specific papers for specific applications, the surface chemistry, the pore structure and the cost of the paper should be carefully considered.[199] Note that the role of each of these parameters is not fully understood yet; for example, it is not clear at this point which of these parameters are predominantly responsible for the poor performance of membranes without the ETH 500 additive.

Approximately 2.5 g of polyurethane was dissolved in 40 mL of THF, and this solution was then applied to both sides of the filter paper using a glass capillary tube, forming polyurethane barriers against hydrophilic samples approximately 2 mm in width. The Ag/AgCl electrodes were patterned on paper by stencil printing. A hand-cut Frisket Film (low tack, Grafix, Maple Heights, OH, USA) was used as the stencil, and Ag/AgCl ink was applied to the openings of the stencil using a rubber brush. This was followed by a curing process at 100 ºC for 15 min.

To form approximately 1-mm wide sensing and reference membranes, a 10 µL microcapillary was used to apply the corresponding precursor solutions onto the filter

paper. The resulting membrane widths were 1.4 ± 0.1 mm for the sensing membranes and 1.3 ± 0.1 mm for the reference membranes (n = 10). Where necessary, the viscosity of the precursor solutions was adjusted by dilution with additional aliquots of corresponding solvents for better penetration into the filter paper. To ensure full penetration of the membrane components through the entire thickness of the paper, the precursor solutions were applied to both sides of the paper twice each.

Potentiometric Measurements. Electrode potentials were measured with an EMF 16 high-impedance voltmeter (input impedance 10 TΩ) controlled by EMF Suite 1.03 software (Lawson Labs, Malvern, PA, USA). Two copper alligator clips were used to connect the two Ag/AgCl electrodes to the voltmeter. All of the devices were used without preconditioning, i.e., without exposure of the Ag/AgCl electrodes and the reference membrane to aqueous solutions prior to measurements. A series of samples containing different concentrations of Cl^- and K^+ was obtained by sequential dilution of a KCl solution. A series of blood serum samples with various Cl^- concentrations was prepared by adding small amounts of a 0.8 M KCl solution into tenfold diluted blood serum; samples of blood serum containing various K^+ concentrations were obtained by adding small amounts of a 0.8 M KCl solution into undiluted blood serum. Activity coefficients were calculated according to a two-parameter Debye–Hückel approximation.[177] After the samples and reference electrolytes were applied to the corresponding sensing zones, it took approximately 20 s for the solutions to be wicked onto the sensing membranes. Then, the emf response over the following 30 s was collected and analyzed.

4.3 Results and Discussion

4.3.1 Evaluation of HHCAE Membrane as Sensing Membrane for Potentiometric Ion Sensing

Commercial high-capacity ion-exchange membranes are commonly used in fuel cells and electrodialysis, but their applications in potentiometric sensors have not been explored until recently.[200] To evaluate the suitability of a commercial HHCAE Fumion® FAA-3 ionomer as anion exchanger for potentiometric ion sensing, the precursor solutions for the preparation of HHCAE membranes were allowed to penetrate a piece of filter paper to form a sensing membrane. The resulting sensing membrane was assembled into a conventional ISE body, as shown in Figure 4.1a, with a 1 mM KCl inner filling solution in contact with a Ag/AgCl wire as inner reference. The potentiometric Cl^- responses of these ISEs were tested with a commercial double-junction reference electrode. As the calibration curve in Figure 4.1b shows, these electrodes exhibited Nernstian responses with a slope of –57.4 ± 0.5 mV/decade and E^o = 10.3 ± 2.2 mV (n = 3), demonstrating their suitability for potentiometric ion sensing.

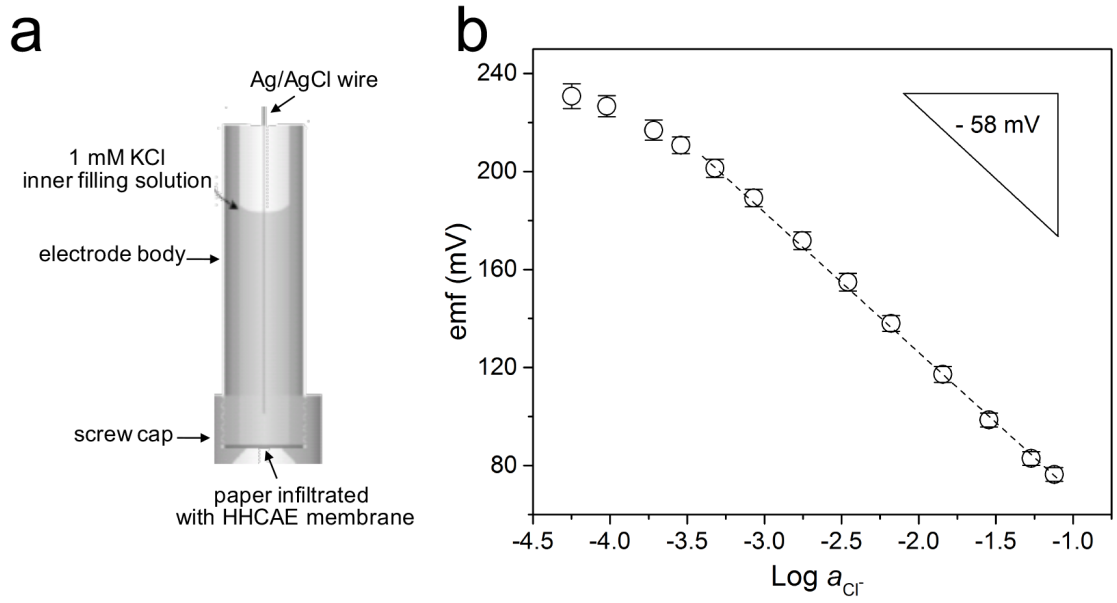

Figure 4.1 (a) Schematic representation of a conventional ion-selective electrode (ISE) with a sensing membrane composed of a filter paper infiltrated with an HHCAE membrane as anion exchanger membrane. (b) Potentiometric Cl^- responses of the ISEs shown in (a) tested with a commercial double-junction reference electrode. The calibration curve is based on three individual electrodes; error bars represent standard deviations.

4.3.2 Design and Sensing Mechanism of Paper-Based Ion-Sensing Platform

The paper-based ion-sensing platform was fabricated by integrating a potentiometric cell into a piece of filter paper (Figure 4.2a). To define microfluidic channels that contain aqueous solutions, a polyurethane-based hydrophobic barrier was deposited into paper. Polyurethane is used because it is affordable, readily available, inkjet-printable,[190] and it avoids the melting process that is required for wax-printed barriers used in previously reported paper-based devices.[191] As a potentiometric cell, this

device contains an ISE with a sensing membrane and a reference electrode with a reference membrane; both of the membranes are embedded into paper. The sensing membrane can be an ionophore-doped ISE membrane, or a hydrophilic high-capacity ion-exchange membrane that is particularly suitable for biological samples.[200] For a demonstration of clinical applications, we used a commercial HHCAE membrane (Fumion® FAA-3 ionomer) and a valinomycin-doped ISE membrane for Cl^- and K^+ sensing, respectively. The reference membrane was loaded with an ionic liquid that can leach into the adjacent aqueous solutions on a slow but continuous basis, thus providing sample-independent potentials.[84,89] It avoids direct contact between the sample and reference electrolyte, thus eliminating undesirable liquid-junction potentials that can cause large measuring errors.[90] Analogous to a conventional ISE that contains a AgCl-coated Ag wire as an inner reference coupled with an inner filling solution, this paper-based device utilizes stencil-printed Ag/AgCl electrodes coupled with 0.1 M KCl reference electrolyte as inner references for both the ISE and reference electrode.

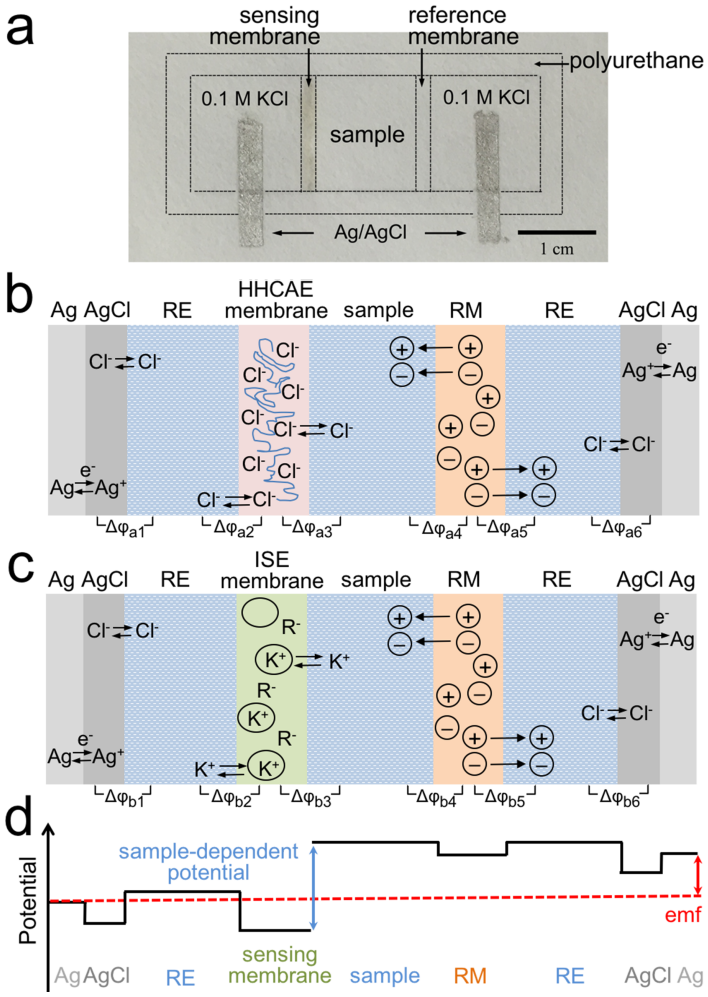

Figure 4.2 (a) Photograph of a paper-based ion-sensing device. (b) Schematic representation of all relevant interfaces in a Cl^- sensor with an HHCAE membrane, ionic liquid-doped reference membrane (RM), and two Ag/AgCl electrodes contacting a 0.1 M KCl reference electrolyte (RE). (c) Paper-based K^+ sensor with a sensing membrane doped with ionophore (shown as an ellipse) and ionic sites (R^-). (d) Electrical potential profile across the sensing device.

To ensure calibration-free operation, each interfacial potential within the cell has to be well defined and highly reproducible.[30,201] For this device (Figure 4.2b), the interfacial potential at the interface between the Ag/AgCl electrode and reference electrolyte ($\Delta\varphi_{a1}$ and $\Delta\varphi_{a6}$) is defined by the redox reaction $AgCl(s) + e^- \leftrightarrow Ag(s) + Cl^-(aq)$, which is fixed by using a 0.1 M KCl reference electrolyte. At the sample/reference membrane ($\Delta\varphi_{a4}$) and reference membrane/reference electrolyte interfaces ($\Delta\varphi_{a5}$), the interfacial potentials are governed by partitioning of the ionic liquid between the membrane and aqueous phases, making them sample-independent. For the sensing membrane, the distribution of the primary ion (Cl^- or K^+) between the membrane and adjacent aqueous solutions determines the two interfacial potentials ($\Delta\varphi_{a2/b2}$ and $\Delta\varphi_{a3/b3}$); therefore, their concentration dependence can be quantitatively predicted by the Nernst equation.[1,5] Since $\Delta\varphi_{a2/b2}$ is controlled by 0.1 M KCl reference electrolyte, $\Delta\varphi_{a3/b3}$ is the only sample-dependent potential within the cell. The measured electromotive force (emf) is the sum of all interfacial potentials of the cell (Figure 4.2d), which are well-defined and, therefore, reproducible and predictable. Consequently, the response of the device can be theoretically predicted, and is, in principle, calibration-free.

The structural features of the device were characterized by scanning electron microscopy (SEM). As shown by a top view (Figure 4.3a and Figure 4.3b), the surface of the cellulose fibers is fully coated by the sensing components (e.g., Ag/AgCl electrode and reference membrane). The sample/sensing membrane interface is located in the cross-section of the paper, into which the membrane is embedded. As the SEM images of the cross-section show (Figure 4.3c and Figure 4.3d), the voids between the cellulose

fibers are filled by the sensing membrane, forming a homogenous sensing network and providing good contact between the sample and sensing components.

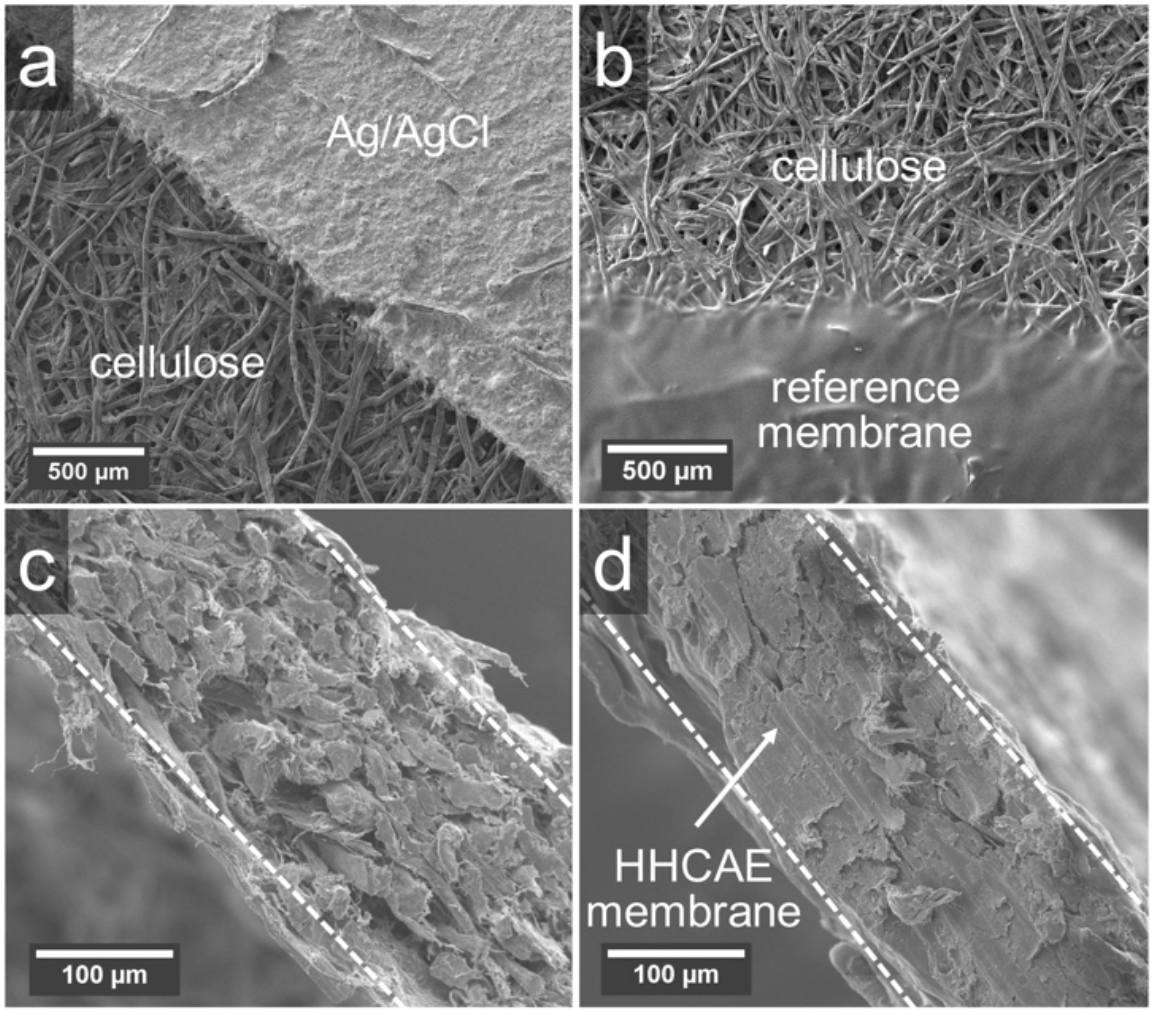

Figure 4.3 SEM images of the device: (a) Top view showing the Ag/AgCl electrode. (b) Top view showing the reference membrane. (c) Cross-section of the paper not infiltrated with a sensing membrane. (d) Cross-section of paper infiltrated with an HHCAE membrane.

Figure 4.4 shows a device placed on a piece of a polyvinyl chloride sheet as a mechanical support, with the two Ag/AgCl electrodes connected to a voltmeter using alligator clips. For a measurement, 20 µL of the 0.1 M KCl reference electrolyte is applied to each of the areas close to the Ag/AgCl electrodes, and 20 µL of the sample is applied to the sample zone. In principle, the sample volume could be further reduced by patterning smaller sensing areas into paper using inkjet printing. Due to the single-use nature of the device, at least ten individual devices are needed for a calibration curve with ten different concentrations.

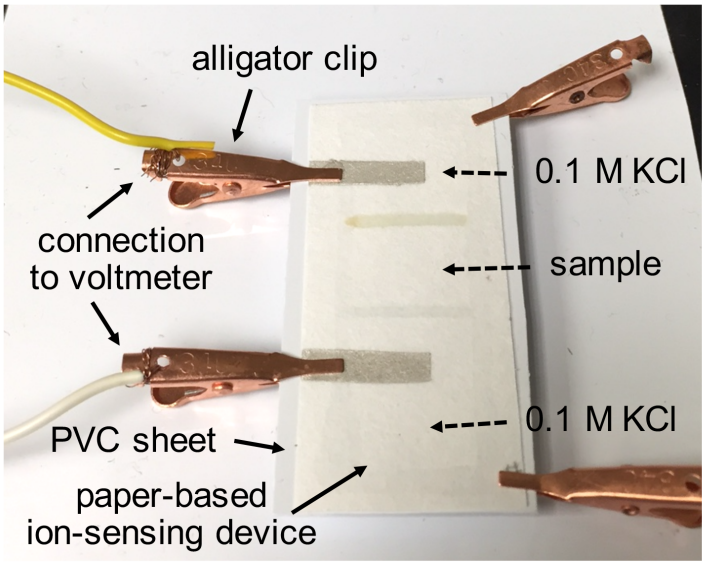

Figure 4.4 Photograph of a paper-based ion-sensing platform placed on a PVC sheet as a supporting substrate, with two alligator clips on the left for the emf measurements and two clips on the right to balance the device.

4.3.3 Paper-Based Cl^--Sensing Platform with HHCAE Sensing Membranes

The Fumion® FAA-3 ionomer anion exchanger was obtained from the manufacturer with Br^- as counterions. To ensure an accurate Cl^- response, Cl^- substitution was required before device fabrication. When paper-based devices with membranes prepared from ion exchanger in Br^- form were used for Cl^- sensing (Figure 4.5, open circle), a sub-Nernstian response was obtained with a reduced slope of -46.3 mV/decade but a surprisingly high linearity (R^2 = 0.9886). The Cl^- response of these devices was significantly improved by using Cl^--loaded HHCAE membranes, leading to a Nernstian slope of –57.3 mV/decade with an R^2 value of 0.9976.

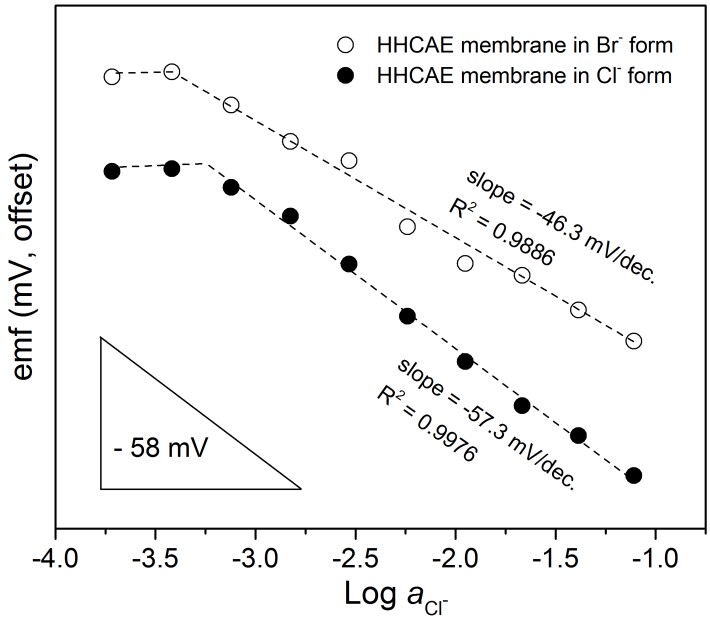

Figure 4.5 Potentiometric Cl^- calibration curves of paper-based ion-sensing devices using Br^--loaded (open circle) and Cl^--loaded (solid circle) HHCAE membranes for Cl^- sensing. Each data point is based on one device.

When the optimized HHCAE membrane is used for Cl^- detection with samples of aqueous solutions (Figure 4.6a), these devices exhibit highly reproducible responses with an E^o of –63.6 ± 2.0 mV and the theoretically predicted (Nernstian) slope of –56.6 ± 1.0 mV/decade in the range from $10^{-0.7}$ to $10^{-3.1}$ M, which covers the clinically relevant range. This E^o and slope reproducibility are similar as for conventional ISEs with HHCAE membrane-infiltrated papers as sensing membranes (E^o = 10.3 ± 2.2 mV and slope = –57.4 ± 0.5 mV/decade, see Figure 4.1). When a 0.1 M KCl solution is used as both the sample and reference electrolyte, a symmetrical potentiometric cell is formed, and the theoretical emf is 0 mV.[202] As Figure 4.6a shows, the measured emf is 0.3 ± 2.1 mV (n = 3), correlating well with the predicted value. Although the HHCAE membrane exhibits limited selectivity towards various hydrophilic anions, it is chosen specifically for clinical Cl^- sensing (98–107 mM in blood serum) because its use reduces interference from lipophilic ions (e.g., Br^- or SCN^-)[203] and biofouling caused by lipids,[200] and also resists Donnan failure at high ion concentrations due to its high ion-exchange capacity.[204]

The performance of paper-based Cl^- sensors was also tested in biological samples. A series of blood serum samples with different Cl^- concentrations was prepared by adding 0.8 M KCl aqueous solutions into tenfold diluted blood serum samples with a certified Cl^- concentration (99 mM for undiluted blood serum). As shown in Figure 4.6b, reproducible and Nernstian responses are obtained in diluted blood serum samples with a slope of –55.7 ± 1.0 mV/decade and an E^o of –68.8 ± 1.6 mV. The resistance of the

devices is 1.2 ± 0.8 MΩ (n = 27), demonstrating that they are compatible with affordable low-impedance voltmeters as a readout tool.

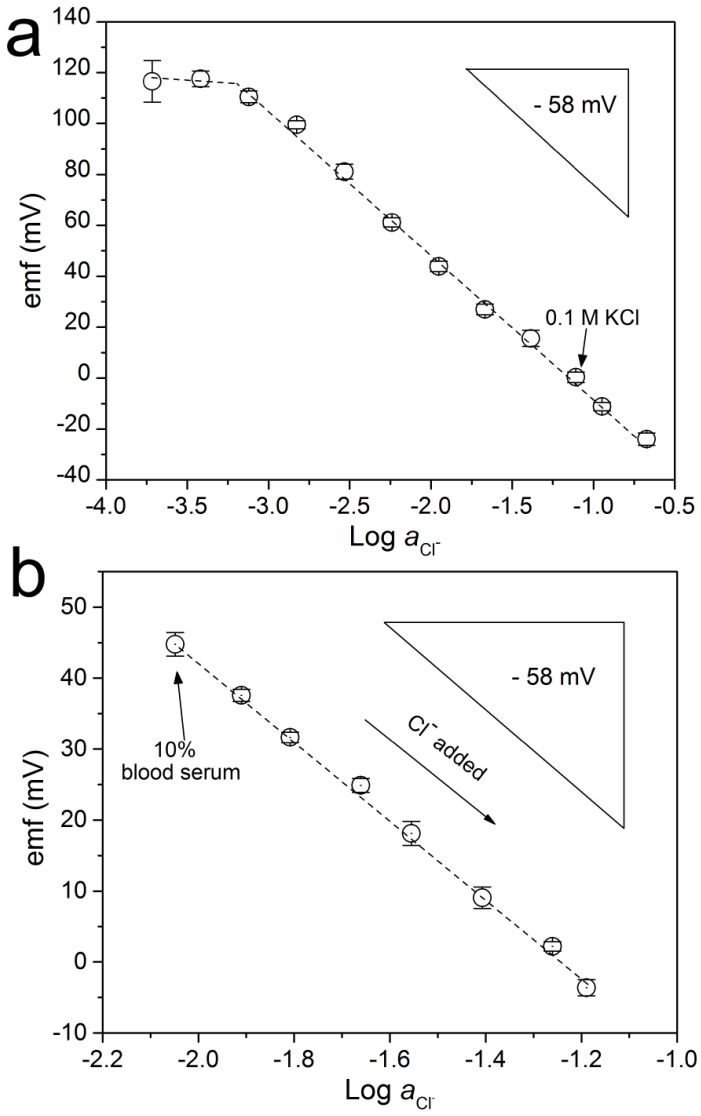

Figure 4.6 Cl^- response of paper-based Cl^- sensors with HHCAE sensing membranes. (a) Potentiometric Cl^- response curve of paper-based Cl^- sensors to aqueous KCl solutions. (b) Potentiometric Cl^- response curve of paper-based Cl^- sensors to tenfold diluted blood serum samples. Each data point is based on three individual devices.

4.3.4 Paper-Based K^+-Sensing Platform with Ionophore-Doped Sensing Membranes

Besides functioning with HHCAE membranes for Cl^- sensing, the paper-based ion-sensing platform is also compatible with ISE membranes exhibiting high selectivity. This is essential for K^+ sensing in blood, since the K^+ level (3.5–5.1 mM) in blood serum is much lower than that of the interfering ion Na^+ (135–145 mM).[203]

In this study, a valinomycin-doped K^+-ISE membrane was used as the sensing membrane, with 20 wt % of an inert electrolyte (ETH 500) as a membrane additive. The effect of ETH 500 was evaluated by testing paper-based devices with K^+-ISE membranes without and with ETH 500 as a membrane additive. As shown in Figure 4.7, the devices without ETH 500 exhibit a non-satisfactory response slope of 48.8 mV/decade with an R^2 of 0.9759. The quality of the K^+ response curve was improved by adding 20 wt % ETH 500 into the K^+-ISE membrane, leading to a linear slope of 53.3 mV/decade with an R^2 of 0.9989. The exact reason of this effect is unknown, but it is very likely that the addition of ETH 500 improved the sensor response by reducing the resistance of the sensing membrane. After adding 20 wt % of ETH 500 into the ISE membranes, the resistance of the devices decreased from 10.9 ± 1.2 MΩ (n = 8) to 4.4 ± 0.8 MΩ (n = 21).

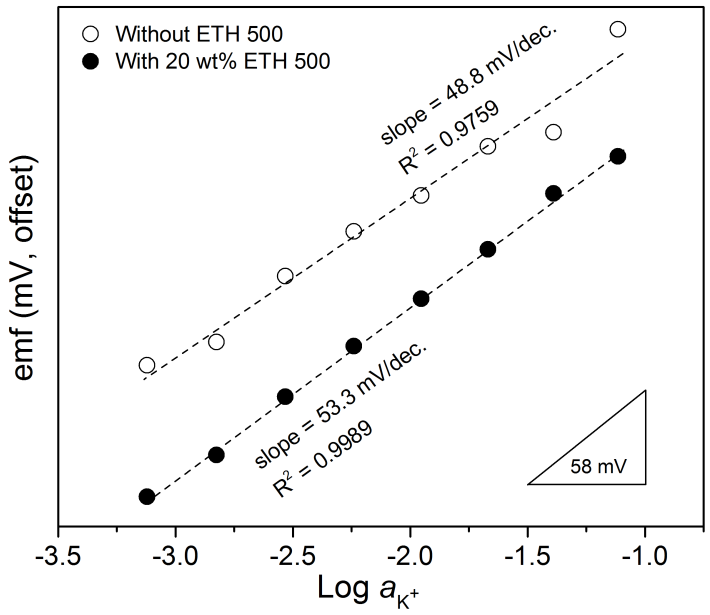

Figure 4.7 Potentiometric K^+ calibration curves of paper-based ion-sensing devices using K^+-ISE membranes without (open circle) and with (solid circle) 20 wt % ETH 500 as membrane additive. Each data point is based on one device.

The response curve of the optimized devices with samples of KCl solutions is shown in Figure 4.8a, where highly reproducible responses are obtained in a clinically relevant range from $10^{-1.0}$ to $10^{-3.1}$ M, with a linear slope of 53.3 ± 0.7 mV/decade and an E^o value of 59.6 ± 1.6 mV. Interestingly, the experimentally observed lower detection limit is $10^{-3.1}$ M, which is higher than for a conventional valinomycin-based K^+-ISE. Similar behavior was reported previously, where paper was used as a sampling tool for Ag^+ detection.[156] The reason for the different detection limit is not yet known, but it is likely that the slightly anionic surface of cellulose contributes to this behavior.[199] When a 0.1 M KCl solution was used as sample, the observed emf was –0.9 ± 1.9 mV (n = 3), matching well with the predicted value (i.e., 0 mV). Compared to devices with HHCAE

membranes, the cell resistance increases to 4.4 ± 0.8 MΩ (n = 21) with the K^+-ISE membranes, but is still sufficiently low to be compatible with low-cost voltmeters.

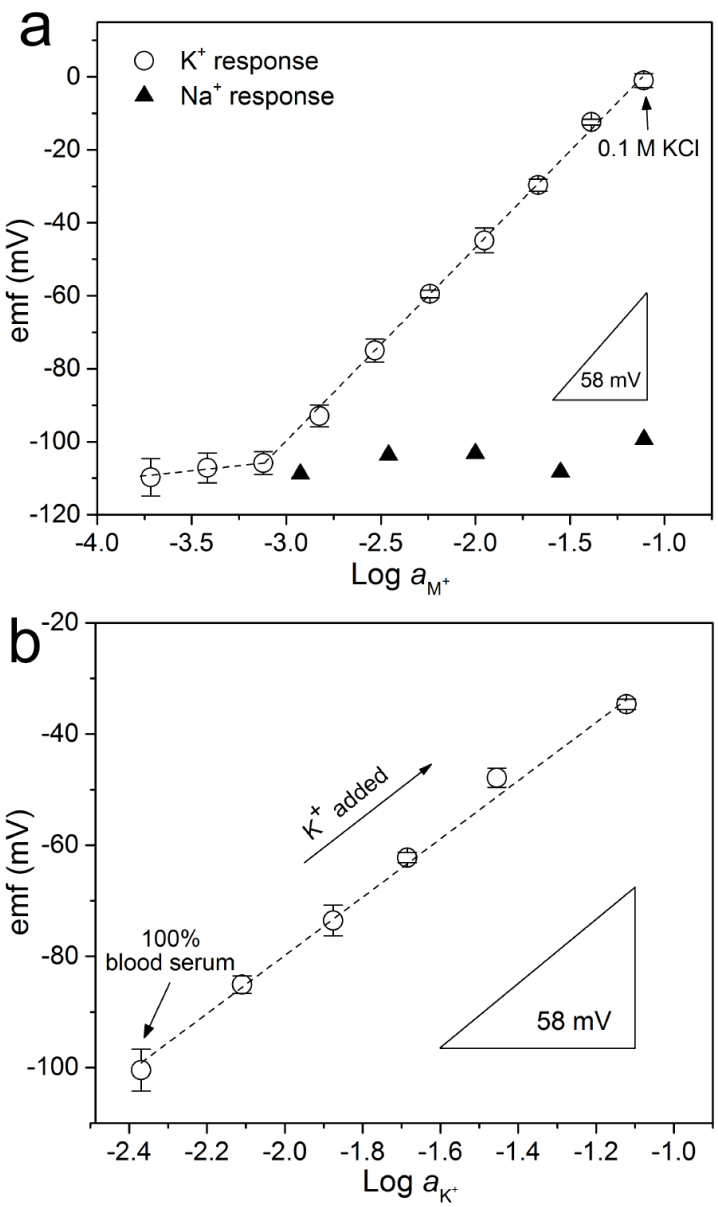

Figure 4.8 Paper-based K^+ selective sensors: (a) Response to K^+ and Na^+ (aqueous samples). (b) Response to K^+ in a background of undiluted blood serum. Each K^+ data point is from three individual devices.

The selectivity of the K^+-sensing device was evaluated by testing its response with NaCl solutions. As shown in Figure 4.8b, no significant Na^+ response is recorded even at high Na^+ concentrations (0.1 M). Finally, K^+ calibrations were performed with a series of samples of undiluted blood serum containing various K^+ concentrations with a high Na^+ background (certified as 140 mM). It can be seen in Figure 4.8b that these devices exhibit reproducible responses in undiluted blood serum with a well-retained linear slope of 53.6 ± 1.8 mV/decade and an E^o of 27.6 ± 3.2 mV, demonstrating their high sensitivity and selectivity in biological media. By using different ISE membranes, sensors for other clinically relevant ions can also be fabricated in the same way.

According to the U.S. Code of Federal Regulations, in clinical laboratories the acceptable measuring error is ± 5% for Cl^- and ±0.5 mM for K^+,[93] which corresponds to a variation in emf of approximately 1.1 mV and 2.6 mV, respectively. In this study, the obtained E^o variations of paper-based ion sensors in blood serum samples are ±1.6 mV (Cl^-) and ±3.2 mV (K^+), which are close to the requirement for calibration-free ion sensing. Improvement of the E^o reproducibility for practical uses may be achieved by detailed sensor optimization (e.g., through the selection of the ionic liquid and mass production using inkjet printing). Further improvements of the E^o reproducibility (e.g., to ±0.2 mV)[205] may be achieved with highly reproducible all-solid-state ISEs and reference electrodes coupled with robust redox buffers,[50,69,90] which are under development.

4.4 Conclusions

In conclusion, a disposable and low-cost paper-based ion-sensing platform was developed with a potentiometric cell embedded into paper. These devices are simple to

use, do not need any pretreatment ("conditioning"), and only require a low sample volume of 20 μL. They are compatible with HHCAE and ionophore-doped ISE membranes to detect clinically relevant ions in biological samples with high sensitivity and reproducibility, and could be potentially adapted to detect other charged analytes by changing the sensing membrane.

4.5 Acknowledgements

This work was supported by the University of Minnesota Initiative for Renewable Energy and the Environment. J.H. thanks the Krogh family for a Lester C. and Joan M. Krogh Fellowship.

Chapter 5

All-Solid-State Paper-Based Ion-Sensing Platform with Colloid-Imprinted Mesoporous Carbon as Solid Contact

Parts of this chapter relate to U.S. patent application (14/716564) titled "Ion-Selective Electrodes and Reference Electrodes with a Solid Contact Having Mesoporous Carbon" by Hu, J.; Stein, A.; and Bühlmann, P. filed on 26 May 2015.

Wenyang Zhao contributed to this chapter by taking the SEM images.

5.1 Introduction

Due to its abundance, low-cost and suitability for mass manufacturing, paper has recently been explored as a substrate to fabricate disposable analytical platforms for various analytes.[196,206-210] Compared to their conventional counterparts that usually rely on expensive consumables and frequent maintenance, paper-based analytical devices are more affordable and simpler to use. These features make them very attractive for clinical applications, especially in developing countries with limited resources.

Ion sensing has long been an interest in analytical chemistry, and is of vital importance in many fields such as clinical analysis, process management and environmental analysis.[1,5,7] With the growing demand for point-of-care and in-field testing applications, increased research efforts have been focused on novel miniaturized ion-sensing systems with small sample volumes, simple operation, reduced cost, and increased manufacturability. Paper is frequently used as a key component in these devices.[201]

Depending on the specific sensor design, paper provides different functions for the ion sensors reported in the literature. It is commonly used as a disposable microfluidic sampling tool to replace conventional sample holders (e.g., beakers or tubing), because paper transports fluids by capillary forces. It was reported that paper can be sandwiched between an all-solid-state ISE and a reference electrode to transport the sample solutions from other areas to the sensing electrodes.[155,156] With the addition of a complexing agent in a pretreated microfluidic paper substrate, a separation system was achieved in which the transport of interfering ions was significantly slowed down by complexation, and thus

only the target ion could reach the sensing electrodes.[211] Besides microfluidic sampling, paper can also serve as a porous matrix to mechanically support the other components of the sensor. For example, strip-type ion-sensing devices were developed with carbon nanotubes[154,158] or graphene[87] deposited onto a paper substrate as the ion-to-electron transducer, and Li^+ measurements in whole blood were demonstrated with such sensor design.[154] With an additional hydrophobic layer of sputtered gold and poly(3-octylthiophene) on top of a carbon nanotube-coated conductive paper, nanomolar detection limits for Cd^{2+}, Ag^+, and K^+ were achieved.[139] In another report, a suspension of gold nanoparticles was printed onto a paper substrate, followed by an infrared sintering process to produce gold electrodes. The electrodes were subsequently coated with the conductive polymer poly(3,4-ethylenedioxythiophene) as the solid contact to construct a flexible paper-based potentiometric ion sensor.[212] When paper was used both as a microfluidic sampling tool and a mechanical support, a three-dimensional paper-based ion sensor was developed with a conventional reusable poly(vinyl chloride) sensing membrane sandwiched between two disposable paper substrates containing sample and reference zones. With careful sensor assembly, various clinically relevant ions could be detected with aqueous sample solutions.[153]

Although many attractive features (e.g., a low detection limit and suitability for biological samples) have been demonstrated with the aforementioned state-of-the-art paper-based ion-sensing devices, these devices all require cumbersome pretreatment protocols including sensor conditioning and calibration, which may impede their practical use, especially when they are used by less skilled operators. To address this issue,

Chapter 4 introduced a conditioning-free and calibration-free paper-based ion-sensing platform that is designed for single-use operation. The device is based on a conventional potentiometric cell that is imbedded into the paper substrate, with an inner reference system composed of Ag/AgCl electrodes and KCl reference electrolytes.[213] Because of a symmetrical cell design and a precise control of each interfacial potential, the response of this paper-based ion-sensing platform can be theoretically predicted, and the device can be used to detect ion concentrations in undiluted blood serum without prior sensor calibration. The use of the Ag/AgCl/KCl inner reference system, however, complicates the measuring protocol by requiring the supply and application of a KCl reference electrolyte. Therefore, it is desirable to eliminate the KCl reference electrolyte and further simplify the sensor operation.

This chapter explores the possibility of constructing an all-solid-state paper-based ion-sensing device that only needs one droplet of sample, but does not need any sensor pretreatment (i.e., conditioning and calibration) or supply reagents (i.e., reference electrolyte). This is the ultimate goal for a robust and simple paper-based ion sensor that can provide useful measurements in real-life applications. The device described in this chapter relies on several building blocks that were discussed in the previous chapters. It contains an all-solid-state ion-selective electrode (ISE) and an all-solid-state reference electrode that are both based on colloid-imprinted mesoporous (CIM) carbon, and these two miniaturized electrodes are integrated into the paper substrate with a symmetrical cell design. Unlike the device in Chapter 4 that employs a conventional Ag/AgCl/KCl inner reference system, a redox buffer is doped into the ISE and reference membranes to

control the interfacial potentials at the CIM carbon/ISE membrane and CIM carbon/reference membrane interfaces. For this purpose, two types of redox buffers were evaluated, i.e., either the tetrakis(pentafluorophenyl)borate salts of cobalt(II/III) tris(4,4'-dinonyl-2,2'-bipyridyl) ($[Co(II/III)(C_9,C_9\text{-bipy})_3](TPFPB)_{2/3}$)[50] or 7,7,8,8,-tetracyanoquinodimethane (TCNQ) and its anion-radical derivative potassium-tetracyanoquinodimethane (KTCNQ).[52,214] As a proof of concept, an all-solid-state paper-based Cl^--sensing platform was constructed and tested with both aqueous and blood serum samples. It was found that the proposed sensor design is feasible, and the sensor performance is strongly dependent on the redox buffer doped into the sensing membranes.

5.2 Experimental

Materials. Reagents were obtained from the following sources: Fumion® FAA-3 ionomer anion exchanger from FuMA-Tech GmbH (Bietigheim-Bissingen, Germany), the ionic liquid 1-methyl-3-octylimidazolium bis(trifluoromethylsulfonyl)imide $[C_8min^+][C_1C_1N^-]$ from IoLiTec (Tuscaloosa, AL, USA), TCNQ, tetraethylammonium tetrafluoroborate ($TEABF_4$), *o*-nitrophenyl octyl ether (*o*-NPOE), high molecular weight poly(vinyl chloride) (PVC) from Sigma-Aldrich (St. Louis, MO, USA), Tecoflex SG-80A polyurethane from Thermedic Polymer Products (Woburn, MA, USA), and Autonorm™ freeze-dried blood serum from SERO (Stasjonsveien, Norway). All chemicals were used as received without further purification. Deionized water was purified to a resistivity of 18.2 MΩ/cm with a Milli-Q PLUS reagent-grade water system (Millipore, Bedford, MA, USA). CIM carbon,[69] KTCNQ,[215] and the redox couple

consisting of [Co(II)(C_9,C_9-bipy)$_3$](TPFPB)$_2$ and [Co(III)(C_9,C_9-bipy)$_3$](TPFPB)$_3$[50] were prepared as previously reported.

Precursor Solutions of Sensing Membranes and Reference Membranes. Fumion® FAA-3 ionomer anion exchanger was used as the sensing membrane and loaded with Cl^- counter ions using a previously reported procedure.[213] 150 mg of Cl^--loaded Fumion® FAA-3 ionomer was dissolved in 2 mL of methanol under magnetic stirring. Precursor solutions for reference membranes were prepared by dissolving 60 mg of the ionic liquid [C_8min^+][$C_1C_1N^-$], 120 mg of PVC as a polymeric matrix, and 120 mg of *o*-NPOE as plasticizer in 2 mL of anhydrous THF. The redox buffers containing 1.4 mmol/kg of [Co(II/III)(C_9,C_9-bipy)$_3$](TPFPB)$_{2/3}$ or 3 mmol/kg of TCNQ/KTCNQ were added into both the sensing membrane and reference membrane precursor solutions as inner reference components.

Fabrication of All-Solid-State Paper-Based Ion-Sensing Platform. Paper-based sample zones and microfluidic channels were defined by patterning polyurethane lines that penetrated the whole thickness of filter paper (Whatman Grade 589/2 white ribbon, GE Healthcare, Chicago, IL, USA) pieces. Approximately 2.5 g of polyurethane was dissolved in 40 mL of THF, and this solution was then applied to both sides of the filter paper using a glass capillary tube, forming polyurethane barriers against hydrophilic samples approximately 2 mm in width.

To form approximately 1-mm wide sensing and reference membranes, a 10 μL microcapillary was used to apply the corresponding precursor solutions onto the filter paper. Where necessary, the viscosity of the precursor solutions was adjusted by dilution

with additional aliquots of corresponding solvents for better penetration into the filter paper. To ensure full penetration of the membrane components through the entire thickness of the paper, the precursor solutions were applied to both sides of the paper twice each.

The CIM carbon-sensing membrane suspension was prepared by ultrasonicating 75 mg of CIM carbon in 1 mL of the sensing membrane precursor solution for 30 min. In a similar way, CIM carbon-reference membrane suspensions were prepared by ultrasonicating for 30 min 60 mg of CIM carbon in 1 mL of the precursor solution containing the reference membrane components. The resulting sensing and reference suspensions were then applied onto paper using a capillary to form a homogenous mixture of CIM carbon and the corresponding membranes, with an effort to maximize the contact area between this homogenous mixture and the membrane.

Electrochemical Measurements. Electrode potentials were measured with an EMF 16 high-impedance voltmeter (input impedance 10 TΩ) controlled by EMF Suite 1.03 software (Lawson Labs, Malvern, PA, USA). Two copper alligator clips were used to connect the two CIM carbon-based sensing and reference electrodes to the voltmeter. A series of samples containing different concentrations of Cl^- and K^+ was obtained by sequential dilution of a KCl solution. A series of blood serum samples with various Cl^- concentrations was prepared by adding small amounts of a 0.8 M KCl solution into tenfold diluted blood serum. Activity coefficients were calculated according to a two-parameter Debye–Hückel approximation.[177] After the samples and reference electrolytes were applied to the corresponding sensing zones, it took approximately 10 s for the

solutions to be wicked onto the sensing and reference membranes. Then, the emf response over the following 30 s was measured.

Cyclic voltammograms of TCNQ and KTCNQ were obtained at room temperature with a CHI600C potentiostat (CH Instruments, Austin, TX). A three-electrode setup was used, with a gold electrode as the working electrode, a Pt wire as the counter electrode, and a Ag wire in 10 mM $AgNO_3$/acetonitrile as a nonaqueous reference electrode. A 0.1 M $TEABF_4$ acetonitrile solution was used as a supporting electrolyte solution.

5.3 Results and Discussion

5.3.1 Design of All-Solid-State Paper-Based Ion-Sensing Platform

The all-solid-state paper-based ion-sensing platform was fabricated by integrating a CIM carbon-based ISE and a CIM carbon-based reference electrode onto the paper substrate (Figure 5.1a). CIM carbon was chosen as the solid contact material not only because it exhibits a low amount of redox-active impurities, which is desirable for constructing electrodes with high electrode-to-electrode reproducibility, but also because it is compatible with mass production techniques that can be used to fabricate paper-based sensors on a large scale (e.g., printing).[69] Both CIM carbon-based sensing and reference electrodes are contacted with the corresponding sensing and reference membranes, which are applied separately and embedded into the paper. For a demonstration, the commercial Fumion® FAA-3 ionomer films were used as an anion exchanger for Cl^- sensing, and the ionic liquid $[C_8min^+][C_1C_1N^-]$ was doped into the

reference membrane to provide a sample-independent reference potential. Similar to the paper-based device described in Chapter 4, the all-solid-state paper-based ion-sensing platform utilizes a polyurethane-based hydrophobic barrier that defines a sample zone. In this sensor design, paper serves both as a microfluidic sampling tool as well as a supportive porous matrix into which the sensing components are embedded.

To ensure single-use operation and calibration-free ion sensing, high electrode E° reproducibility with multiple devices is required.[201] This can be achieved by precisely defining each interfacial potential within the device (see Figure 5.1b). To this end, a redox buffer (i.e., $[Co(II/III)(C_9,C_9\text{-bipy})_3](TPFPB)_{2/3}$ or TCNQ/KTCNQ) was doped into both the sensing and reference membranes to control the phase boundary potentials at the CIM carbon/sensing membrane interface ($\Delta\varphi_1$) and the CIM carbon/reference membrane interface ($\Delta\varphi_4$). In addition, the interfacial potentials at the sensing membrane/sample interface ($\Delta\varphi_2$) and the sample/reference membrane interface ($\Delta\varphi_3$) were defined by the partition of the primary ion (i.e., Cl^-) and the ionic liquid (i.e., $[C_8min^+][C_1C_1N^-]$), respectively. Therefore, the only sample-dependent interfacial potential was the phase boundary potential at the sensing membrane/sample interface ($\Delta\varphi_2$), with all other interfacial potentials being sample-independent but well-defined. The measured overall electromotive force (emf) was the electrical potential difference between the two CIM carbon-based electrodes, which was the sum of all interfacial potentials within the cell (Figure 5.1c). By such a design, the correlation between the measured emf and the concentration of Cl^- can be established.

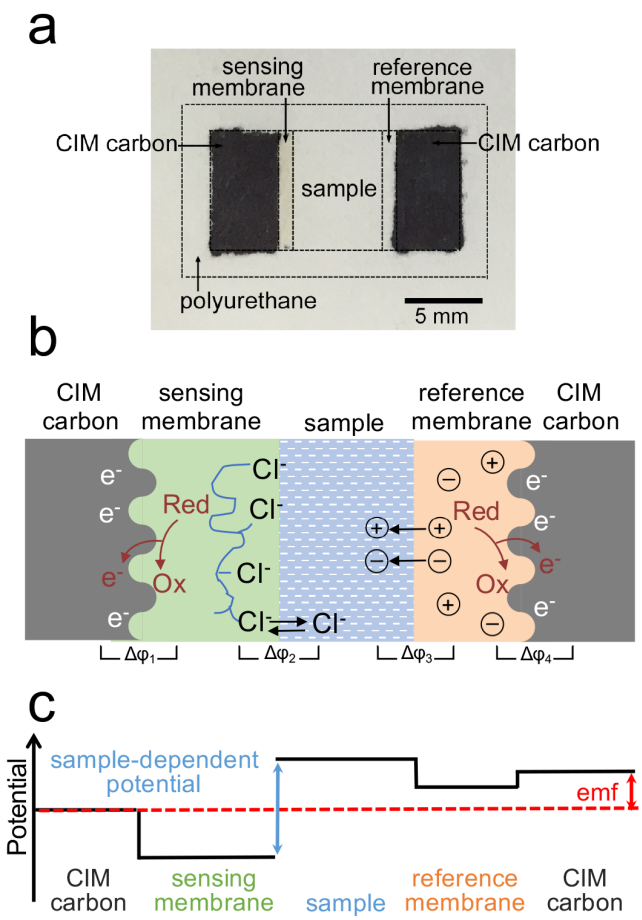

Figure 5.1 (a) Photograph of an all-solid-state paper-based ion-sensing device with a CIM carbon-based ISE, a CIM carbon-based reference electrode, and a microfluidic sample zone defined by polyurethane. (b) Schematic representation of all relevant interfaces in a paper-based Cl^- sensor with a commercial anion exchanger Fumion® FAA-3 ionomer film as the sensing membrane and an ionic liquid-doped and plasticized PVC film as reference membrane. Both membranes are doped with a redox buffer containing a redox couple, shown as "Red" and "Ox". (c) Electrical potential profile across the all-solid-state paper-based ion-sensing platform, with the only sample-dependent interfacial potential being the phase boundary potential at the sensing membrane/sample interface.

The paper-based ion-sensing platform was characterized by scanning electron microscopy (SEM) to reveal the structural features of the device. Figure 5.2a presents the non-ordered pore structure of the paper substrate made from hydrophilic cellulose fibers. The cellulose fibers can be coated and penetrated by the sensing membrane, thus creating a sensing interface between the sample and the membrane (Figure 5.2b and f). Instead of utilizing a conventional ISE coupled with an Ag/AgCl electrode and KCl reference electrolyte, the sensing membrane was contacted with a CIM carbon-based ISE on the other side (Figure 5.2c), in which the ionic signal (i.e., the ion concentration) was converted to an electronic signal (i.e., an electrical potential) through the electrical double layer at the CIM carbon/sensing membrane interface. A magnified image of the CIM-carbon based electrode shows a particle size of approximately 10 μm (Figure 5.2d), and smaller CIM carbon particles may be achieved through ball milling or probe sonication to make the device fabrication process compatible with printing as a large-scale manufacturing method. The highly porous surface of CIM carbon can be seen in the high magnification image in Figure 5.2e. When CIM carbon was mixed with the precursor solution of the sensing membrane under sonication, the sensing components could infiltrate the highly interconnected mesopores of CIM carbon to form a bicontinuous, ionically and electronically conducting structure with a large interfacial contacting area. Therefore, effective ion-to-electron transduction could be achieved. A cross-sectional view of the device is available in Figure 5.2f. It can be seen that the sensing membrane penetrated the entire thickness of the paper substrate, and a good contact was formed between the sensing membrane and the CIM carbon transduction layer.

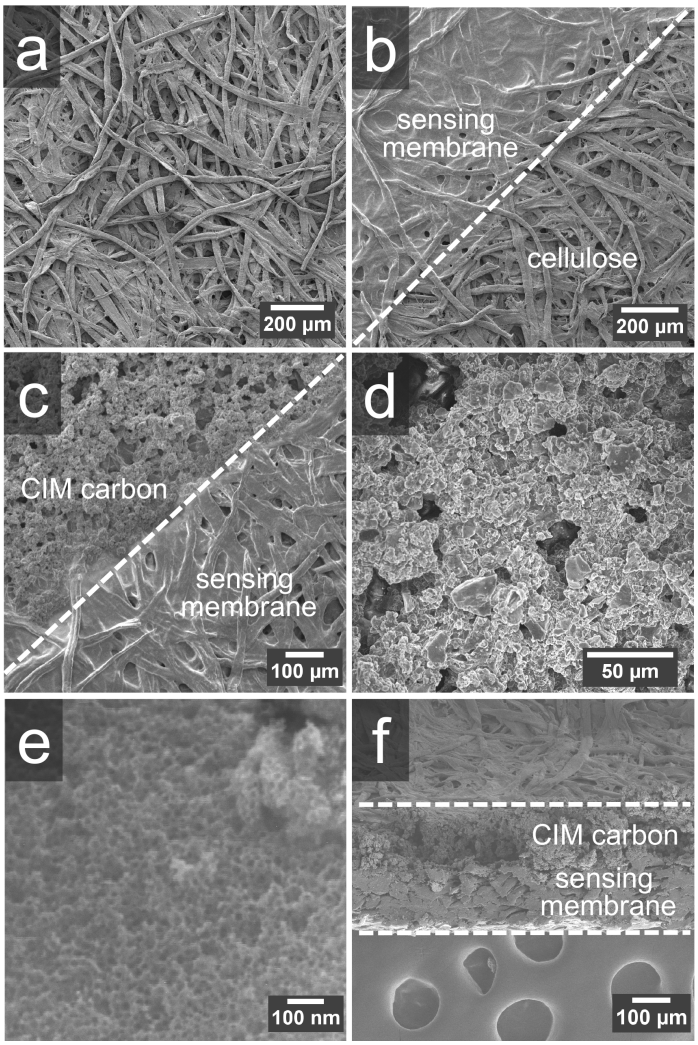

Figure 5.2 SEM images of the all-solid-state paper-based ion-sensing platform. (a) Top view of the paper substrate. (b) Top view of the device showing the interface between the sensing membrane and the sample zone. (c) Top view of the device showing the interface between CIM carbon-based sensing electrode and the sensing membrane. (d) Magnified view of the CIM carbon-based sensing electrode. (e) High magnification image of uncoated CIM carbon showing the mesopores. (f) Cross-sectional view of the all-solid-state paper-based ion-sensing platform showing the sensing membrane-infiltrated paper substrate with the CIM carbon-based sensing electrode.

5.3.2 All-Solid-State Paper-Based Ion-Sensing Platform with a [Co(II/III)(C_9,C_9-bipy)$_3$](TPFPB)$_{2/3}$ Redox Buffer

The potentiometric Cl^- response of the all-solid-state paper-based ion-sensing platform was evaluated with both aqueous KCl solutions and tenfold diluted blood serum samples containing different concentrations of Cl^-. For each measurement, 20 μL of the sample was applied to the sample zone of the device, and the potential difference between the two CIM carbon-based electrodes was measured once the sample reached the sensing and reference membranes.

When [Co(II)(C_9,C_9-bipy)$_3$](TPFPB)$_2$ and [Co(III)(C_9,C_9-bipy)$_3$](TPFPB)$_3$ were doped into the sensing and reference membranes as the redox buffer, the devices exhibited a potential drift of –0.17 ± 0.03 mV/s (n = 8) when KCl solutions were used as samples (Figure 5.3a). This potential drift is approximately one order of magnitude higher than that of the device described in Chapter 4 (i.e., –0.012 ± 0.028 mV/s, n = 8), but is relatively consistent so that meaningful data can still be extracted. Calibration curves for Cl^- were obtained by collecting the average potentials of the devices over the first 30 s of measurements. As presented in Figure 5.3b, a good Nernstian response was obtained, with a slope of –60.6 mV/decade and an R^2 value of 0.991. The observed linear range of the all-solid-state paper-based Cl^- sensor is from $10^{-1.1}$ to $10^{-3.1}$ M, with a lower detection limit of $10^{-3.14}$ M. This lower detection limit is very close to that of the device described in Chapter 4 (i.e., $10^{-3.10}$ M), and is mostly limited by the high-capacity anion exchange film used as the sensing membrane.[204,213]

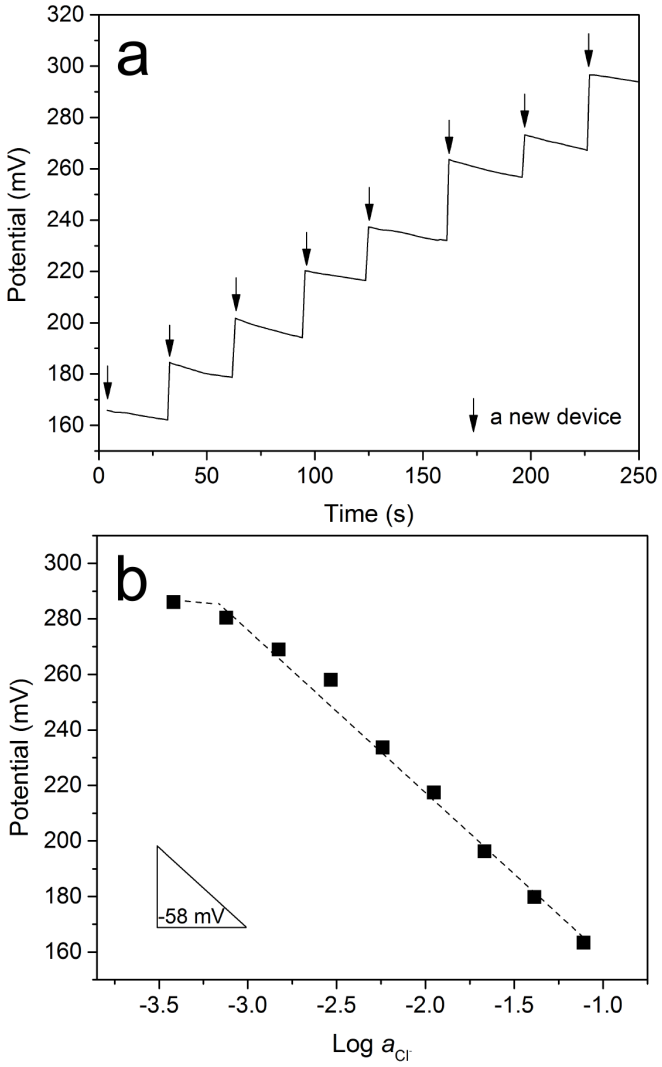

Figure 5.3 Potentiometric Cl^- responses of the all-solid-state paper-based ion-sensing platform with a redox buffer containing $[Co(II/III)(C_9,C_9\text{-bipy})_3](TPFPB)_{2/3}$. The response was obtained with KCl solutions. (a) Potential trace of the paper-based Cl^- sensors under different Cl^- concentrations, each arrow indicating a different Cl^- concentration and a new device. (b) Potentiometric Cl^- calibration curve of the paper-based Cl^- sensors. Each data point is based on one device.

To explore the suitability of the all-solid-state paper-based ion sensors for clinical applications, the response of the Cl^- sensor was also tested with tenfold diluted blood serum samples containing different concentrations of Cl^- ions (Figure 5.4). The potential drift of the device is –0.034 ± 0.075 mV/s (n = 10), with a much larger device-to-device variation as compared to the drift observed with KCl solutions. The corresponding calibration curve is depicted in Figure 5.4b, in which the recorded data deviates significantly from the mathematical linear fit. Based on linear regression, the response slope is –59.9 mV/decade, but the R^2 value of 0.628 is low.

The poor performance of the all-solid-state paper-based ion sensors with biological samples is not surprising, though. It is known that the redox buffer $[Co(II/III)(C_9,C_9\text{-bipy})_3](TPFPB)_{2/3}$ can leach from the hydrophobic sensing membrane into hydrophilic sample solutions, thus leading to large potential drifts and decreased electrode-to-electrode E° reproducibility.[50] Compared to aqueous KCl solutions, blood serum samples are more lipophilic, which accelerates the loss of redox buffer out of the sensing membrane into the sample. This can possibly explain the loss of good response linearity when switching from KCl solutions to biological samples, even though the measuring period was only about 1 min.

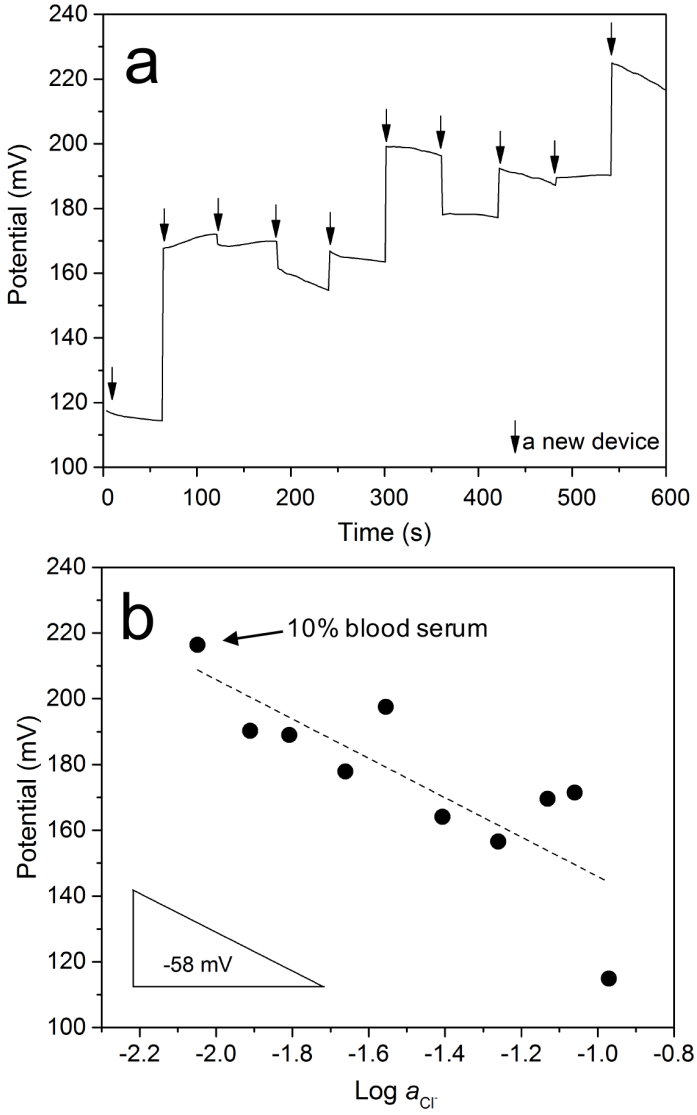

Figure 5.4 Potentiometric Cl^- responses of all-solid-state paper-based ion-sensing platform with a redox buffer containing $[Co(II/III)(C_9,C_9\text{-bipy})_3](TPFPB)_{2/3}$. The response was obtained with tenfold diluted blood serum solutions. (a) Potential trace of the paper-based Cl^- sensors under different Cl^- concentrations, each arrow indicating a different Cl^- concentration and a new device. (b) Potentiometric Cl^- calibration curve of the paper-based Cl^- sensors. Each data point is based on one device.

5.3.2 All-Solid-State Paper-Based Ion-Sensing Platform with a TCNQ/KTCNQ Redox Buffer

Besides [Co(II/III)(C_9,C_9-bipy)$_3$](TPFPB)$_{2/3}$, a redox couple consisting of TCNQ and its ion-radical salt KTCNQ was also evaluated as a redox buffer. TCNQ has long been of interest in molecular electronics due to its exceptional ability to accept electrons to form simple and stable charge-transfer complexes and ion-radical salts.[215-220] TCNQ ion-radical salts were used in potentiometric ion sensors as early as in the 1970s, where they were employed as solid-state ion-selective membranes based on the selective distribution of the primary ion (e.g., Ag^+) between the sample solution and the TCNQ ion-radical salts (e.g., AgTCNQ).[51]

Recent publications by Paczosa-Bator et al. report outstanding electrochemical performance of all-solid-state ISEs based on TCNQ, NaTCNQ, or a mixture of the two.[52,214] When TCNQ was used as the ion-to-electron transducer between a glassy carbon electrode and a K^+-ISE membrane, high electrode E° reproducibility was achieved with a standard deviation of E° as low as 1.4 mV.[52] In follow-up work, TCNQ and NaTCNQ were mixed with various carbon nanomaterials (i.e., graphene, carbon nanotubes, ordered mesoporous carbon CMK-3, and carbon black) with a 1:1:1 weight ratio to serve as the solid contact. The resulting all-solid-state ISEs all exhibited good electrode E° reproducibility with a standard deviation of E° less than 4.0 mV. The reported potential stability is remarkable as well, with a drift less than 10 μV/h over a measuring period of 72 h.[214] It should be noted that in these two papers, a high E° reproducibility was observed after the electrodes had been conditioned in aqueous

solutions for 24 h. This is very different from the all-solid-state K^+-ISEs based on the [Co(II/III)(C_9,C_9-bipy)$_3$](TPFPB)$_{2/3}$ redox buffer, which exhibited significantly decreased E° reproducibility upon electrode conditioning due to the loss of the redox buffer (i.e., standard deviation of E° increased from 0.7 mV after 1 h of conditioning to 16.3 mV after 24 h of electrode conditioning).[50] Therefore according to the reported data, TCNQ and its ion-radical salt may not suffer as much from the leaching problem as the [Co(II/III)(C_9,C_9-bipy)$_3$](TPFPB)$_{2/3}$ redox buffer does, and appear to be an effective redox buffer pair.

To evaluate the suitability of TCNQ/$TCNQ^-$ as a redox buffer, cyclic voltammograms for TCNQ and KTCNQ were collected. TCNQ is known to exhibit two reversible one-electron redox processes, in which TCNQ is first reduced to $TCNQ^{\cdot -}$ and then further reduced to $TCNQ^{2-}$.[221,222] As shown in Figure 5.5, two pairs of well-defined redox peaks are observed with a peak separation of 59 mV and 63 mV, indicating fast and reversible electron transfer. The calculated standard potentials (i.e., the midpoint potential, (E_{pa} + E_{pc})/2) are –248 mV and –786 mV (vs. Ag/Ag^+) for the $TCNQ^{\circ/\cdot -}$ and $TCNQ^{\cdot -/2-}$ redox processes, respectively. The potential separation of these two processes is 538 mV, which matches well with the literature value (i.e., 550 mV).[222] Since the observed standard potential of the $TCNQ^{\circ/\cdot -}$ redox process is close to 0 V, both the oxidized and reduced species within the redox couple are expected to be stable. Therefore, the TCNQ/KTCNQ couple can be considered a good candidate to prepare a redox buffer because of its fast and reversible electron transfer process, as well as its chemical and electrochemical stability.

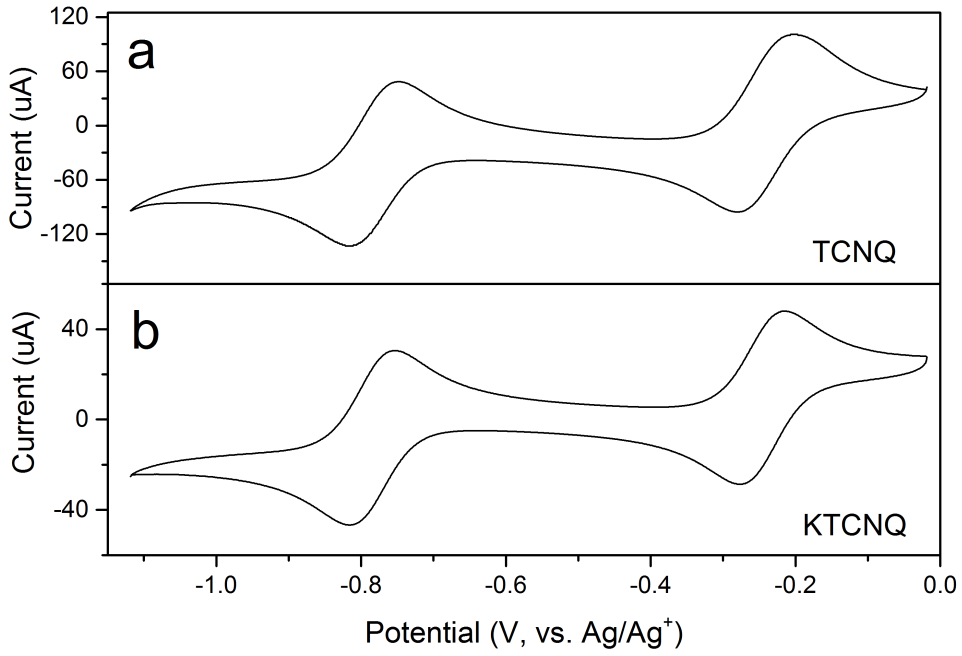

Figure 5.5 Cyclic voltammograms for 1 mM TCNQ (top) and 0.5 mM KTCNQ (bottom) dissolved in acetonitrile solutions containing 0.1 M $TEABF_4$ as a supporting electrolyte. Scan rate = 100 mV/s.

To further evaluate the effectiveness of E° control of the TCNQ/KTCNQ redox buffer in potentiometric ion sensing, 3 mmol/kg of TCNQ and KTCNQ with 1:1 molar ratio were doped into the sensing membrane to construct CIM carbon-based all-solid-state bulk ISEs. The electrodes contained CIM carbon films sandwiched between gold electrodes and hydrophilic high-capacity anion exchanger sensing membrane that were doped with TCNQ/KTCNQ (the same electrode configuration as in Figure 2.3). To study the effect of electrode conditioning on the E° reproducibility, Cl^- calibrations were performed both without conditioning and after conditioning the electrodes in a 1 mM KCl solution for 24 h.

When the electrodes were tested with aqueous KCl solutions without conditioning (Figure 5.6a), a linear response was obtained with a close to Nernstian slope of –53.9 ± 1.2 mV/decade and a fairly reproducible E° of –47.0 ± 4.3 mV (n = 5). This E° reproducibility is in good agreement with literature, where TCNQ/NaTCNQ was used with other nanostructured carbon materials to construct all-solid-state ISEs (i.e., standard deviation of E°: 2.4 mV for graphene, 3.7 mV for carbon nanotubes, 3.2 mV for carbon black, and 3.2 mV for ordered mesoporous carbon CMK-3).[214] After conditioning the electrodes for 24 h, however, larger electrode-to-electrode variations were observed, with the standard deviation of E° increasing to 14.0 mV (Figure 5.6b). This behavior differs from the high electrode reproducibility reported by Paczosa-Bator et al.,[214] but is very similar to that of all-solid-state K^+-ISEs based on the $[Co(II/III)(C_9,C_9\text{-bipy})_3](TPFPB)_{2/3}$ redox buffer, whose standard deviation of E° increased from 0.7 to 16.3 mV after conditioning the electrodes in an aqueous solution for additional 23 h.[50]

The all-solid-state ISEs with the TCNQ/KTCNQ redox buffer were also tested with tenfold diluted blood serum samples. It can be seen from Figure 5.6c and 5.6d that after 24 h of electrode conditioning, the sub-Nernstian slope improved from –39.4 ± 3.4 mV/decade to –53.8 ± 1.0 mV/decade, but was accompanied by a significantly decreased E° reproducibility from –33.8 ± 4.4 mV to 10.4 ± 19.0 mV (n = 6). It is therefore concluded that TCNQ/KTCNQ may be used as a redox buffer for single-use devices but with a large ISE measuring error of approximately 4 mV, and decreased electrode-to-electrode E° reproducibility can be expected when the device is used for long-term measurements, most likely due to the leaching of TCNQ/KTCNQ into the sample.

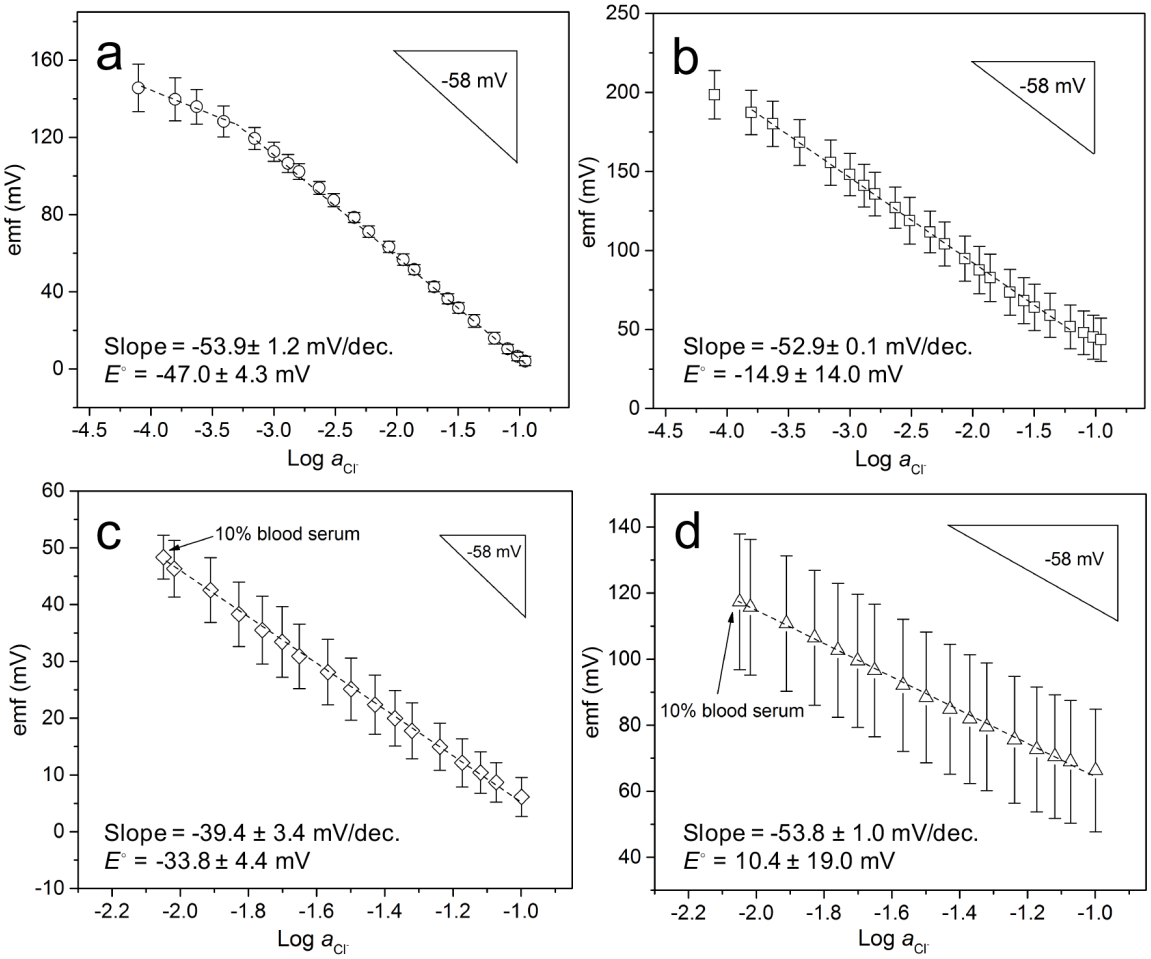

Figure 5.6 Potentiometric Cl^- calibration curves of CIM carbon-based all-solid-state bulk electrodes with a TCNQ/KTCNQ redox buffer doped in the sensing membrane. (a) Response to KCl solutions without electrode conditioning. (b) Response to KCl solutions after conditioning the electrodes in a 1 mM KCl solution for 24 h. (c) Response to tenfold diluted blood serum samples without electrode conditioning. (d) Response to tenfold diluted blood serum samples after conditioning the electrodes in a 1 mM KCl solution for 24 h. n = 5 for electrodes tested with KCl aqueous solutions and n = 6 for electrodes tested with blood serum samples.

The TCNQ/KTCNQ couple was also used to dope the sensing and reference membranes of the all-solid-state, paper-based ion-sensing platform, and the performance of the resulting device is shown in Figure 5.7. Compared to the device with $[Co(II/III)(C_9,C_9\text{-bipy})_3](TPFPB)_{2/3}$ redox buffer, a similar Nernstian response was acquired with a slope of –63.6 mV/decade in KCl solutions, but with decreased linearity ($R^2 = 0.984$). When the devices were tested with tenfold diluted blood serum samples, the Nernstian response appears to be preserved, but with a lower R^2 value of 0.856. Therefore, TCNQ/KTCNQ is not a satisfactory redox buffer for this application, and a more robust redox buffer is still needed to improve the measuring accuracy of the all-solid-state paper-based ion sensors.

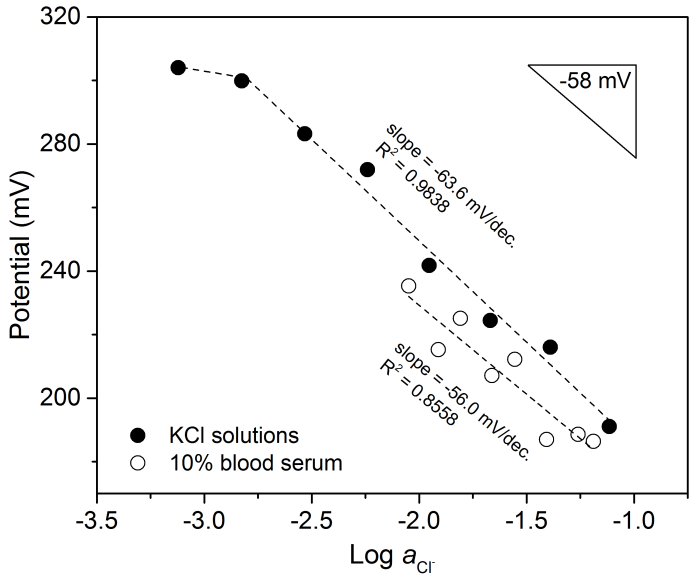

Figure 5.7 Potentiometric Cl^- responses of all-solid-state paper-based ion-sensing platform with a TCNQ/KTCNQ redox buffer doped in the sensing and reference membranes. The response was measured with KCl solutions (solid circle) and tenfold diluted blood serum samples (open circle). Each data point is based on one device.

5.4 Conclusions

This chapter explores the possibility of constructing a pretreatment-free all-solid-state paper-based ion-sensing platform that is based on a CIM carbon solid contact and a redox buffer. The transduction mechanism of the sensor, in which each interfacial potential was well defined, was discussed in detail, and proof-of-concept ion sensors were constructed with two types of redox buffers $[Co(II/III)(C_9,C_9\text{-bipy})_3](TPFPB)_{2/3}$ and TCNQ/KTCNQ. While the feasibility of the sensor design was demonstrated with aqueous KCl solutions, the sensor performance relies strongly on the redox buffer used in the system, and a more robust redox buffer system is required for this all-solid-state paper-based ion sensor to function in real-life applications. It appears that the leaching of the redox buffer is still a key problem, even for devices like this that are designed for single use. Therefore, covalent attachment of the redox buffer to the sensing membrane or CIM carbon will be a promising solution. Once such covalent attachment is successfully implemented, this sensor design should be revisited to pursue robust all-solid-state paper-based ion-sensing platforms that can be eventually commercialized and used with real-life samples.

5.5 Acknowledgements

This work was supported by the University of Minnesota Initiative for Renewable Energy and the Environment, as well as Medtronic PLC through an industrial fellow program enabled by the Industrial Partnership for Research in Interfacial and Materials Engineering (IPRIME). J.H. thanks the Krogh family for a Lester C. and Joan M. Krogh Fellowship, and Carl Schu for valuable discussions.

5.6 Appendix

Several additional experiments were performed for the development of all-solid-state paper-based ion-sensing platforms described in this chapter, and the results are presented in this Appendix.

Pre-conditioning Devices in a Humid Environment. To improve the potential stability of the all-solid-state paper-based ion-sensing platforms, the paper-based devices were pre-conditioned by exposing them to a humid environment for 30 h prior to measurement. It was hypothesized that the relatively large potential drift observed in Figure 5.3 was related to the water uptake process of the dry sensing and reference membranes once they were in contact with aqueous samples, and a pre-conditioning process under humidity could pre-saturate the sensing and reference membranes with water, thus eliminating the large potential drift during the actual measurement.

The devices were pre-conditioned in a closed desiccator that was filled with water at the bottom for 30 h. After the pre-conditioning, Cl^- responses were collected with aqueous KCl solutions and the results are shown in Figure 5.8. Compared to the potential response in Figure 5.3, the pre-conditioned devices appear to exhibit a more stable potential output, as presented in Figure 5.8a. The Cl^- response curve, however, is meaningless with a slope of –23.1 mV/decade and an R^2 value of 0.193 (Figure 5.8b). It is very likely that the redox buffer doped in the sensing and reference membranes leached out into the wetted sample zones during the pre-conditioning process, thus leading to the loss of Nernstian response of the devices.

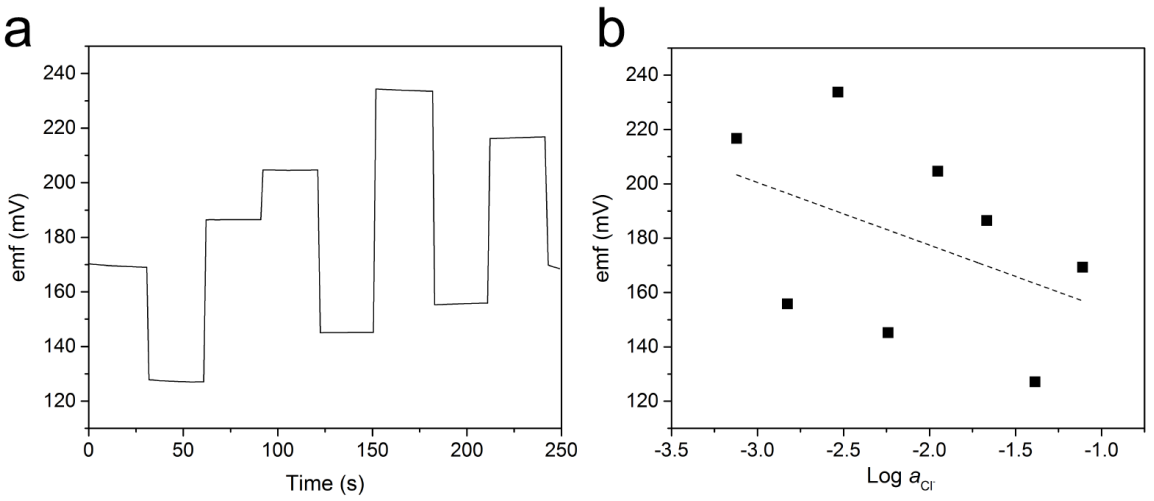

Figure 5.8 Potentiometric Cl^- responses of an all-solid-state paper-based ion-sensing platform with a redox buffer containing $[Co(II/III)(C_9,C_9\text{-bipy})_3](TPFPB)_{2/3}$. The devices were pre-conditioned under humidity for 30 h, and the response was obtained with aqueous KCl solutions. (a) Potential trace of paper-based Cl^- sensors under different Cl^- concentrations. (b) Potentiometric Cl^- calibration curve of the paper-based Cl^- sensors. Each data point is based on one device.

Hybrid Devices with a $[Co(II/III)(C_9,C_9\text{-bipy})_3](TPFPB)_{2/3}$ Redox Buffer. To better understand the behavior of the all-solid-state paper-based ion-sensing platform in blood serum samples, hybrid devices that comprise either an all-solid-state ISE with a conventional reference electrode, or a conventional ISE with an all-solid-state reference electrode were constructed and tested. Herein the conventional ISE or reference electrode refers to a stencil-printed Ag/AgCl electrode with 0.1 M KCl reference solution, coupled with an ISE or reference membrane. Based on the results reported in Chapter 4, it was assumed that the conventional ISE and reference electrode exhibit good response in blood serum samples.

The responses of the hybrid devices were obtained with 10-fold diluted blood serum samples, and the corresponding calibration curves are presented in Figure 5.9. It can be seen that the hybrid device with a CIM carbon-based all-solid-state ISE and a conventional reference electrode exhibits a response slope of –67.1 mV/decade (R^2 = 0.917), whereas the device containing a conventional ISE and a CIM carbon-based all-solid-state reference electrode has a response slope of –33.9 mV/decade and an R^2 value of 0.889. The results show that diluted blood serum samples affect both the all-solid-state ISE and reference electrode, and the observed effect is higher on the reference electrode side than the ISE side.

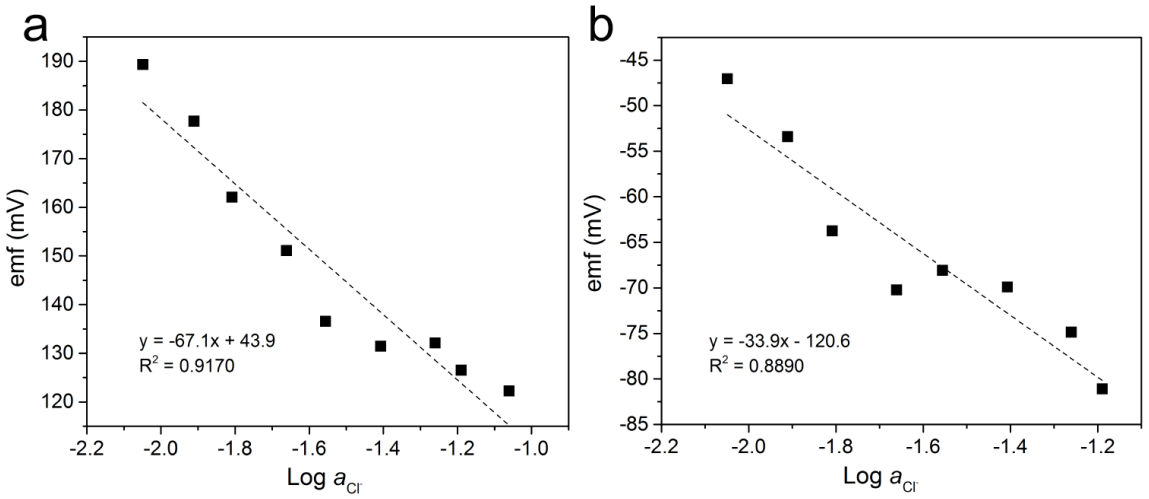

Figure 5.9 Potentiometric Cl^- responses of hybrid ion-sensing devices with a redox buffer containing $[Co(II/III)(C_9,C_9\text{-bipy})_3](TPFPB)_{2/3}$. The responses were measured with 10-fold diluted blood serum samples. (a) Device with a CIM carbon-based all-solid-state ISE and a conventional reference electrode. (b) Device with a conventional ISE and a CIM carbon-based all-solid-state reference electrode.

Devices with $[Co(II/III)(C_9,C_9\text{-bipy})_3](TPFPB)_{2/3}$ Redox Buffer Not Contacting Samples. As it was hypothesized that the leaching of the redox buffer caused the loss of good linearity of the all-solid-state ion sensors in diluted blood serum samples, devices were constructed in a way to avoid the direct contact between the redox buffer and the sample, thus possibly eliminating the problem of leaching. Herein, the redox buffer $[Co(II/III)(C_9,C_9\text{-bipy})_3](TPFPB)_{2/3}$ was doped into the sensing/reference membranes that were mixed with CIM carbon to construct the all-solid-state ISE/reference electrodes, but it was not doped into the sensing/reference membranes that contact samples.

When the new devices were tested with aqueous KCl solutions, a super-Nernstian response was obtained with a slope of –65.8 mV/decade and an R^2 value of 0.956 (Figure 5.10). The response is inferior compared to the devices with the redox buffer contacting samples (i.e., slope of –60.6 mV/decade and an R^2 value of 0.991, as shown in Figure 5.3). Similar results were observed with 10-fold diluted blood serum samples, in which a sub-Nernstian response was obtained with a slope of –48.1 mV/decade and an R^2 value of 0.709 (Figure 5.10). It can be concluded that the avoidance of the contact between redox buffer and sample did not improve the linearity and reproducibility of the sensor in diluted blood serum samples. It is likely that by using such sensor design, an uncontrolled interface between the redox-buffer-doped and non-redox-buffer-doped membranes was introduced into the system, thus affecting the reproducibility of the sensor.

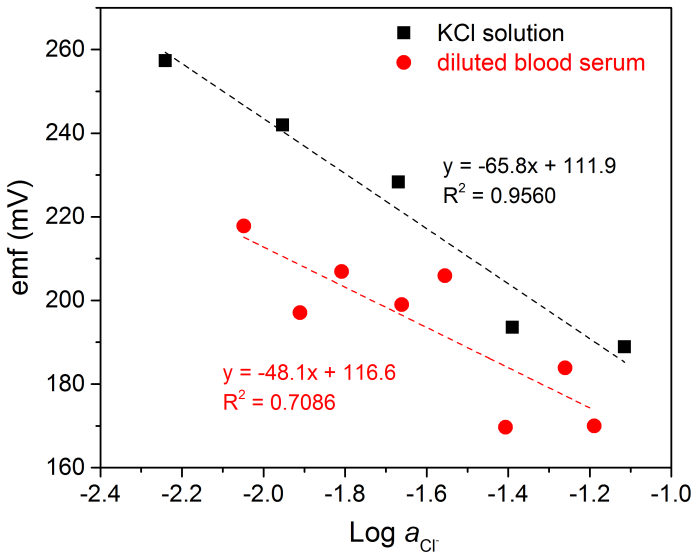

Figure 5.10 Potentiometric Cl^- responses of an all-solid-state, paper-based ion-sensing platform with the redox buffer $[Co(II/III)(C_9,C_9\text{-bipy})_3](TPFPB)_{2/3}$. The redox buffer was doped into the sensing/reference membranes that were mixed with CIM carbon to construct the all-solid-state ISE/reference electrodes, but was not doped into the sensing/reference membranes that contact the samples. The responses were collected both with aqueous KCl solutions (black square) and 10-fold diluted blood serum samples (red circle).

Chapter 6

Redox Buffers Covalently Attached to Colloid-Imprinted Mesoporous Carbon

Parts of this chapter relate to U.S. patent application (15/655457) entitled "Electrochemical Sensors with a Chemically Attached Molecular Redox Buffer" by Hu, J.; Stein, A.; Bühlmann, P.; and Zhen, V. X. filed on 20 July 2017.

Xue Zhen contributed to this chapter by providing valuable suggestions on experimental procedures and data interpretation.

6.1 Introduction

Driven by the growing demand for point-of-care and onsite measuring applications, modern chemical sensor research has focused on the development of new materials and methodologies that enable robust sensors with less maintenance and simple measuring protocols.[7,201,223] Ion-selective electrodes (ISEs) represent a large subgroup of chemical sensors that are routinely used in various fields, such as process management and clinical analysis. Over the past 40 years, ISEs have evolved into well-established analytical tools, with sensors for more than 60 different analytes.[1,5,30] However, conventional ISEs have to be recalibrated frequently, which requires calibrating solutions and either automated mechanisms or trained personnel to perform the calibration protocols. Therefore, the elimination of sensor calibration can significantly simplify the use of ISEs and open up opportunities for new applications, such as single-use ion sensors.

There are two key parameters to construct an ISE calibration curve: the slope and the intercept (i.e., electrode standard potential, or E°). The variation in the calibration slope depends on the robustness of the ISE sensing membrane and is generally negligible. Thus, the reason for frequent electrode recalibration usually lies in the unacceptable repeatability of the electrode E° values. Since there is no E° control mechanism for conventional ISEs, the E° can be quite different (as large as 10 mV) for multiple ISEs even though they are fabricated in a same way. Also, the E° of an individual electrode can drift significantly in an unpredictable way, which can lead to large measuring errors if the electrode is not recalibrated prior to measurements. Therefore, to claim calibration-free

ion-sensing operations, the electrode E° must be well-controlled in such a way that the device-to-device reproducibility is maintained during the entire life time of the sensor. Different applications require different measurement accuracies. For example, an accuracy of ±0.05 pH unit is typically acceptable for a pH electrode used in industrial process, which corresponds to an ISE response of approximately ±2.9 mV. Clinical applications usually require higher measurement accuracy. According to the U.S. Code of Federal Regulations, in clinical laboratories the acceptable measuring errors for K^+ and Na^+ are ± 0.5 mM and ± 4 mM, respectively.[93] This leads to an acceptable error of approximately 2.8 mV for a K^+-ISE and 0.7 mV for a Na^+-ISE. Therefore, no Na^+ calibration would be needed in clinical laboratories if for multiple Na^+-ISEs the E° variation is smaller than 0.7 mV during the entire life time of the sensor. A type of electrode with such E° reproducibility can be referred to as calibration-free.

The introduction of all-solid-state ISEs opens up great opportunities for the development of calibration-free ion sensors because of the possibility of fine-tuning the properties of the solid contact materials.[201] All-solid-state ISEs with high device-to-device reproducibility have become a major target in the field, with many approaches reported to control the electrode E° as discussed in Section 1.2.1 in Chapter 1. These approaches include tuning the oxidation states of conductive polymers,[100-102] utilizing intercalation compounds with well-defined redox potentials,[47,54] and introducing redox buffers as membrane additives.[49,50,53,214] Among them, the redox buffer approach is the most promising method because of its ability to precisely control the electrode E° by tuning the composition of the redox buffer. A well-defined redox buffer contains both the

oxidized and reduced species of a redox couple. Similar to a pH buffer whose pH can be controlled by an acid and its conjugate base, the electrical potential of a redox buffer is determined by its standard redox potential and the ratio of the oxidized and reduced species of the redox couple, which can be predicted by the Nernst equation[103]:

$$E = E^{\circ'} + \frac{RT}{n\mathrm{F}} \ln \frac{a_{\mathrm{ox}}}{a_{\mathrm{red}}} \tag{6.1}$$

where E is the electrical potential of the redox buffer, $E^{\circ'}$ is the standard reduction potential of the redox couple, R is the ideal gas constant, F is the Faraday constant, T is the temperature, n is the number of moles of electrons transferred in the redox reaction, and a_{ox} and a_{red} are the activities of the oxidized and reduced species of the redox couple, respectively.

When a well-defined redox buffer is doped in the sensing membrane, the interfacial potential at the solid contact/ISE membrane interface can be controlled and stabilized. This was previously demonstrated with redox buffers consisting of cobalt(II/II) tris(1,10-phenanthroline) or of the more hydrophobic cobalt(II/III) tris(4,4'-dinonyl-2,2'-bipyridyl) complexes. Results showed that the electrode E° values correlated well with the ratios of Co(II) and Co(III) species as predicted by the Nernst equation, and were highly reproducible with a standard deviation less than 1 mV.[49,50] When the redox buffer containing the cobalt(II/III) tris(4,4'-dinonyl-2,2'-bipyridyl) complex was combined with colloid-imprinted mesoporous (CIM) carbon as the solid contact, all-solid-state ISEs could be fabricated with an initial E° standard deviation as low as 0.7 mV.[69] The redox buffer, however, leached out of the ISE membrane during the measurement, thus causing large potential drifts and reduced E° reproducibility over time.

After conditioning the electrodes in an aqueous solution for 24 h, the standard deviation of electrode E° increased from 0.7 mV to 16.3 mV for an all-solid-state ISE based on the cobalt(II/III) tris(4,4'-dinonyl-2,2'-bipyridyl) redox buffer.[50] Therefore, to construct robust calibration-free all-solid-state ISEs with a meaningful life time, the redox buffer must be immobilized within the sensor to ensure high electrode E° reproducibility as well as stability.

To address this issue, this chapter explores the possibility of covalently attaching a redox buffer to the surface of CIM carbon to develop CIM carbon-based redox buffer. CIM carbon is an ideal substrate to anchor redox buffer, not only because its highly accessible surface with a large specific surface area onto which the redox buffer can be attached, but also because it contains low amounts of redox-active impurities that can act as redox interferences.[69] Surface modification was performed to immobilize anchoring points to the surface of CIM carbon, and cobalt-based complexes were then attached through click chemistry (copper(I)-catalyzed azide-alkyne cycloaddition) or amide coupling reactions. Each step of the modification was characterized using surface analysis techniques. It was found that a cobalt-based redox buffer can be attached to CIM carbon with a relatively low surface loading of 0.1 atom%, and the open circuit potential of CIM carbon films can be affected by the oxidation states of the attached redox buffer. To achieve robust all-solid-state ISEs with highly reproducible electrode E° values, however, a higher surface loading of the redox buffer is required. Possible approaches of achieving such high surface loading are discussed in Section 7.2.

6.2 Experimental

Materials. Reagents were obtained from the following sources: Teflon dispersion (60 wt% in H_2O), ethynylferrocene, ferrocenecarboxylic acid, sodium ascorbate, 4-nitrobenzene diazonium tetrafluoroborate, disodium sulfide, *N*-(3-dimethylaminopropyl)-*N*'-ethylcarbodiimide hydrochloride (EDC·HCl), 1-hydroxybenzotriazole (HOBt), *N*,*N*-diisopropylethylamine (DIPEA), tetraethylammonium tetrafluoroborate ($TEABF_4$), tetrabutylammonium perchlorate ($TBAClO_4$), *o*-nitrophenyl octyl ether (*o*-NPOE), high molecular weight poly(vinyl chloride) (PVC), valinomycin, potassium tetrakis(4-chlorophenyl)borate, potassium hexafluorophosphate (KPF_6) from Sigma-Aldrich (St. Louis, MO, USA), 5-ethynyl-2,2′-bipyridine from Ark Pharm (Arlington Heights, IL, USA), 5-carboxy-2,2'-bipyridine from Enamine (Monmouth Junction, NJ, USA), 4-(4,6-dimethoxy-1,3,5-triazin-2-yl)-4-methylmorpholinium chloride (DMTMM), tris(benzyltriazolylmethyl)amine, tetrakis(4-carboxyphenyl)porphyrin (TCPP) from TCI Chemicals (Tokyo, Japan), lithium tetrakis(pentafluorophenyl)borate ethyl etherate (LiTPFPB) from Gelest (Morrisville, PA, USA) and cobalt(II) tetrakis(4-carboxyphenyl)porphyrin (Co(II)TCPP) from Porphychem (Dijon, France). All chemicals were used as received without further purification. Deionized water was purified to a resistivity of 18.2 MΩ/cm with a Milli-Q PLUS reagent-grade water system (Millipore, Bedford, MA, USA). CIM carbon,[69] 4-azidobenezene diazonium tetrafluoroborate,[224] and cobalt(III) tetrakis(4-carboxyphenyl)porphyrin chloride (Co(III)TCPP)[225] were prepared according to previously reported procedures.

Preparation of CIM Carbon Film. CIM carbon powder was combined with 5

wt% Teflon binder and pressed under a roller press to form a film of ~100–200 μm thickness. The film was then cut into individual electrodes using a 7/32 inch punch, and dried at 110 ˚C under vacuum overnight.

Synthesis of Cobalt Bipyridine Complexes. The cobalt(II) tris(5-ethynyl-2,2'-bipyridine) complex was synthesized by dissolving 11 mg of $CoCl_2 \cdot 6H_2O$ and 25 mg of 5-ethynyl-2,2'-bipyridine in 3 mL of methanol. The solution was heated at 70 ˚C for 2 h to form the complex. After the solution was cooled down, 80 mg of LiTPFPB was added into the solution to form a precipitate. The precipitate was filtered, washed with hexanes, and redissolved in methanol. The cobalt(II) tris(5-ethynyl-2,2'-bipyridine) complex was obtained by evaporating methanol under vacuum.

The cobalt(II) tris(5-carboxy-2,2'-bipyridine) complex was synthesized by dissolving 24 mg of $CoCl_2 \cdot 6H_2O$ and 60 mg of 5-carboxy-2,2'-bipyridine in 5 mL of methanol. The obtained solution was heated at 50 ˚C for 2 h to form the complex. The solution was then evaporated to obtain the cobalt(II) tris(5-carboxy-2,2'-bipyridine) complex.

The cobalt(II) tris(2,2'-bipyridine) complex was synthesized by dissolving 200 mg of $CoCl_2 \cdot 6H_2O$ and 400 mg of 2,2'-bipyridine in 10 mL of water. The solution was heated at 50 ˚C for 2 h. Then, 323 mg of KPF_6 was added into the solution to obtain a precipitate. The precipitate was filtered out, washed with water, and dried under vacuum. The cobalt(III) tris(2,2'-bipyridine) complex was synthesized by dissolving 500 mg of $CoSO_4 \cdot 7H_2O$ and 920 mg of 2,2'-bipyridine in 25 mL of water. 30% H_2O_2 was added dropwise into the above solution under stirring until all the cobalt (II) was oxidized to

cobalt (III) (confirmed by the disappearance of paramagnetic broad peaks higher than 10 ppm in proton nuclear magnetic resonance spectroscopy, or proton NMR). 985 mg of KPF_6 was then added into the mixture to obtain a precipitate. The precipitate was filtered out, washed with water, and dried under vacuum.

Covalent Attachment of Redox-Active Molecules on CIM Carbon through Click Chemistry. An electrolyte was prepared in an ice bath by dissolving 1 mM 4-azidobenzene diazonium tetrafluoroborate and 0.1 M supporting electrolyte $TEABF_4$ in acetonitrile. CIM carbon films were presoaked in the electrolyte for 1 h to ensure the electrolytes could diffuse into the mesopores, and bubbles were observed on the CIM carbon surface, indicating good electrolyte wetting. After presoaking, CIM carbon film was put on top of a gold electrode and mechanically held there using an electrode body.

To modify the CIM carbon with $–N_3$ surface functional groups, a potential scan of 0.2 V to -0.6 V (vs Ag/Ag^+ with 10 mM Ag^+) was applied to the CIM carbon film with a scan rate of 25 mV/s for 5 cycles. N_3-modified CIM carbon films were washed with acetonitrile and soaked in acetonitrile on a shaker overnight to remove physically absorbed unreacted diazonium salts. The click reaction was conducted by soaking azide-modified CIM carbon film overnight on a shaker in a dimethyl sulfoxide/water solution containing 1 mM of ethynylferrocene or cobalt(II) tris(5-ethynyl-2,2'-bipyridine) complex, 1 mM of copper sulfate, 10 mM of sodium ascorbate (to reduce Cu(II) to Cu(I) catalyst), and 1 mM of tris(benzyltriazolylmethyl)amine as the Cu(I) stabilizer. After the reaction, the CIM carbon film was thoroughly washed with dimethyl sulfoxide and methanol overnight with the assistance of a shaker.

Covalent Attachment of Redox-Active Molecules on CIM Carbon through Amide Coupling. For $–NO_2$ attachment, an electrolyte was prepared by dissolving 0.1 M of 4-nitrobenzene diazonium tetrafluoroborate and 0.1 M of $TEABF_4$ in acetonitrile. CIM carbon films were presoaked in the electrolyte for 1 h to ensure the electrolytes could diffuse into the mesopores. A potential scan of 0.5 V to -0.2 V (vs Ag/Ag^+ with 10 mM Ag^+) was applied to the CIM carbon film with a scan rate of 25 mV/s for 3 – 5 cycles. The modified CIM carbon films were washed thoroughly with acetonitrile and soaked in acetonitrile and methanol on a shaker overnight to remove physically absorbed unreacted diazonium salts.

To reduce $–NO_2$ to $–NH_2$ groups, CIM-NO_2 was soaked in a 0.8 M solution of disodium sulfide ethanol/water (1:1 v/v) at 50 ˚C overnight. The resulting CIM-NH_2 films were washed thoroughly with ethanol and water using a shaker.

Amide coupling reactions between CIM-NH_2 films and redox-active molecules with –COOH groups were performed using DMTMM or EDC/HOBt as the coupling reagents. For amide coupling reactions involving ferrocenecarboxylic acid and Co(III)TCPP, CIM-NH_2 films were soaked in a methanol solution containing 2 mM of ferrocenecarboxylic acid (or 1 mM of Co(III)TCPP) and 2 mM of DMTMM for 24 h. The resulting CIM carbon films were washed thoroughly with methanol using a shaker. For amide coupling reactions that involve cobalt(II) tris(5-carboxy-2,2’-bipyridine) complex, the CIM-NH_2 films were soaked for 24 h in a dimethylformamide solution containing 2 mM of cobalt(II) tris(5-carboxy-2,2’-bipyridine) chloride, 2 mM of EDC·HCl, 2 mM of HOBt, and 2 mM of DIPEA. The resulting carbon films were washed

with dimethylformamide and ethanol extensively with the assistance of a shaker.

Preparation of CIM Carbon-Based Redox Buffer and K^+-ISEs. The cobalt(II) tris(5-carboxy-2,2'-bipyridine)-modified CIM carbon films were soaked for 24 h in a dimethylformamide solution containing 5 mM Co(II) tris(bipyridine) and 5 mM Co(III) tris(bipyridine) complexes. The resulting carbon films were thoroughly washed with dimethylformamide, ethanol, and methanol using a shaker, and dried under vacuum to obtain a CIM carbon-based redox buffer.

A K^+-ISE membrane precursor solution was prepared by dissolving 66 mg of PVC as polymer matrix, 132 mg of o-nitrophenyl octyl ether as plasticizer, 2.0 mg of valinomycin as ionophore, and 0.67 mg of potassium tetrakis(4-chlorophenyl) borate (75 mol % with respect to the ionophore) to provide for ionic sites in 1 mL of anhydrous tetrahydrofuran. 40 μL of the precursor solution was dropcast onto the redox buffer-modified CIM carbon film that was placed on a gold electrode. The solvent tetrahydrofuran was allowed to evaporate overnight, thus forming a homogenous sensing membrane on the modified CIM carbon film. The gold electrode coated with CIM carbon film and the sensing membrane was then mounted into a cylindrical electrode body custom-made from DuPont Delrin acetal resin, as described in Section 2.1.

Electrochemical Measurements. Unless otherwise noted, cyclic voltammograms were collected at room temperature in a solution containing 0.1 M of $TEABF_4$. A three-electrode electrochemical cell was used with Ag/Ag^+ (with 10 mM Ag^+) as the reference, modified electrode as the working electrode, and a Pt wire as the counter electrode. Potentiometric measurements were conducted using a two-electrode setup, with an

aqueous double-junction Ag/AgCl electrode (with a 1.0 M LiOAc bridge electrolyte and AgCl-saturated 3.0 M KCl inner reference electrolyte) as the reference electrode.

Surface Analysis. Fourier-transform infrared (FTIR) spectra of functionalized CIM carbon samples were obtained using KBr pellets with a Nicolet Magna-IR 760 spectrometer. The modified CIM carbon films were also characterized by X-ray photoelectron spectroscopy (XPS) using a Surface Science SSX-100 instrument with an Al anode (Kα X-rays at 1486.66 eV) operated at 10 kV and 20 mA. Measurements were performed at room temperature, with a high vacuum below 10^{-8} Torr in the analysis chamber.

6.3 Results and Discussion

6.3.1 Strategies to Prepare CIM Carbon-Based Redox Buffer

Figure 6.1a shows a schematic representation of an all-solid-state redox buffer based on CIM carbon, in which both oxidized and reduced species of a redox couple are covalently attached to the carbon surface. To maximize buffer capacity (i.e., the ability to resist electrical potential change caused by redox interference), the molar ratio of the oxidized and reduced species should be 1:1. When CIM carbon-based redox buffer is used as the solid contact in an all-solid-state ISE, the interfacial potentials at the CIM carbon/ISE membrane interface ($\Delta\varphi_2$) and at the CIM carbon/conducting substrate interface ($\Delta\varphi_3$) can be controlled by the redox buffer attached to CIM carbon, thus enabling highly reproducible and stable electrode E°.

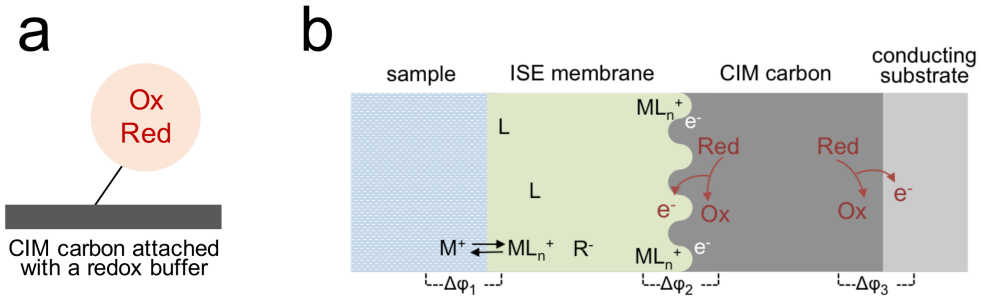

Figure 6.1 Schematic representations of a CIM carbon-based redox buffer and its application in all-solid-state potentiometric ion sensors. (a) A redox couple comprising both oxidized and reduced species is covalently attached to the surface of CIM carbon. (b) All relevant interfaces of an all-solid-state ISE with a CIM carbon-based redox buffer and a cation (M^+) selective membrane that contains an electrically neutral ionophore (L) and anionic sites (R^-).

A few requirements must be fulfilled for an adequate redox buffer. First and foremost, a well-defined redox buffer should have a well-defined redox potential. Conductive polymers usually exhibit high redox capacitance, but a continuum of less well-defined redox potentials that can be related to the inhomogeneity in crystallinity, conformation, film morphology, and so on.[201] Therefore, compared to molecular redox species that exhibit well-defined redox potentials, conductive polymers are less attractive for redox buffer applications. Besides well-defined redox potentials, both the oxidized and reduced species of the redox buffer should be chemically and electrochemically stable with reversible redox activity. In this regard, the standard reduction potential of the redox couple should be close to 0 V (vs Ag/AgCl) so that the redox couple cannot be

easily oxidized or reduced by redox-active interferents that are present in the system. Although ferrocene is a well-studied redox molecule with a suitable standard reduction potential of 0.40 V (vs SHE), it cannot be used for redox buffer applications because its oxidized form ferrocenium ion is not stable under certain circumstances. It was reported that Cl^- ions can induce the degradation of ferrocenium ions into non-reducible $FeCl_4^-$ in both organic electrolytes and ferrocene-doped ISE membranes, which can lead to irreversible redox chemistry.[226] Furthermore, the redox couple should also exhibit fast electron-transfer rates, thus enabling adequate ion-to-electron transduction when the redox buffer is used as the transducer layer in an all-solid-state ISE. Based on the above considerations, cobalt complexes were chosen as promising candidates for redox buffers because of their well-defined and reversible redox chemistry, fast electron-transfer kinetics, as well as good chemical and electrochemical stability.[49,50,227]

To immobilize the redox buffer to CIM carbon, surface functionalization of CIM carbon is needed to create anchoring points for the following attachment. Numerous approaches have been reported to modify the surface of carbon materials. For example, surface oxidation can be performed to introduce oxygen-containing functional groups (e.g., phenol, ketone, lactone) to the carbon surface, which serve as starting points for the subsequent reactions for attachment.[228] However, surface oxidation is usually conducted in an uncontrolled way (e.g., by boiling the carbon material in concentrated nitric acid) that can generate large amounts of hydrophilic redox-active surface functionalities, which can interfere with the grafted redox buffer and also induce water-layer formation at the solid contact/ISE membrane interface. Therefore surface oxidation is not suitable for the

preparation of CIM carbon-based redox buffer. Compared to surface oxidation, electrografting allows surface modification to proceed in a controlled manner that results in a cleaner electrode surface, and thus is more suitable for the preparation of all-solid-state redox buffer based on CIM carbon.[229-231]

Herein, the surface of CIM carbon is functionalized using the electrografting method through the diazonium chemistry. Two types of subsequent chemical reactions were evaluated, as depicted in Figure 6.2. The first reaction was click chemistry (copper(I)-catalyzed azide-alkyne cycloaddition), where azide ($–N_3$) groups were introduced to CIM carbon through the electrochemical reduction of an aryl diazonium salt that bears the azide group (i.e., 4-azidobenzene diazonium tetrafluoroborate). A click reaction was then performed to attach a cobalt tris(5-ethynyl-2,2′-bipyridine) complex to the surface of CIM carbon through a triazole linkage (Figure 6.2a). The second reaction was an amide coupling reaction, in which nitro ($–NO_2$) groups were first attached to CIM carbon via diazonium chemistry (i.e., 4-nitrobenzene diazonium tetrafluoroborate) and then reduced to amino ($–NH_2$) groups. The amide coupling reaction was then conducted to immobilize a cobalt tris(bipyridine) complex or cobalt porphyrin complex derivative with –COOH groups (Figure 6.2b). In each case, a ferrocene derivative (i.e., ethynylferrocene or ferrocenecarboxylic acid) was used as a model molecule to demonstrate the feasibility of covalently attaching a redox-active molecule to the surface of CIM carbon using this type of chemical reaction.

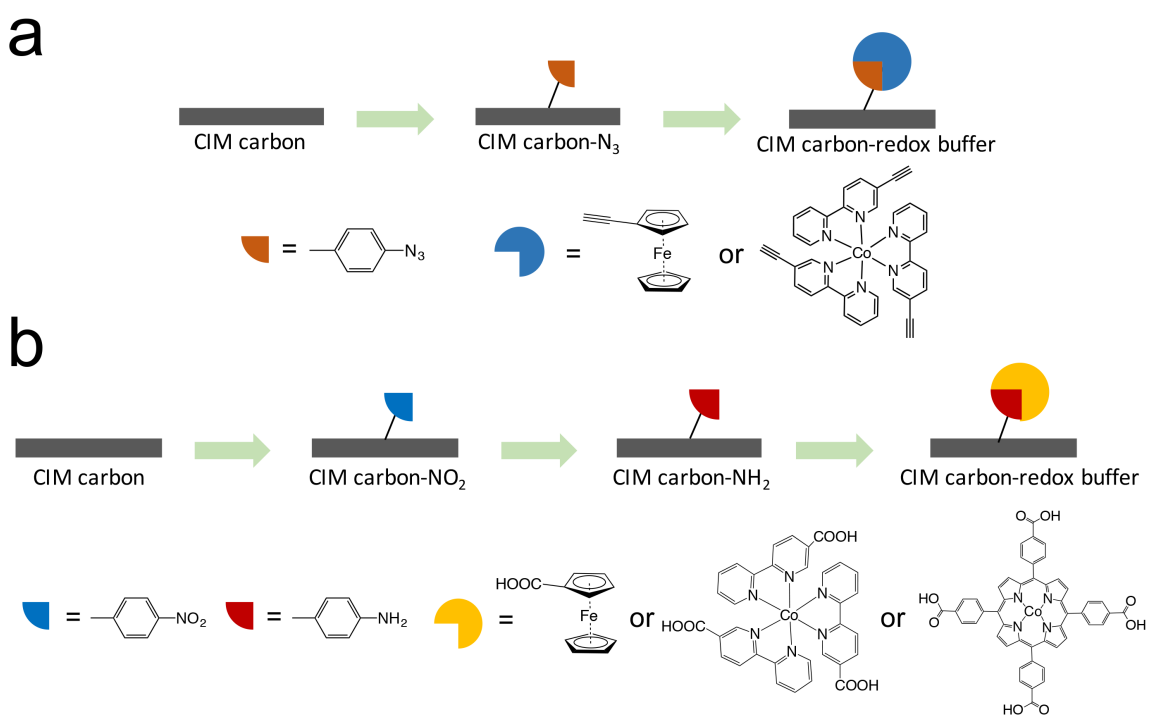

Figure 6.2 Schematic representations of the covalent attachment of redox-active molecules onto the surface of CIM carbon. (a) Click chemistry. Azide groups are first introduced to the surface of CIM carbon, followed by subsequent click reaction to covalently attach redox-active molecules through a triazole linkage. (b) Amide coupling reaction. Nitro groups are first attached to CIM carbon, followed by reduction to amino surface functional groups. An amide coupling reaction is then performed to attach redox-active molecules with carboxylic groups through an amide linkage.

6.3.2 Surface Modification of CIM Carbon through Electrochemical Reduction of Diazonium Salts

Figure 6.3 represents typical cyclic voltammograms of $–N_3$ and $–NO_2$ attachments to CIM carbon through the electrochemical reduction of aryl diazonium salts. It is well known that diazonium salts can be reduced through a one-electron transfer process to produce dinitrogen and a phenyl radical that can directly react with the electrode surface. The corresponding cathodic reduction potential depends on the functional group that is attached to the phenyl ring.[230] For both 4-azidobenzene diazonium and 4-nitrobenzene diazonium salts, a broad irreversible cathodic wave can be observed during the first scan, which corresponds to the cleavage of dinitrogen from diazonium salts. On the following scans, the intensity of the cathodic wave decreased significantly due to the blocking of the electrode by the organic groups that were attached to the electrode surface. Interestingly, a second cathodic reduction wave at about 0.13 V showed up for 4-nitrobenzene diazonium salt (Figure 6.3b). This phenomenon was observed in literature as well, especially when the concentration of the diazonium salt was high. Previous studies suggest that this second cathodic reduction wave may be attributed to the adsorption and reduction of diazonium salts at different sites of the electrode.[232,233]

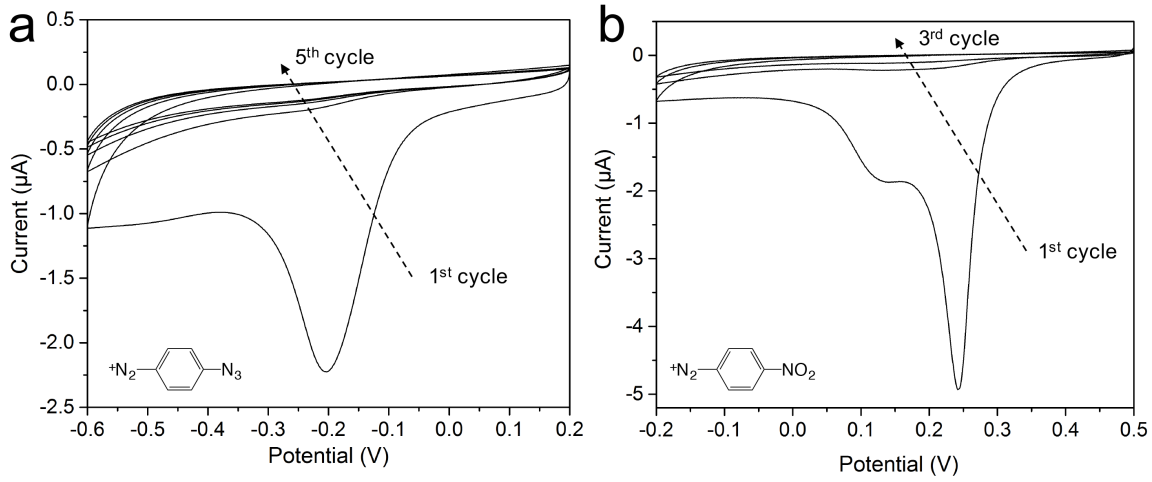

Figure 6.3 Typical cyclic voltammograms of CIM carbon that had been surface-modified through the electrochemical reduction of diazonium salts. (a) Surface modification with 1 mM of 4-azidobenzene diazonium tetrafluoroborate. (b) Surface modification with 0.1 M of 4-nitrobenzene diazonium tetrafluoroborate. Scan rate = 25 mV/s, supporting electrolyte: 0.1 M $TEABF_4$, reference potential: Ag/Ag^+, 10 mM Ag^+.

6.3.3 Covalent Attachment through Click Chemistry

Azide Attachment to CIM Carbon. The first step of the click chemistry approach is to covalently attach azide functional groups to the surface of CIM carbon. FTIR spectroscopy was used to detect the presence of azide groups on the CIM carbon film (Figure 6.4). Azide groups usually exhibit IR absorptions near 2100 cm^{-1} due to the asymmetrical vibrations.[234] The observed absorptions were at 2120 cm^{-1} and 2093 cm^{-1}, in agreement with observations for previously reported azide-modified carbon nanofibers (i.e., 2113 cm^{-1} and 2083 cm^{-1}).[235] The reason for the presence of two absorption peaks is not clear yet, but it is possible that the two peaks correspond to the phenyl azides attached to basal- and edge-planes of CIM carbon.

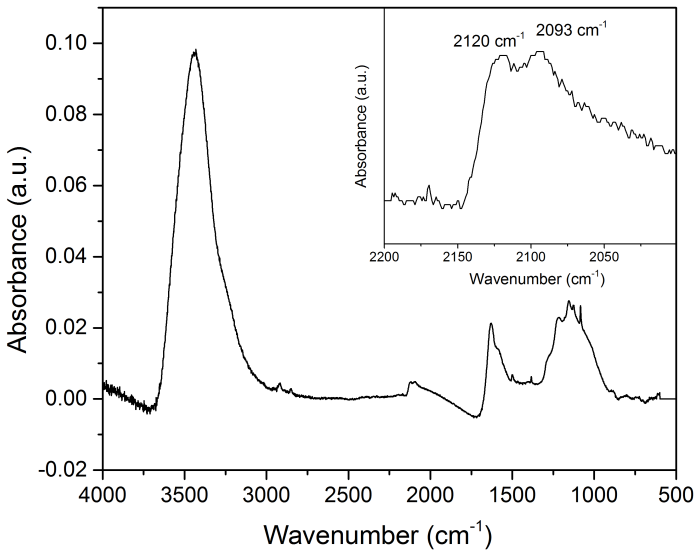

Figure 6.4 FTIR spectrum of CIM carbon films modified with $–N_3$ surface groups. An expanded view showing the evidence of the presence of $–N_3$ groups is presented in the inset.

XPS was also used to confirm the presence of $–N_3$ groups on the surface of CIM carbon. Compared to unmodified CIM carbon that does not contain nitrogen (Figure 6.5, black trace), it can be clearly seen that a N_{1s} peak appears in the survey scan of azide-modified CIM carbon (Figure 6.5, red trace). By integrating the areas of the peaks in XPS, the N content was calculated to be 4.40 atom%, so that the surface loading of $–N_3$ was 1.47% (each $–N_3$ contains 3 N atoms) with respect to all the atoms on the carbon surface. Assuming an accessible surface area of 442 m^2/g for CIM carbon,[69] the surface coverage of $–N_3$ groups was estimated to be 1.6 molecules/nm^2. This value is approximately double that of the previously reported azide coverage on planar graphitic surfaces (i.e., 0.7 molecules/nm^2) through a chemical modification method.[236]

The high-resolution N_{1s} spectrum of the azide-modified CIM carbon shows two peaks at 400.8 eV and 404.3 eV with an area ratio of 7:3 (Figure 6.5, inset). This N_{1s} spectrum is characteristic for the azide group, and is consistent with previously reported values for azide attached to glassy carbon (i.e, 400 eV and 404 eV, area ratio of 2:1).[237] The observed fluorine originated from the Teflon binder that was used to make the CIM carbon film. Based on the results obtained from FTIR and XPS, it can be concluded that $-N_3$ groups were successfully attached to the surface of CIM carbon.

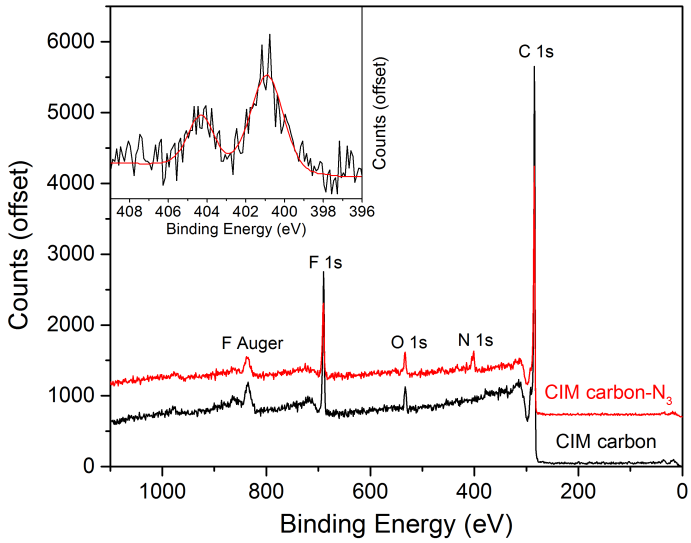

Figure 6.5 XPS spectra of CIM carbon films before (black) and after (red) modification with $-N_3$ surface groups. The high-resolution N_{1s} spectrum of N_3-modified CIM carbon is presented in the inset.

Ferrocene Attachment to CIM Carbon through Click Chemistry. Before attaching the cobalt complex, ethynylferrocene was first attached to azide-modified CIM carbon to demonstrate the feasibility of immobilizing a redox-active molecule on the surface of CIM carbon using click chemistry. Ferrocene was chosen because of its fast charge transfer ability and because it has been well studied, thus enabling a better understanding of the system. The obtained ferrocene-modified CIM carbon film was characterized by XPS. Fe_{2p} peaks from ferrocene can be clearly observed in the XPS spectrum for the ferrocene-modified CIM carbon (Figure 6.6, red trace). Based on XPS data, the surface Fe content was calculated to be 0.65 atom%, indicating a yield of 44%. If the reaction efficiency was 100%, the theoretical surface loading of Fe from ferrocene would equal the surface loading of $–N_3$ anchoring points, which is 1.47 atom%.

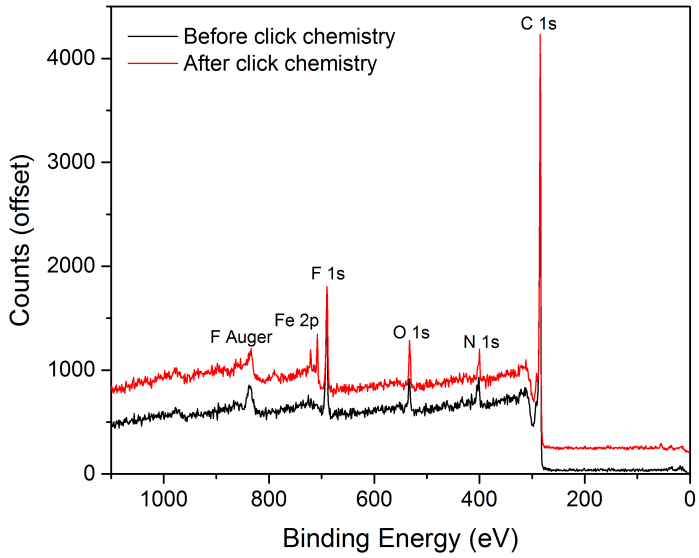

Figure 6.6 XPS spectra of N_3-modified CIM carbon films before (black) and after (red) click reactions to attach ethynylferrocene to CIM carbon. The Fe_{2p} peaks can be observed at about 710 eV ($Fe_{2p(3/2)}$) and 723 eV ($Fe_{2p(1/2)}$).

Using the same click chemistry conditions, ethynylferrocene was also successfully attached to an azide-modified planar glassy carbon electrode. This can be demonstrated by the cyclic voltammogram of the resulting electrode, as shown in Figure 6.7a. With a scan rate of 100 mV/s, a pair of well-defined and reversible redox peaks arising from ferrocene was observed, with a peak separation as low as 28 mV. A plot of scan rate and peak currents (Figure 6.7b) shows that both anodic and cathodic peak currents are proportional to the scan rate, with high coefficients of determination (R^2 = 0.9997 and 0.9999). This result confirms that the observed redox activity is indeed a surface-controlled process, and the above experiments demonstrate that it is feasible to graft redox-active molecules to the surface of CIM carbon through click chemistry.

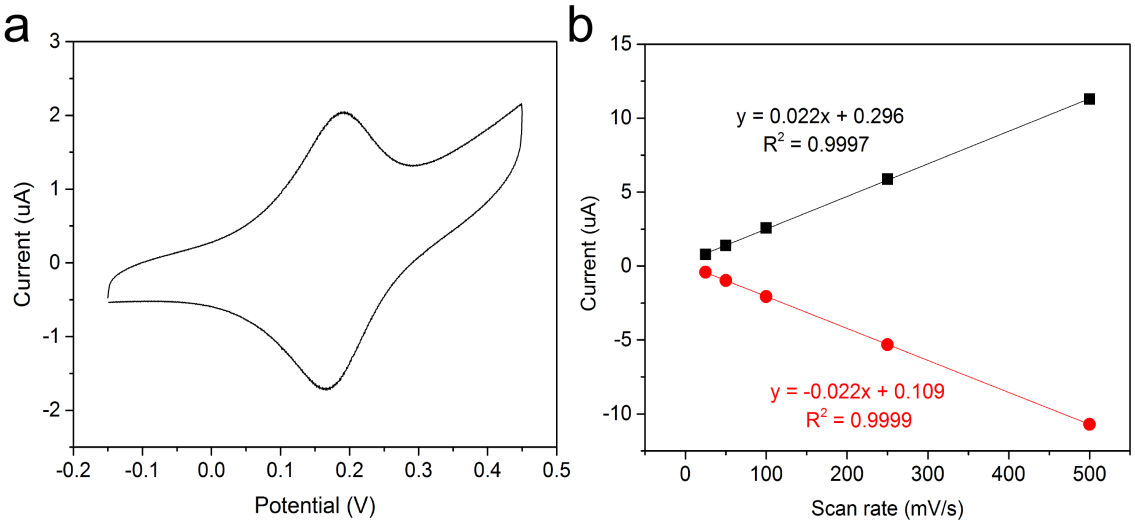

Figure 6.7 (a) Cyclic voltammogram of ferrocene attached to a planar glassy carbon electrode using click chemistry reaction. The scan rate was 100 mV/s and the reference was Ag/Ag^+, 10 mM Ag^+. The dependence of anodic and cathodic peak currents on the scan rates are shown in panel b.

Attachment of Cobalt(II) Tris(5-ethynyl-2,2′-bipyridine) to CIM Carbon Using Click Chemistry. Following the demonstration of ferrocene attachment, the cobalt complex cobalt(II) tris(5-ethynyl-2,2′-bipyridine) was attached to azide-modified CIM carbon films using the same click chemistry reaction. For a control experiment, cobalt(II) tris(2,2′-bipyridine) without ethynyl groups (necessary for click chemistry reaction) was tested as well. The XPS spectra of the two samples are shown in Figure 6.8a.

Strong evidence showing the completion of the click reaction between azide-modified CIM carbon and cobalt(II) tris(5-ethynyl-2,2′-bipyridine) was obtained from XPS high-resolution N_{1s} spectra. As previously discussed, $–N_3$ groups exhibit two peaks at 400 eV and 404 eV in the high-resolution XPS N_{1s} spectrum, and these two peaks can become one broadened peak at 400 eV due to the formation of a triazole linkage after the completion of click reaction.[236,237] This feature was observed when the cobalt complex was attached to CIM carbon, as shown in Figure 6.8b (top). For the control experiment with the cobalt(II) tris(2,2′-bipyridine) complex, two distinct N_{1s} peaks remained, corresponding to the unreacted $–N_3$ surface functional groups on CIM carbon.

The cobalt surface loading, however, is 0.05 atom%, which is much lower than that of ferrocene (i.e., 0.65 atom%) attached to CIM carbon using the same click chemistry method. Also, it was found that the Cu(I) catalyst used in click chemistry reactions could contaminate the surface of CIM carbon, possibly due to the formation of a Cu complex with the bipyridine ligands. This Cu impurity may interfere with the redox buffer and eventually affect the E° reproducibility of the resulting all-solid-state ISEs.

Therefore, extra steps of Cu removal are required to prepare electrodes using click chemistry reactions.

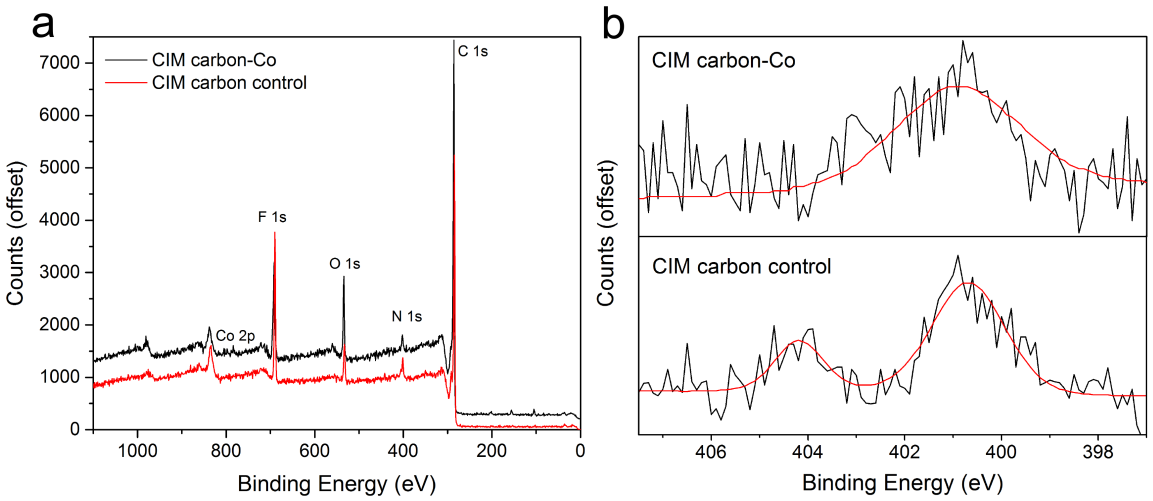

Figure 6.8 XPS spectra of the control sample (red) and cobalt(II) tris(5-ethynyl-2,2′-bipyridine) complex attached to CIM carbon (black) using click chemistry reaction (a). The corresponding high-resolution XPS N_{1s} spectra are shown in panel b.

6.3.4 Covalent Attachment through Amide Coupling

Nitro and Amine Attachment to CIM Carbon. In a similar way to the $–N_3$ attachment, $–NO_2$ surface functional groups were grafted to CIM carbon through the reduction of diazonium salts. The successful attachment of $–NO_2$ groups was evidenced by the IR absorptions at 1520 and 1344 cm^{-1} (vs reported values of 1520 and 1340 cm^{-1}), which correspond to the asymmetric and symmetric stretching of $–NO_2$ groups, respectively.[230,231] The absence of an N_2^+ IR absorption in the range of 2130–2300 cm^{-1} indicates that the observed nitro groups are covalently attached rather than physically absorbed to the carbon surface (Figure 6.9a). The N surface loading was calculated to be

1.60 atom% (or an estimated surface coverage of 1.7 molecules/nm^2) on the basis of XPS data (Figure 6.9b), which agreed well with the results of $–N_3$ attachment (i.e., 1.6 molecules/nm^2). The presence $–NO_2$ groups was further confirmed by a strong characteristic peak at 406 eV in the high-resolution XPS N_{1s} spectrum (Figure 6.10, top).[230,238]

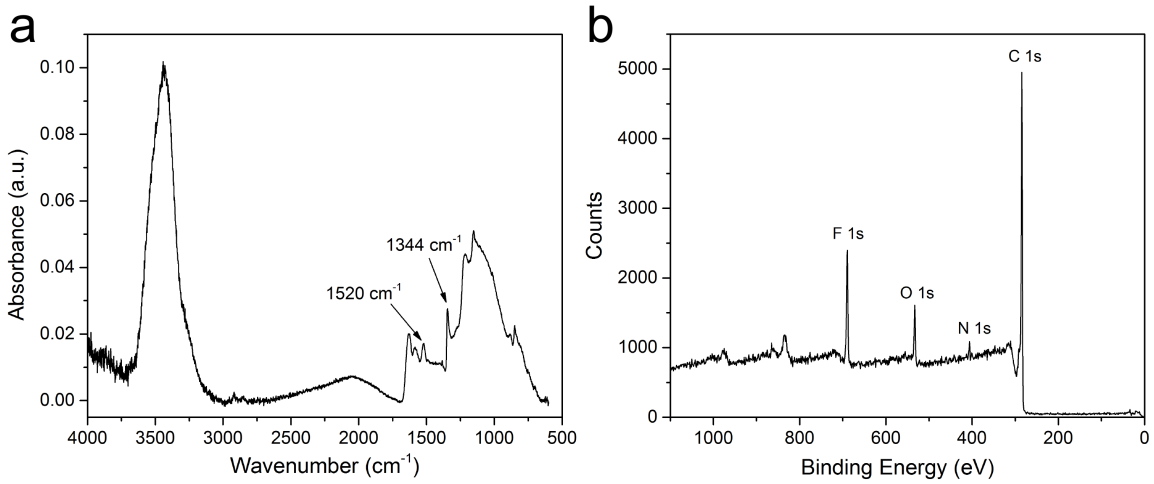

Figure 6.9 FTIR (a) and XPS (b) spectra of CIM carbon films modified with $–NO_2$ surface groups.

Both electrochemical and chemical approaches were evaluated to reduce the surface $–NO_2$ groups to $–NH_2$ groups on CIM carbon. For the electrochemical approach, a constant cathodic potential of –0.8 V was applied to a nitro-modified CIM carbon film for 2 h. But it can be seen in Figure 6.10 (middle) that this method was insufficient in terms of $–NO_2$ reduction as an XPS N_{1s} peak at 406 eV, characteristic for nitro groups, was still present after the treatment. For the chemical reduction approach, the $–NO_2$ groups attached to CIM carbon were successfully reduced to $–NH_2$ groups using Na_2S as a reducing agent. After the chemical reduction, the XPS N1s peak at 406 eV in nitro-

modified CIM carbon films disappeared, and a strong peak at 400 eV was observed (Figure 6.10, bottom), corresponding to $–NH_2$ groups on the surface of CIM carbon.[238,239] These results demonstrate that CIM carbon can be modified with $–NH_2$ surface groups through this two-step process.

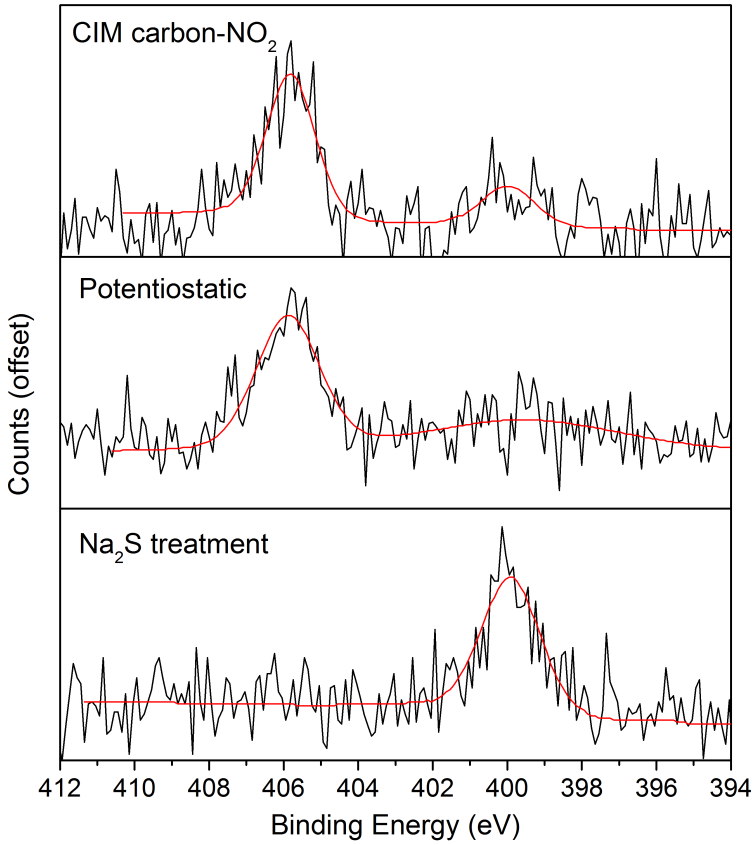

Figure 6.10 High-resolution XPS N_{1s} spectra of CIM carbon films. (top) CIM carbon film modified with $–NO_2$ surface groups. (middle) Electrochemical reduction of $–NO_2$ to $–NH_2$ surface groups by a potentiostatic approach. Applied potential = –0.8 V, time = 2 h. (bottom) Chemical reduction of $–NO_2$ to $–NH_2$ surface groups by Na_2S treatment.

Ferrocene Attachment to CIM Carbon through Amide Coupling. To evaluate the feasibility of covalently attaching a redox-active molecule onto CIM carbon using an amide coupling reaction, ferrocenecarboxylic acid was used to react with amine-modified CIM carbon films with DMTMM as the amide coupling reagent. For a control experiment, CIM carbon films were also soaked in a solution containing ferrocenecarboxylic acid but without the DMTMM amide coupling reagent.

XPS data reveal the successful attachment of ferrocene to CIM carbon (Figure 6.11). Compared to the control sample that did not exhibit any Fe signal, strong Fe_{2p} XPS peaks were observed for the ferrocene-modified CIM carbon film. This comparison also demonstrates that the observed Fe on CIM carbon was covalently attached rather than physically absorbed. The surface loading of Fe was calculated to be 1.05 atom% and was relatively high compared to the surface loading of the initial $–NO_2$ anchoring points (i.e., 1.60%). The ferrocene surface coverage was estimated to be 1.1 molecules/nm^2, which is on the same level as a previously reported ferrocene coverage on carbon nanofibers through covalent linkage (i.e., 0.9 molecules/nm^2).[235]

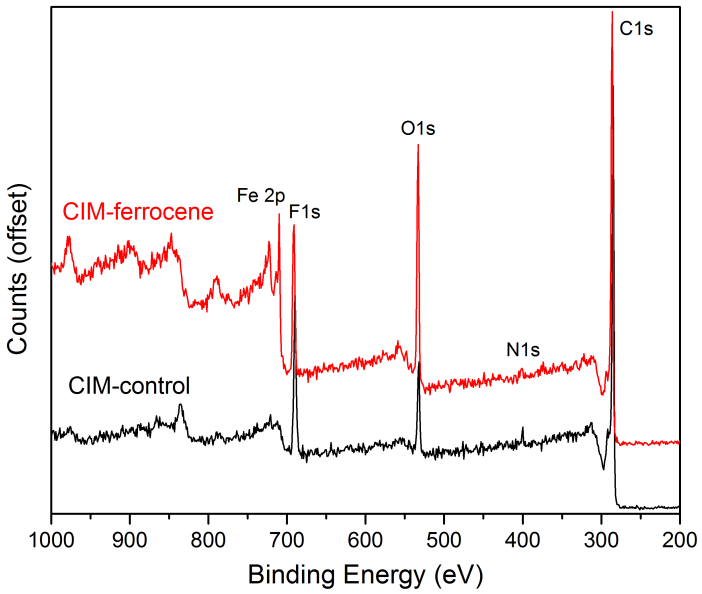

Figure 6.11 XPS spectra of the control sample (black) and ferrocenecarboxylic acid attached to CIM carbon (red) using an amide coupling reaction.

Using the same DMTMM-catalyzed amide coupling reaction, ferrocenecarboxylic acid was also successfully attached to a planar glassy carbon electrode. As shown in Figure 6.12a, the resulting electrode exhibited a pair of well-defined redox peaks with a peak separation of 45 mV for a scan rate of 100 mV/s. A plot of the dependence of peak currents on the scan rates (Figure 6.12b) shows that both anodic and cathodic peak currents are proportional to the scan rate, with high coefficients of determination (R^2 = 0.9991 and 0.9982). These results confirm that the observed redox activity is due to a surface-controlled process, and they demonstrate that it is feasible to attach a redox-active molecule on CIM carbon and glassy carbon through an amide coupling reaction.

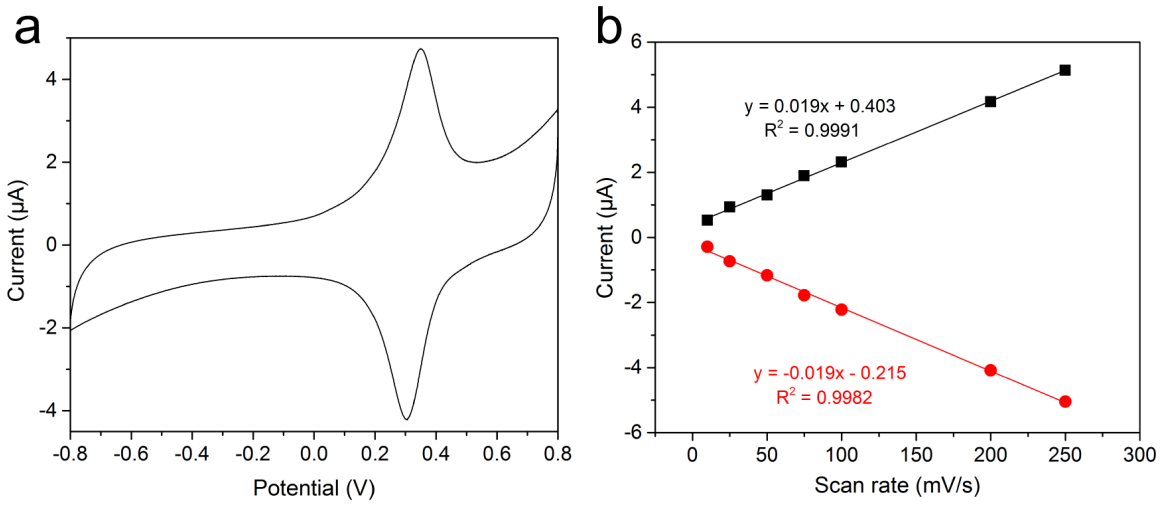

Figure 6.12 Cyclic voltammogram of ferrocenecarboxylic acid attached to a planar glassy carbon electrode through amide coupling (a). Scan rate = 100 mV/s, reference potential: Ag/Ag^+, 10 mM Ag^+. The dependence of anodic and cathodic peak currents on the scan rates is shown in panel b.

Cobalt Porphyrin Attachment to CIM Carbon through Amide Coupling. To covalently attach a redox buffer to CIM carbon through an amide coupling reaction, two cobalt complexes with carboxylic acid groups were evaluated. The first was the cobalt(III) porphyrin complex Co(III)TCPP. Co(III)TCPP was synthesized according to previously reported procedures,[225] and its suitability for redox buffer application was studied using cyclic voltammetry.

A typical cyclic voltammogram of dissolved Co(III)TCPP is shown in Figure 6.13. It can be seen that Co(III)TCPP exhibits three pairs of redox peaks, which resembles the behavior of cobalt tetraphenyl porphyrin complexes without the carboxylic groups.[240] From the cathodic to anodic potentials, the three one-electron transfer reactions

can be attributed to the Co(II)/Co(III) process (Figure 6.13, I), the formation of Co(III) π cation radical (Figure 6.13, II), and the formation of dication (Figure 6.13, III), respectively.[240] The midpoint potential (i.e., the average of the reduction and oxidation peak potentials) of the Co(II)/Co(III) process was 0.193 V versus Ag/Ag^+, indicating good electrochemical stability of the Co(II/III)TCPP redox couple. Therefore, the Co(II/III)TCPP redox couple may be a good candidate for redox buffer.

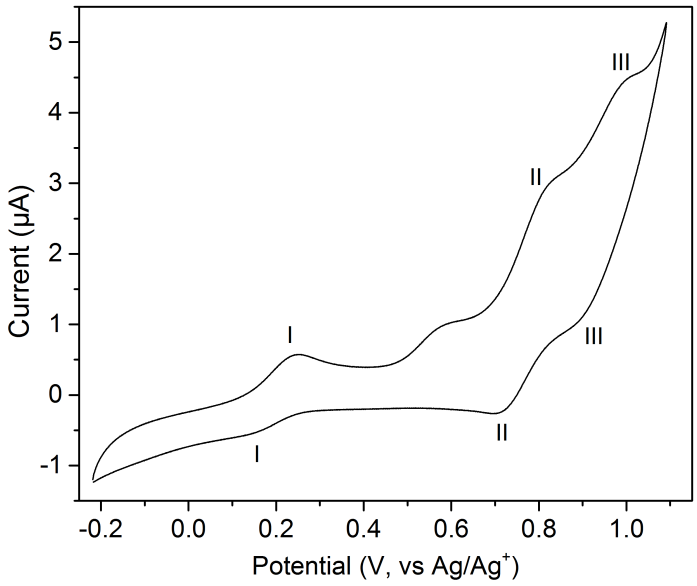

Figure 6.13 Cyclic voltammogram of 0.5 mM Co(III)TCPP dissolved in tetrahydrofuran with 0.1 M supporting electrolyte $TBAClO_4$. Three redox processes can be observed, which correspond to Co(II)/Co(III), the formation of Co(III) π cation radical, and the formation of dication, respectively. Scan rate = 100 mV/s, reference potential: Ag/Ag^+.

The DMTMM-catalyzed amide coupling reaction was used to attach Co(III)TCPP to amine-modified CIM carbon. The reaction conditions were the same as those used for successful attachment of ferrocenecarboxylic acid, and a control experiment without the coupling reagent DMTMM was performed as well. After reaction, an XPS survey scan showed two weak Co_{2p} peaks around 780 eV (Figure 6.14a, black trace), with a relatively low cobalt surface loading of 0.30 atom% compared to the surface loading of anchoring points (i.e., 1.60 atom%) and that of ferrocene immobilized using the same method (i.e., 1.05 atom%). The high-resolution XPS Co_{2p} spectrum revealed two distinct peaks at 780 eV and 785 eV (Figure 6.14b), which corresponded to $Co_{2p(3/2)}$ and $Co_{2p(1/2)}$, respectively. For the control experiment without amide coupling reagent, no cobalt was detected from an XPS survey scan (Figure 6.14a, red trace). This confirms that the observed cobalt on CIM carbon was not physically absorbed but indeed covalently attached.

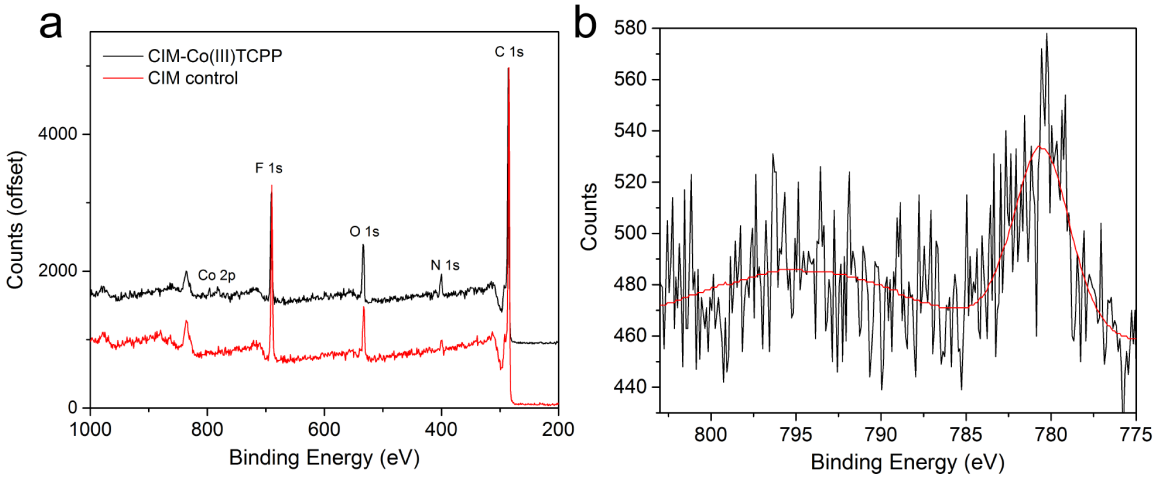

Figure 6.14 XPS spectra of Co(III)TCPP-modified CIM carbon film (black, a) and the control sample (red, a). The high-resolution XPS Co_{2p} spectrum of the Co(III)TCPP-modified CIM carbon is presented in panel b, revealing two distinct peaks corresponsing to $Co_{2p(3/2)}$ (780 eV) and $Co_{2p(1/2)}$ (795 eV).

Attempts were made to increase the surface cobalt loading by increasing the efficiency of the amide coupling reaction. A reported mechanism of DMTMM-catalyzed amide coupling reaction reveals that in homogenous solutions, the –COOH groups have to be deprotonated by $–NH_2$ groups for the reaction to proceed.[241] In the CIM carbon system, however, $–NH_2$ groups were grafted on the surface of CIM carbon so that they may not be readily available to deprotonate the –COOH groups. Therefore, different concentrations (i.e., 0.1 mM and 0.5 mM) of two types of bases (i.e., NaOH and DIPEA) were added into the reaction mixture to assist the deprotonation of the –COOH groups. The resulting cobalt surface loading, however, remained in the range of 0.15 to 0.30 atom% based on XPS data (Figure 6.15), showing no improvement compared to results obtained without an additional base as shown above.

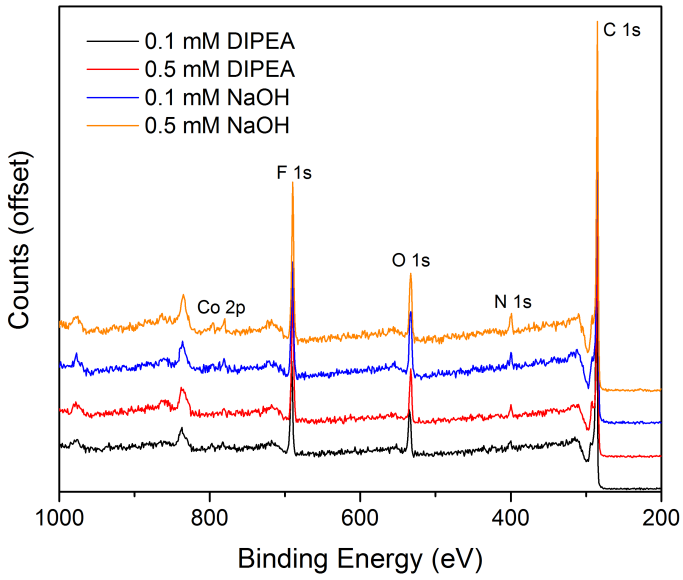

Figure 6.15 XPS spectra of Co(III)TCPP-modified CIM carbon films. The amide coupling reactions were performed with NaOH or DIPEA added to the reaction.

Although the achievable surface cobalt loading was relatively low, attempts of preparing the redox buffer with Co(II/III)TCPP were made. Several trials of synthesizing Co(II)TCPP were made under the protection of nitrogen and argon, but failed because the obtained product was oxidized to Co(III) based on proton NMR. Co(II)TCPP was also obtained from a commercial source, but was readily oxidized to Co(III) in methanol and tetrahydrofuran. Therefore, Co(II)TCPP is challenging to obtain, possibly because it could be readily oxidized, and a glove box may be required to synthesize Co(II)TCPP with high purity and perform the subsequent amide coupling reaction.

Attachment of Cobalt(II) Tris(5-carboxy-2,2'-bipyridine) to CIM Carbon through Amide Coupling. The second cobalt complex evaluated was cobalt(II) tris(5-carboxy-2,2'-bipyridine). To determine its suitability for the application of a redox buffer, the cyclic voltammogram of cobalt(II) tris(5-carboxy-2,2'-bipyridine) was collected. As shown in Figure 6.16a, well-defined and reversible redox peaks were observed. The midpoint potential of cobalt(II) tris(5-carboxy-2,2'-bipyridine) was 0.153 V (vs Ag/AgCl) with a peak separation of 81 mV, indicating good electrochemical stability and fast electron-transfer kinetics of the cobalt(II/III) tris(5-carboxy-2,2'-bipyridine) redox couple. Therefore, the cobalt tris(5-carboxy-2,2'-bipyridine) complex is considered to be a good candidate for application as a redox buffer.

The amide coupling reaction between cobalt(II) tris(5-carboxy-2,2'-bipyridine) and amine-modified CIM carbon films was performed using EDC/HOBt as the coupling reagents. EDC/HOBt were used as the coupling reagents instead of DMTMM because of their solubility in dimethylformamide, a solvent that can dissolve the cobalt(II) tris(5-carboxy-2,2'-bipyridine) complex with hexafluorophosphate as the counter ion. After the reaction, an analysis based on an XPS survey spectrum revealed that the cobalt surface loading obtained by this approach was 0.20 atom% (Figure 6.16b). This surface loading is on a similar level as that of cobalt(III) porphyrin (i.e., 0.15 – 0.30 atom%), but much lower than that of ferrocene (i.e., 1.05 atom%).

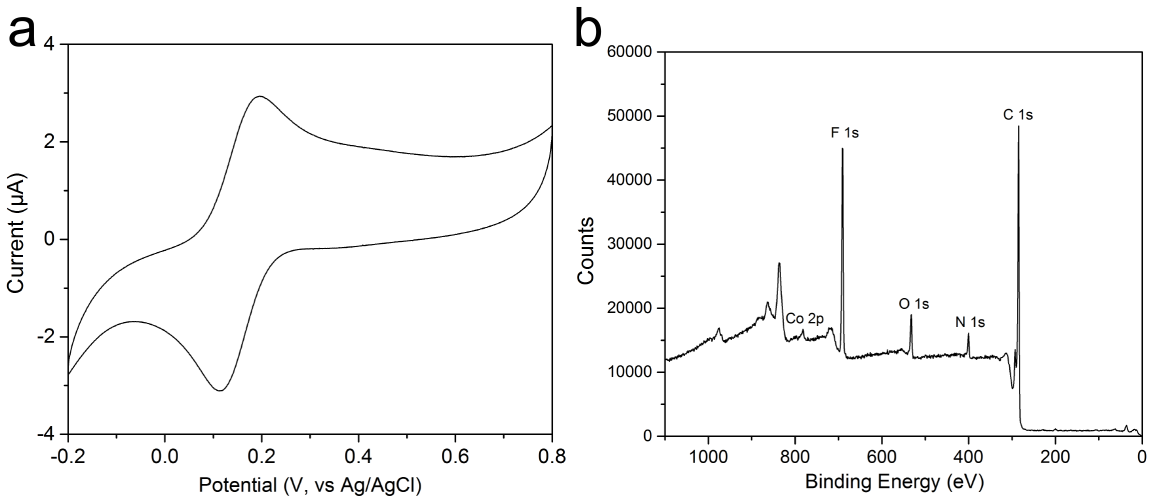

Figure 6.16 Cyclic voltammogram of 0.5 mM cobalt(II) tris(5-carboxy-2,2'-bipyridine) dissolved in 0.1 M phosphate-buffered saline (a). Scan rate = 100 mV/s, reference potential: Ag/AgCl. (b) XPS spectrum of the cobalt(II) tris(5-carboxy-2,2'-bipyridine) attached to CIM carbon.

Redox Buffer Based on Cobalt(II/III) Tris(5-carboxy-2,2′-bipyridine) Attached to CIM Carbon. In spite of the relatively low cobalt surface loading, a redox buffer based on cobalt(II/III) tris(5-carboxy-2,2′-bipyridine) attached to CIM carbon was prepared and evaluated. To maximize buffer capacity, the oxidation states of the surface cobalt needs to be tuned to reach a 1:1 ratio of the Co(II) and Co(III) species. This can be achieved through electron transfer by soaking the cobalt(II) tris(5-carboxy-2,2'-bipyridine)-modified CIM carbon film in a solution containing both Co(II) and Co(III) species.

Herein, cobalt(II) tris(5-carboxy-2,2'-bipyridine)-modified CIM carbon films were soaked in dimethylformamide solutions containing different ratios of Co(II) and Co(III) species (i.e., 10 mM Co(II) tris(bipyridine), 5 mM Co(II) tris(bipyridine) + 5 mM

Co(III) tris(bipyridine), and 10 mM Co(III) tris(bipyridine)) to obtain CIM carbon films with different surface cobalt oxidation states (i.e., CIM-Co(II), CIM-Co(II/III) and CIM-Co(III)). Thorough washing was performed afterwards to remove the Co(II) and Co(III) complexes that were not attached to the surface and were merely introduced to control the redox states of the covalently attached species. XPS results revealed that the obtained CIM carbon films exhibited cobalt surface loadings in the range of 0.10 – 0.20 atom% (Figure 6.17), similar to that of cobalt(II) tris(5-carboxy-2,2'-bipyridine)-modified CIM carbon prior to the adjustment of surface cobalt oxidation states (i.e., 0.20 atom%).

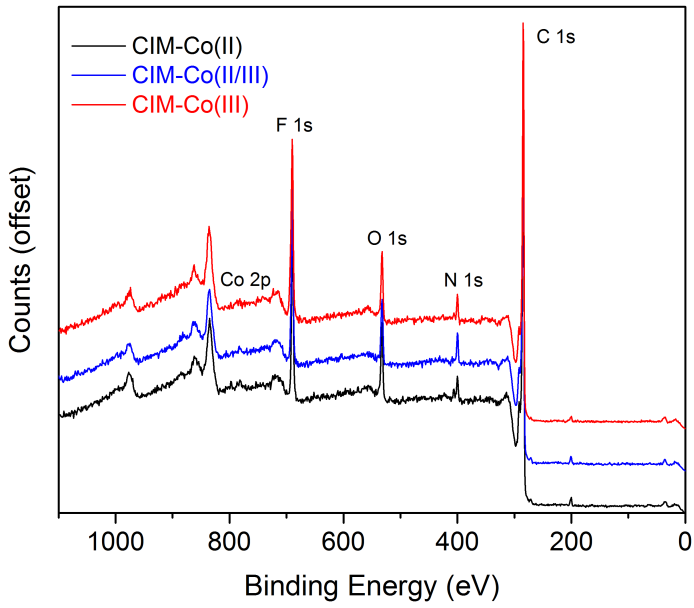

Figure 6.17 XPS spectra of CIM carbon films modified with cobalt complexes with different oxidation states. Black: CIM carbon with Co(II) only. Blue: CIM carbon with 1:1 molar ratio of Co(II) and Co(III). Red: CIM carbon with Co(III) only.

To evaluate the effectiveness of controlling interfacial potentials using a redox buffer covalently attached to CIM carbon, the open circuit potentials of the obtained CIM carbon films (i.e., CIM-Co(II), CIM-Co(II/III) and CIM-Co(III)) were tested. For each sample, two individual carbon films were prepared and measured. As Figure 6.18a shows, the open circuit potentials of the two individual electrodes bearing the same cobalt oxidation states are close to each other, and the potentials for all cobalt-modified CIM carbon films are stable during the measuring period of 120 s. The dependence of open circuit potentials on the surface cobalt oxidation states is summarized in Figure 6.18b. It can be seen that the average open circuit potentials are –267.0 mV for CIM-Co(II) films, –223.5 mV for CIM Co(II/III) films, and –176.8 mV for CIM-Co(III) films. This result demonstrates that the open circuit potential of CIM carbon films can be affected by the surface cobalt oxidation states, even with a low cobalt surface loading of 0.10 – 0.20 atom%. It is assumed that the low amount of redox-active impurities on the surface of CIM carbon is of particular importance for the proper functioning of the redox buffer covalently attached to CIM carbon with such a low surface loading. Otherwise, the open circuit potentials of CIM carbon would have been determined by the redox-active surface impurities rather than the redox buffer.

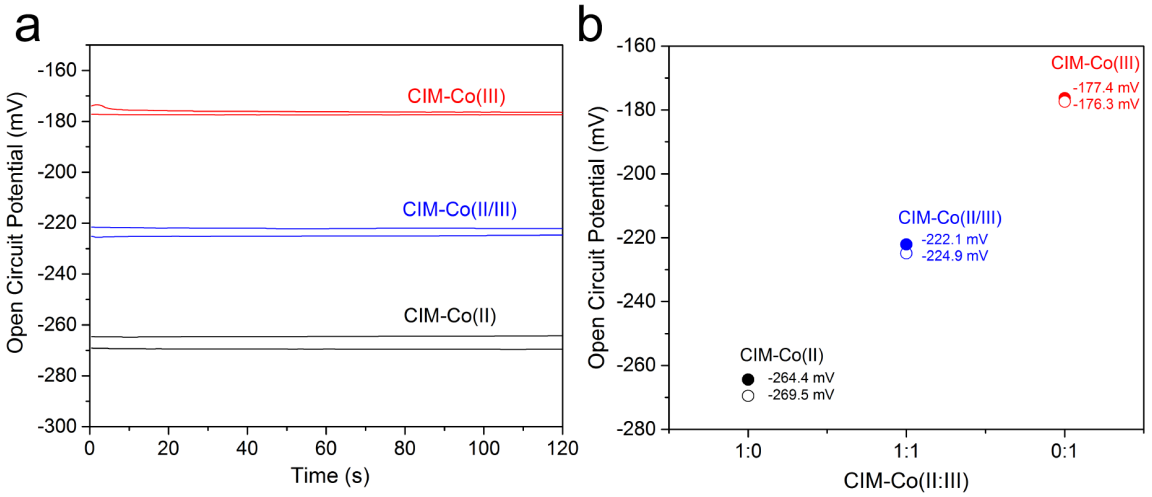

Figure 6.18 Open circuit potentials of CIM carbon films loaded with surface cobalt species with different oxidation states (a). Reference potential: Ag/Ag^+, 10 mM Ag^+. The dependence of open circuit potentials on the surface cobalt oxidation states is shown in panel b. Two individual electrodes were prepared and tested for each cobalt oxidation state.

Finally, all-solid-state ISEs were fabricated to evaluate the effectiveness of the CIM carbon-based redox buffer for electrode E° control in potentiometric ion sensing. The all-solid-state ISE contained a CIM-Co(II/III) film as the solid contact, sandwiched between a gold electrode and a K^+-ISE membrane based on plasticized PVC. A total number of five individual electrodes were prepared, and their K^+ responses were measured without electrode conditioning (i.e., soaking the electrode in a 1 mM KCl solution). The individual calibration curves before electrode conditioning are shown in Figure 6.19a, and the electrode E° based on five electrodes is 322.8 ± 53.0 mV. It can be

seen in Figure 6.19a that the potential of a specific electrode (green trace) differs significantly from that of the rest of other four electrodes, and this may be attributed to significant variations in the manual electrode fabrication process.

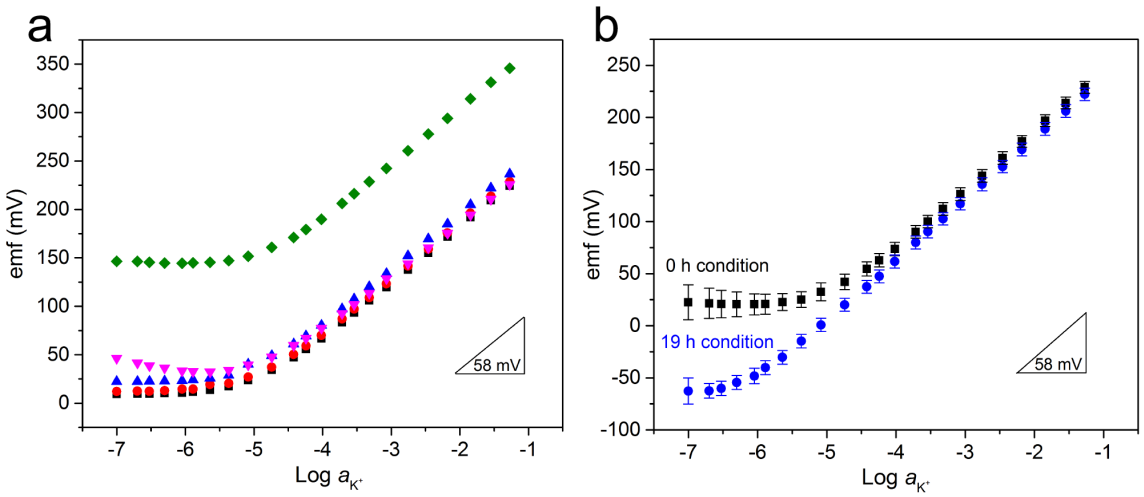

Figure 6.19 Potentiometric K^+ calibration curves (0 h conditioning) of five individual all-solid-state ISEs (represented by different colors) that are based on CIM carbon redox buffer as the solid contact (a). (b) Calibration curves without the green trace without electrode conditioning and after 19 h electrode conditioning.

If one excludes that specific electrode (green trace in Figure 6.19a), the rest of the four electrodes exhibit an electrode E° of 299.3 ± 7.0 mV without electrode conditioning. After conditioning of the electrodes in a 1 mM KCl solution for 19 h, the electrode E° remained stable and was 296.9 ± 6.9 mV. This standard deviation of E° (i.e., 7.0 mV and 6.9 mV) is very similar to previous results of CIM carbon-based ISEs without redox buffer as the membrane additive (i.e., 7.3 mV).[69] Therefore, although the redox buffer attached to CIM carbon with a low surface loading can affect the open circuit potential of CIM carbon, it cannot sufficiently control the interfacial potential at the CIM carbon/ISE

membrane interface to the extent needed for calibration-free ion sensing (e.g., E° variation < 2.8 mV for K^+ measurements in clinical laboratories). Higher redox buffer surface loading is required (i.e., > 1.0 atom%) to achieve all-solid-state ISEs with higher electrode E° reproducibility.

Interestingly, despite the relatively large electrode-to-electrode E° variation, the E° stability of the prepared all-solid-state ISEs is remarkable. Between the first contact of the dry electrodes with aqueous solutions and 19 h of electrode conditioning in a 1 mM KCl solution, the electrode E° remained very stable with a potential change as low as 2.4 mV. This E° shift is much lower than that of electrodes based on cobalt(II/III) tris(4,4'-dinonyl-2,2'-bipyridyl) redox buffer with the same plasticized PVC membrane matrix (i.e., potential drift up to 44 mV within the first 1 h of dry electrodes contacting aqueous solutions),[50] and is even smaller than that of electrodes based on hydrophobic silicone rubber membranes and poly(3-octylthiophene) solid contacts that are designed to quickly reach water uptake equilibrium (i.e., penitential drift of 4 mV during the first 4 h of contacting with aqueous solutions).[118] The exact reason for such high initial electrode E° stability is still unknown, but the stability may be attributed to combined effects of E° control from the redox buffer attached to CIM carbon as well as the hydrophobic nature of the CIM carbon surface. High initial electrode E° stability is essential for single-use and easy-to-use ion sensors without the requirement of cumbersome electrode conditioning. Research efforts may be directed to this direction to realize conditioning-free ion sensing operations.

6.4 Conclusions

In conclusion, two approaches (i.e., click chemistry and amide coupling) were evaluated to graft a redox buffer to the surface of CIM carbon to prepare CIM carbon-based redox buffer. For each approach, anchoring points were successfully attached to CIM carbon, followed by successful covalent attachment of ferrocene derivatives with a high surface loading. It was therefore demonstrated that covalent attachment of redox-active species to the surface of CIM carbon is feasible.

Several cobalt complexes were also attached to the surface of CIM carbon through click chemistry or amide coupling reactions. It was found that the achievable cobalt surface loading was relatively low compared to the iron loading in ferrocene-modified CIM carbon samples, and it is very likely that the low cobalt surface loading arises from the low stability of cobalt complexes on the electrode surface. When cobalt(II) tris(5-carboxy-2,2'-bipyridine) was grafted to CIM carbon through amide coupling, a cobalt surface loading of 0.20 atom% was achieved, and a redox buffer based on cobalt(II/III) tris(5-carboxy-2,2'-bipyridine)-modified CIM carbon was prepared. Results showed that the open circuit potential of cobalt(II/III) tris(5-carboxy-2,2'-bipyridine)-modified CIM carbon can be affected by the surface cobalt oxidation states, even at low cobalt surface loadings. To achieve high electrode-to-electrode E° reproducibility, however, higher redox buffer surface loadings (> 1.0 atom%) are required.

Future work should be focused on identifying redox-active complexes that are stable on the electrode surface and can also fulfill the requirements outlined in Section

6.3.1. Several alternative approaches to increasing the surface loading of redox buffer have been proposed and are discussed in detail in Section 7.2. Once a more effective method is identified, the application of redox buffers covalently attached to CIM carbon should be re-evaluated for potentiometric ion sensing, and robust calibration-free and conditioning-free all-solid-state ion sensors can be developed.

6.5 Acknowledgements

This work was supported by Medtronic PLC through a sponsored research project. J.H. thanks the Krogh family for a Lester C. and Joan M. Krogh Fellowship, and the Graduate School of University of Minnesota for a Doctoral Dissertation Fellowship. We greatly appreciate the contributions by Dr. James Carney, Dr. Ping Yang and Dr. Trisha Dunn through their valuable comments throughout the project.

Chapter 7

Conclusions and Outlook

7.1 Summary of Results

The first objective of this dissertation was to develop a novel solid contact material to fabricate high-performance all-solid-state potentiometric sensors, including all-solid-state ion-selective electrodes (ISEs) and reference electrodes. This objective was successfully achieved by introducing colloid-imprinted mesoporous (CIM) carbon as a new solid contact material, as described in Chapter 2 and Chapter 3. CIM carbon exhibits several unique properties that are desirable for an ion-to-electron transducer material. It comprises interconnected mesopores that can be infiltrated with an ISE sensing phase, providing large interfacial contact area with high double layer capacitance. As a result, the all-solid-state ISEs and reference electrodes based on CIM carbon exhibit remarkable potential stability, and they are the most stable all-solid-state potentiometric sensors reported so far. Besides high double layer capacitance, CIM carbon also contains very low amounts of redox-active impurities on its surface, which is very desirable for the construction of all-solid-state potentiometric sensors with high electrode-to-electrode reproducibility. When combined with a hydrophobic redox buffer as internal reference, highly reproducible all-solid-state ISEs can be achieved, with a variation of standard electrode potential as low as 0.7 mV. Furthermore, the possibility of sensor miniaturization was explored by integrating CIM carbon-based reference electrodes into a paper-based ion-sensing platform. It was demonstrated that the conventional Ag/AgCl/KCl reference system can be successfully replaced by a miniaturized CIM carbon-based reference electrode.

The second objective of this dissertation research was to develop affordable ion-sensing platforms with simple operations and small sample volumes. This objective was achieved by introducing a pretreatment-free planar paper-based ion-sensing platform, as described in Chapter 4. This paper-based ion sensor employed a conventional ISE and reference electrode that were embedded into the paper substrate. As a potentiometric sensor, each interfacial potential within the cell was well-defined by design so that the response of the device can be theoretically predicted. Consequently, the proposed paper-based ion-sensing platform does not need sensor calibration in principle. As a proof-of-concept, single-use paper-based K^+ and Cl^- sensors were constructed and tested. It was found that these paper-based ion sensors exhibit highly reproducible Nernstian responses with both aqueous solutions and undiluted blood serum samples. To further simplify the use of the device, an all-solid-state paper-based ion-sensing platform was proposed and explored in Chapter 5. CIM carbon-based all-solid-state ISE and reference electrode were integrated onto the paper substrate, creating a sensor design that only requires one droplet of the sample but without the need for other reagents. The all-solid-state ion-sensing platform was designed to be calibration-free by defining each interfacial potential within the potentiometric cell, and the sensor performance strongly relied on the redox buffer that was doped into the sensing membranes. It was found that a more robust redox buffer is needed to construct a fully functional all-solid-state paper-based ion-sensing platform that can be used with biological samples.

The last objective of this dissertation research was to develop an all-solid-state redox buffer by covalently immobilizing a redox buffer on the surface of CIM carbon.

Significant progress was achieved, and an all-solid-state CIM carbon-based redox buffer was developed with a relatively low buffer loading. To covalently attach a redox buffer to CIM carbon, two approaches (i.e., click chemistry and amide coupling reactions) involving multiple steps were proposed and evaluated. It was found that ferrocene derivatives can be successfully attached to CIM carbon with a high surface loading via both click chemistry and amide coupling reactions, whereas the achievable surface loadings of various cobalt-based redox-active complexes were relatively low. When an all-solid-state redox buffer was constructed with cobalt(II/III) tris(5-carboxy-2,2'-bipyridine) attached to CIM carbon, the open circuit potentials of the resulting CIM carbon films can be affected by the oxidation states of the surface cobalt on CIM carbon, demonstrating the effectiveness of this CIM carbon-based all-solid-state redox buffer. To construct robust calibration-free potentiometric ion sensors, however, a CIM carbon-based all-solid-state redox buffer with higher buffer surface loading is needed. Possible approaches to achieving such high buffer capacity are discussed in detail in Section 7.2.

7.2 Outlook

To increase the surface loading of a redox buffer that is covalently attached to CIM carbon, the stability of the redox-active complexes on the electrode surface needs to be improved. For this purpose, a few alternatives have been identified, potentially increasing the redox buffer loading on the surface of CIM carbon.

The first alternative is to use 2,2’-bipyridine-5-acetic acid (Figure 7.1a) as the ligand to bind cobalt on the surface of CIM carbon. Compared to the ligand 2,2’-bipyridine-5-carboxylic acid that was evaluated in Section 6.3.4, 2,2’-bipyridine-5-acetic

acid contains a CH_2 spacer that separates the carboxyl group from bipyridine. As the cobalt metal center strongly withdraws electrons, it may destabilize the amide bond that is essential to attach the complex to CIM carbon. An additional CH_2 spacer between the cobalt center and the carboxyl group can significantly reduce this effect, thus increasing the stability of the amide bond. In this way, a higher cobalt surface loading can be expected.

To further increase the binding ability, a tridentate ligand 2,2':6',2"-terpyridine-4'-acetic acid (Figure 7.1b) can be used. This ligand not only exhibits a $–CH_2$ separator between the carboxyl group and terpyridine, but also contains three nitrogen atoms that are available to bind with cobalt. It has been demonstrated in previous reports that cobalt complexes based on terpyridine exhibit fast and reversible electron-transfer kinetics, and therefore they were used as redox mediators for dye-sensitized solar cells,[227,242] and Li-O_2 batteries.[243] For a preliminary electrochemical study, a cyclic voltammogram of 1 mM cobalt(II) bi(terpyridine) complex was collected (data not shown). A pair of well-defined redox peaks was observed, with a midpoint potential of –0.137 V (vs Ag/Ag^+) and a peak separation of 73 mV. These results further confirm the suitability of cobalt terpyridine complexes for redox buffer applications. Since 2,2':6',2"-terpyridine-4'-acetic acid is commercially available, it is a promising candidate to prepare CIM carbon-based all-solid-state redox buffer with high buffer surface loading.

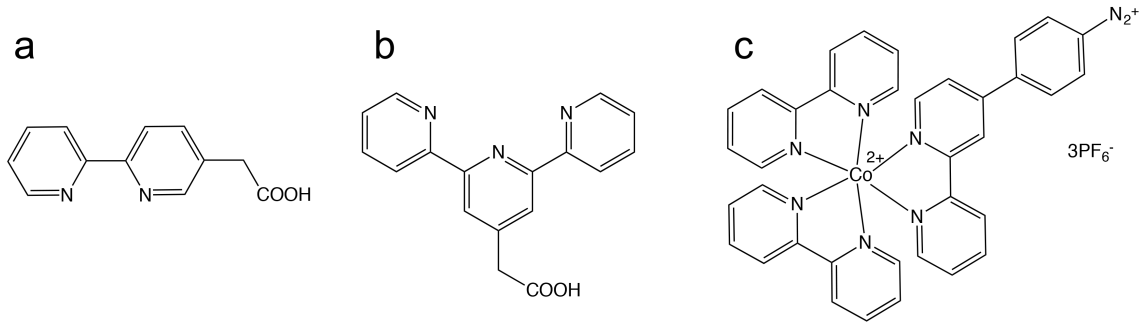

Figure 7.1 Chemical structures of alternative ligands and complexes to attach redox buffers to CIM carbon with potentially high surface loading. (a) 2,2'-Bipyridine-5-acetic acid. (b) 2,2':6',2"-Terpyridine-4'-acetic acid. (c) Diazonium derivative of a cobalt tris(bipyridine) complex that can be attached to an electrode surface via a single-step electrochemical reduction process.

Besides the choice of the ligand, cobalt complexes can also be prepared in the form of diazonium salts (Figure 7.3c) and directly attached to an electrode surface through a single-step electrochemical reduction process as described in Section 6.3.2. The synthetic route and effectiveness of this approach have been demonstrated in previous reports, where diazonium derivatives of ruthenium based complexes were successfully synthesized and attached to the surface of carbon nanotubes,[244] and boron doped diamond.[245] Compared to the previous multi-step approaches that involve click chemistry and amide coupling reactions, this method can significantly simplify the material preparation process, thus making it very attractive for producing CIM carbon-based redox buffers on a large scale.

Once the redox buffer is covalently attached to CIM carbon with a high surface loading, it has great potential to be employed in various applications, where the precise control of interfacial potential can benefit the application.

First and foremost, robust all-solid-state potentiometric ISEs and reference electrodes can be constructed with redox-buffer-modified CIM carbon as the solid contact. Benefiting from the combination of the redox buffer and high double layer capacitance of CIM carbon, sensors with high electrode-to-electrode reproducibility and potential stability can be obtained, and calibration-free ion-sensing operations can be achieved. Due to the high reproducibility and stability, these sensors can be used in a large variety of applications, such as remote environmental sensing, industrial on-line monitoring, and implantable medical devices. Besides bulk electrodes, CIM carbon-based redox buffers can also be used in single-use potentiometric ion sensors, such as the paper-based ion-sensing platform introduced in Chapter 5. Highly reproducible and miniaturized all-solid-state ISEs and reference electrodes can be integrated onto the paper substrate, thus constructing all-solid-state paper-based ion-sensing devices that can be used with biological samples. By changing the components in the ISE membrane, paper-based ion sensors with different types of ISEs and one reference electrode can be fabricated, enabling the detection of multiple ions (e.g., K^+, Na^+, Cl^-) with a single device. Eventually, the method of printing CIM carbon-based redox buffer can be developed to fabricate devices on a large scale.

Beyond current-less potentiometric sensors, CIM carbon-based redox buffers can also benefit electrochemical sensors that rely on current-based techniques, such as ion-

transfer voltammetry.[20,246,247] In ion-transfer voltammetry, an external potential is scanned to facilitate ion transfer between the interface of two immiscible phases (e.g., aqueous and organic phases), thus creating a current response. The formal transfer potential depends on transfer free energy of the specific ion that is related to its identity, and the peak current is dependent on the ion concentration.[248] Similar to all-solid-state potentiometric sensors, conductive polymers can be used as an ion-to-electron transducer to construct all-solid-state voltammetric sensors.[21,22,249] However, as discussed in Section 1.2.1, conducting polymer films usually exhibit a continuum of redox potentials, which may affect the response of the all-solid-state voltammetric sensors, especially when the current flow is high. Therefore, CIM carbon-based redox buffer can be employed to replace conductive polymers as the ion-to-electron transducer. Because the redox potential of CIM carbon-based redox buffer is well defined and the buffer capacity is high, the potential shift caused by current flow can be minimized, and calibration-free all-solid-state voltammetric sensors can be achieved.

Looking beyond this dissertation, exciting opportunities await. The research of CIM carbon-based ion sensors has been brought to a transition point from fundamental inquiry to application-orientated development. It is the author's firm belief that the technology developed in this dissertation will be eventually applied in commercialized ion-sensing devices with low cost, simple operation, high reliability, and small sample volumes.

References

(1) Bakker, E.; Bühlmann, P.; Pretsch, E. *Chem. Rev.* **1997**, *97*, 3083-3132.
(2) Bühlmann, P.; Pretsch, E.; Bakker, E. *Chem. Rev.* **1998**, *98*, 1593-1688.
(3) Johnson, R. D.; Bachas, L. *Anal. Bioanal. Chem.* **2003**, *376*, 328-341.
(4) Amemiya, S. In *Handbook of Electrochemistry*, Zoski, C. G., Ed.; Elsevier: Amsterdam, 2007.
(5) Bobacka, J.; Ivaska, A.; Lewenstam, A. *Chem. Rev.* **2008**, *108*, 329-351.
(6) Lewenstam, A. *Electroanalysis* **2014**, *26*, 1171-1181.
(7) Bakker, E. *Anal. Chem.* **2016**, *88*, 395-413.
(8) Lindner, E.; Gyurcsányi, R. E. *J. Solid State Electrochem.* **2009**, *13*, 51-68.
(9) Ammann, D. *Ion-Selective Microelectrodes: Principles, Designs and Application*; Springer-Verlag: Berlin, 1986.
(10) Morf, W. E. *The Principles of Ion-Selective Electrodes and of Membrane Transport*; Elsevier: New York, NY, 1981.
(11) Pretsch, E. *TrAC, Trends Anal. Chem.* **2007**, *26*, 46-51.
(12) Michalska, A. *Electroanalysis* **2012**, *24*, 1253-1265.
(13) Gyurcsányi, R. E.; Pretsch, E. In *Nanoelectrochemistry*, Mirkin, M. V.; Amemiya, S., Eds.; CRC Press: Boca Raton, FL, 2015.
(14) Hirata, H.; Date, K. *Talanta* **1970**, *17*, 883-887.
(15) Cattrall, R. W.; Freiser, H. *Anal. Chem.* **1971**, *43*, 1905-1906.
(16) Nikolskii, B. P.; Materowa, E. A. *Ion-Sel. Electrode Rev.* **1985**, *7*, 3.
(17) Cattrall, R. W.; Drew, D. M.; Hamilton, I. C. *Anal. Chim. Acta* **1975**, *76*, 269-277.
(18) Hulanicki, A.; Trojanowicz, M. *Anal. Chim. Acta* **1976**, *87*, 411-417.
(19) Lindner, E.; Umezawa, Y. *Pure Appl. Chem.* **2008**, *80*, 85-104.
(20) Bakker, E. *TrAC, Trends Anal. Chem.* **2014**, *53*, 98-105.
(21) Guo, J.; Amemiya, S. *Anal. Chem.* **2006**, *78*, 6893-6902.
(22) Kim, Y.; Rodgers, P. J.; Ishimatsu, R.; Amemiya, S. *Anal. Chem.* **2009**, *81*, 7262-7270.
(23) Jarolimova, Z.; Crespo, G. A.; Afshar, M. G.; Pawlak, M.; Bakker, E. *J. Electroanal. Chem.* **2013**, *709*, 118-125.
(24) Jarolímová, Z.; Crespo, G. A.; Xie, X.; Ghahraman Afshar, M.; Pawlak, M.; Bakker, E. *Anal. Chem.* **2014**, *86*, 6307-6314.
(25) Hupa, E.; Vanamo, U.; Bobacka, J. *Electroanalysis* **2015**, *27*, 591-594.
(26) Vanamo, U.; Hupa, E.; Yrjänä, V.; Bobacka, J. *Anal. Chem.* **2016**, *88*, 4369-4374.
(27) Han, T.; Vanamo, U.; Bobacka, J. *ChemElectroChem* **2016**, *3*, 2071-2077.
(28) Bobacka, J. *Electroanalysis* **2006**, *18*, 7-18.
(29) Yin, T.; Qin, W. *TrAC, Trends Anal. Chem.* **2013**, *51*, 79-86.

(30) Bühlmann, P.; Chen, L. D. In *Supramolecular Chemistry: From Molecules to Nanomaterials*, Jonathan W. Steed, P. A. G., Ed.; John Wiley & Sons, Ltd: New York, NY, 2012.
(31) Bakker, E.; Bühlmann, P.; Pretsch, E. *Talanta* **2004**, *63*, 3-20.
(32) Bobacka, J. *Anal. Chem.* **1999**, *71*, 4932-4937.
(33) Mousavi, Z.; Bobacka, J.; Lewenstam, A.; Ivaska, A. *J. Electroanal. Chem.* **2009**, *633*, 246-252.
(34) Pławińska, Ż.; Michalska, A.; Maksymiuk, K. *Electrochim. Acta* **2016**, *187*, 397-405.
(35) Cadogan, A.; Gao, Z.; Lewenstam, A.; Ivaska, A.; Diamond, D. *Anal. Chem.* **1992**, *64*, 2496-2501.
(36) Bobacka, J.; McCarrick, M.; Lewenstam, A.; Ivaska, A. *Analyst* **1994**, *119*, 1985-1991.
(37) Bobacka, J.; Lindfors, T.; McCarrick, M.; Ivaska, A.; Lewenstam, A. *Anal. Chem.* **1995**, *67*, 3819-3823.
(38) Lindfors, T.; Ivaska, A. *J. Electroanal. Chem.* **2002**, *531*, 43-52.
(39) Lindfors, T.; Ivaska, A. *Anal. Chem.* **2004**, *76*, 4387-4394.
(40) Vázquez, M.; Bobacka, J.; Ivaska, A. *J. Solid State Electrochem.* **2005**, *9*, 865-873.
(41) Veder, J.-P.; De Marco, R.; Patel, K.; Si, P.; Grygolowicz-Pawlak, E.; James, M.; Alam, M. T.; Sohail, M.; Lee, J.; Pretsch, E.; Bakker, E. *Anal. Chem.* **2013**, *85*, 10495-10502.
(42) Liu, D.; Meruva, R. K.; Brown, R. B.; Meyerhoff, M. E. *Anal. Chim. Acta* **1996**, *321*, 173-183.
(43) Fibbioli, M.; Bandyopadhyay, K.; Liu, S.-G.; Echegoyen, L.; Enger, O.; Diederich, F.; Buhlmann, P.; Pretsch, E. *Chem. Commun.* **2000**, *0*, 339-340.
(44) Fibbioli, M.; Bandyopadhyay, K.; Liu, S.-G.; Echegoyen, L.; Enger, O.; Diederich, F.; Gingery, D.; Bühlmann, P.; Persson, H.; Suter, U. W.; Pretsch, E. *Chem. Mater.* **2002**, *14*, 1721-1729.
(45) Grygołowicz-Pawlak, E.; Wyglądacz, K.; Sęk, S.; Bilewicz, R.; Brzózka, Z.; Malinowska, E. *Sens. Actuators, B* **2005**, *111–112*, 310-316.
(46) Gabrielli, C.; Hémery, P.; Liatsi, P.; Masure, M.; Perrot, H. *J. Electrochem. Soc.* **2005**, *152*, H219-H224.
(47) Klink, S.; Ishige, Y.; Schuhmann, W. *ChemElectroChem* **2017**, *4*, 490-494.
(48) Zhou, M.; Gan, S.; Cai, B.; Li, F.; Ma, W.; Han, D.; Niu, L. *Anal. Chem.* **2012**, *84*, 3480-3483.
(49) Zou, X. U.; Cheong, J. H.; Taitt, B. J.; Bühlmann, P. *Anal. Chem.* **2013**, *85*, 9350-9355.
(50) Zou, X. U.; Zhen, X. V.; Cheong, J. H.; Bühlmann, P. *Anal. Chem.* **2014**, *86*, 8687-8692.

(51) Sharp, M.; Johansson, G. *Anal. Chim. Acta* **1971**, *54*, 13-21.
(52) Paczosa-Bator, B.; Pięk, M.; Piech, R. *Anal. Chem.* **2015**, *87*, 1718-1725.
(53) Pięk, M.; Piech, R.; Paczosa-Bator, B. *J. Electrochem. Soc.* **2015**, *162*, B257-B263.
(54) Ishige, Y.; Klink, S.; Schuhmann, W. *Angew. Chem., Int. Ed.* **2016**, *55*, 4831-4835.
(55) Crespo, G. A.; Macho, S.; Bobacka, J.; Rius, F. X. *Anal. Chem.* **2008**, *81*, 676-681.
(56) Cuartero, M.; Bishop, J.; Walker, R.; Acres, R. G.; Bakker, E.; De Marco, R.; Crespo, G. A. *Chem. Commun.* **2016**, *52*, 9703-9706.
(57) Růžička, J.; Rald, K. *Anal. Chim. Acta* **1971**, *53*, 1-12.
(58) Růžička, J.; Lamm, C. G.; Chr. Tjell, J. *Anal. Chim. Acta* **1972**, *62*, 15-28.
(59) Vamvakaki, M.; Chaniotakis, N. A. *Anal. Chim. Acta* **1996**, *320*, 53-61.
(60) Chaniotakis, N.A.; West, S.J., US Patent, 5,840,168, 1998.
(61) Lai, C.-Z.; Fierke, M. A.; Stein, A.; Bühlmann, P. *Anal. Chem.* **2007**, *79*, 4621-4626.
(62) Crespo, G. A.; Macho, S.; Rius, F. X. *Anal. Chem.* **2008**, *80*, 1316-1322.
(63) Fouskaki, M.; Chaniotakis, N. *Analyst* **2008**, *133*, 1072-1075.
(64) Li, J.; Yin, T.; Qin, W. *Anal. Chim. Acta* **2015**, *876*, 49-54.
(65) Ping, J.; Wang, Y.; Wu, J.; Ying, Y. *Electrochem. Commun.* **2011**, *13*, 1529-1532.
(66) Hernández, R.; Riu, J.; Bobacka, J.; Vallés, C.; Jiménez, P.; Benito, A. M.; Maser, W. K.; Rius, F. X. *J. Phys. Chem. C* **2012**, *116*, 22570-22578.
(67) Li, F.; Ye, J.; Zhou, M.; Gan, S.; Zhang, Q.; Han, D.; Niu, L. *Analyst* **2012**, *137*, 618-623.
(68) Miller, P. R.; Xiao, X.; Brener, I.; Burckel, D. B.; Narayan, R.; Polsky, R. *Adv. Healthcare Mater.* **2014**, *3*, 876-881.
(69) Hu, J.; Zou, X. U.; Stein, A.; Bühlmann, P. *Anal. Chem.* **2014**, *86*, 7111-7118.
(70) Ye, J.; Li, F.; Gan, S.; Jiang, Y.; An, Q.; Zhang, Q.; Niu, L. *Electrochem. Commun.* **2015**, *50*, 60-63.
(71) Walcarius, A.; Kuhn, A. *TrAC, Trends Anal. Chem.* **2008**, *27*, 593-603.
(72) Walcarius, A. *Chem. Soc. Rev.* **2013**, *42*, 4098-4140.
(73) Fierke, M. A.; Lai, C.-Z.; Bühlmann, P.; Stein, A. *Anal. Chem.* **2010**, *82*, 680-688.
(74) Paczosa-Bator, B.; Cabaj, L.; Piech, R.; Skupień, K. *Anal. Chem.* **2013**, *85*, 10255-10261.
(75) Yin, T.; Pan, D.; Qin, W. *Anal. Chem.* **2014**, *86*, 11038-11044.
(76) Jaworska, E.; Wójcik, M.; Kisiel, A.; Mieczkowski, J.; Michalska, A. *Talanta* **2011**, *85*, 1986-1989.
(77) Li, J.; Yin, T.; Qin, W. *Sens. Actuators, B* **2017**, *239*, 438-446.
(78) Dohner, R. E.; Wegmann, D.; Morf, W. E.; Simon, W. *Anal. Chem.* **1986**, *58*, 2585-2589.
(79) Mousavi, M. P. S.; Bühlmann, P. *Anal. Chem.* **2013**, *85*, 8895-8901.
(80) Bakker, E. *Electroanalysis* **1999**, *11*, 788-792.

(81) Kisiel, A.; Marcisz, H.; Michalska, A.; Maksymiuk, K. *Analyst* **2005**, *130*, 1655-1662.
(82) Mousavi, Z.; Granholm, K.; Sokalski, T.; Lewenstam, A. *Analyst* **2013**, *138*, 5216-5220.
(83) Lewenstam, A.; Blaz, T.; Migdalski, J. *Anal. Chem.* **2017**, *89*, 1068-1072.
(84) Kakiuchi, T.; Yoshimatsu, T. *Bull. Chem. Soc. Jpn.* **2006**, *79*, 1017-1024.
(85) Rius-Ruiz, F. X.; Kisiel, A.; Michalska, A.; Maksymiuk, K.; Riu, J.; Rius, F. X. *Anal. Bioanal. Chem.* **2011**, *399*, 3613-3622.
(86) Rius-Ruiz, F. X.; Bejarano-Nosas, D.; Blondeau, P.; Riu, J.; Rius, F. X. *Anal. Chem.* **2011**, *83*, 5783-5788.
(87) Ping, J.; Wang, Y.; Fan, K.; Tang, W.; Wu, J.; Ying, Y. *J. Mater. Chem. B* **2013**, *1*, 4781-4791.
(88) Cicmil, D.; Anastasova, S.; Kavanagh, A.; Diamond, D.; Mattinen, U.; Bobacka, J.; Lewenstam, A.; Radu , A. *Electroanalysis* **2011**, *23*, 1881-1890.
(89) Zhang, T.; Lai, C.-Z.; Fierke, M. A.; Stein, A.; Bühlmann, P. *Anal. Chem.* **2012**, *84*, 7771-7778.
(90) Hu, J.; Ho, K. T.; Zou, X. U.; Smyrl, W. H.; Stein, A.; Bühlmann, P. *Anal. Chem.* **2015**, *87*, 2981-2987.
(91) Zou, X. U.; Chen, L. D.; Lai, C.-Z.; Bühlmann, P. *Electroanalysis* **2015**, *27*, 602-608.
(92) Inzelt, G.; Lewenstam, A.; Scholz, F. *Handbook of Reference Electrodes*; Springer-Verlag: Berlin Heidelberg, 2013.
(93) Laboratory Requirements, Code of Federal Regulations, Section *493.931*, Title 42, **2003**.
(94) Abad, J.; Espinosa, N.; Ferrer, P.; Garcia-Valverde, R.; Miguel, C.; Padilla, J.; Alcolea, A.; Castro, G. R.; Colchero, J.; Urbina, A. *Sol. Energy Mater. Sol. Cells* **2012**, *97*, 109-118.
(95) Csahok, E.; Vieil, E.; Inzelt, G. *J. Electroanal. Chem.* **2000**, *482*, 168-177.
(96) Chen, S.; Ni, J.; Hua, M. *J. Polym. Res.* **1997**, *4*, 261–265.
(97) Vorotyntsev, M. A.; Heinze, J. *Electrochim. Acta* **2001**, *46*, 3309-3324.
(98) Kobashi, M.; Takeuchi, H. *Macromolecules* **1998**, *31*, 7273-7278.
(99) Lindfors, T.; Szücs, J.; Sundfors, F.; Gyurcsányi, R. E. *Anal. Chem.* **2010**, *82*, 9425-9432.
(100) Vanamo, U.; Bobacka, J. *Electrochim. Acta* **2014**, *122*, 316-321.
(101) Vanamo, U.; Bobacka, J. *Anal. Chem.* **2014**, *86*, 10540-10545.
(102) He, N.; Papp, S.; Lindfors, T.; Höfler, L.; Latonen, R.-M.; Gyurcsányi, R. E. *Anal. Chem.* **2017**, *89*, 2598-2605.
(103) de Levie, R. *J. Chem. Educ.* **1999**, *76*, 574.

(104) Zou, X. U.; Zhen, X. V.; Hu, J.; Stein, A.; Bühlmann, P. In *48th Heyrovský Discussion, Progress in Electrochemistry at Liquid-Liquid Interfaces and Liquid Membranes*: Třešť, Czech Republic, June 14-19, 2015.
(105) Sun, Q.; Li, W.; Su, B. *J. Electroanal. Chem.* **2015**, *740*, 21-27.
(106) Guzinski, M.; Jarvis, J. M.; Pendley, B. D.; Lindner, E. *Anal. Chem.* **2015**, *87*, 6654-6659.
(107) Guzinski, M.; Jarvis, J. M.; Perez, F.; Pendley, B. D.; Lindner, E.; De Marco, R.; Crespo, G. A.; Acres, R. G.; Walker, R.; Bishop, J. *Anal. Chem.* **2017**, *89*, 3508-3516.
(108) Li, X.; Petrović, S.; Harrison, D. J. *Sens. Actuators, B* **1990**, *1*, 275-280.
(109) Chan, A. D. C.; Harrison, D. J. *Anal. Chem.* **1993**, *65*, 32-36.
(110) Fibbioli, M.; Morf, W. E.; Badertscher, M.; de Rooij, N. F.; Pretsch, E. *Electroanalysis* **2000**, *12*, 1286-1292.
(111) De Marco, R.; Veder, J.-P.; Clarke, G.; Nelson, A.; Prince, K.; Pretsch, E.; Bakker, E. *Phys. Chem. Chem. Phys.* **2008**, *10*, 73-76.
(112) Sundfors, F.; Lindfors, T.; Höfler, L.; Bereczki, R.; Gyurcsányi, R. E. *Anal. Chem.* **2009**, *81*, 5925-5934.
(113) Lindfors, T.; Sundfors, F.; Höfler, L.; Gyurcsányi, R. E. *Electroanalysis* **2009**, *21*, 1914-1922.
(114) He, N.; Lindfors, T. *Anal. Chem.* **2013**, *85*, 1006-1012.
(115) Appiah-Kusi, C.; Kew, S. J.; Hall, E. *Electroanalysis* **2009**, *21*, 1992-2003.
(116) Veder, J.-P.; De Marco, R.; Clarke, G.; Chester, R.; Nelson, A.; Prince, K.; Pretsch, E.; Bakker, E. *Anal. Chem.* **2008**, *80*, 6731-6740.
(117) Veder, J.-P.; Patel, K.; Clarke, G.; Grygolowicz-Pawlak, E.; Silvester, D. S.; De Marco, R.; Pretsch, E.; Bakker, E. *Anal. Chem.* **2010**, *82*, 6203-6207.
(118) Lindfors, T.; Höfler, L.; Jágerszki, G.; Gyurcsányi, R. E. *Anal. Chem.* **2011**, *83*, 4902-4908.
(119) He, N.; Gyurcsanyi, R.; Lindfors, T. *Analyst* **2016**, *141*, 2990-2997.
(120) Sutter, J.; Lindner, E.; Gyurcsányi, R.; Pretsch, E. *Anal. Bioanal. Chem.* **2004**, *380*, 7-14.
(121) Ampurdanés, J.; Crespo, G. A.; Maroto, A.; Sarmentero, M. A.; Ballester, P.; Rius, F. X. *Biosens. Bioelectron.* **2009**, *25*, 344-349.
(122) Hernandez, R.; Riu, J.; Rius, F. X. *Analyst* **2010**, *135*, 1979-1985.
(123) Gyurcsányi, R. E.; Rangisetty, N.; Clifton, S.; Pendley, B. D.; Lindner, E. *Talanta* **2004**, *63*, 89-99.
(124) Yuan, D.; Anthis, A. H.; Ghahraman Afshar, M.; Pankratova, N.; Cuartero, M.; Crespo, G. A.; Bakker, E. *Anal. Chem.* **2015**, *87*, 8640-8645.
(125) Lindner, E.; Cosofret, V. V.; Ufer, S.; Buck, R. P.; Kusy, R. P.; Ash, R. B.; Nagle, H. T. *J. Chem. Soc., Faraday Trans.* **1993**, *89*, 361-367.

(126) Lindfors, T. *J. Solid State Electrochem.* **2009**, *13*, 77-89.
(127) Kankare, J.; Vinokurov, I. A. *Anal. Chem.* **1997**, *69*, 2337-2342.
(128) Vázquez, M.; Bobacka, J.; Ivaska, A.; Lewenstam, A. *Sens. Actuators, B* **2002**, *82*, 7-13.
(129) Sokalski, T.; Ceresa, A.; Zwickl, T.; Pretsch, E. *J. Am. Chem. Soc.* **1997**, *119*, 11347-11348.
(130) Bühlmann, P.; Yajima, S.; Tohda, K.; Umezawa, K.; Nishizawa, S.; Umezawa, Y. *Electroanalysis* **1995**, *7*, 811-816.
(131) Michalska, A.; Konopka, A.; Maj-Zurawska, M. *Anal. Chem.* **2003**, *75*, 141-144.
(132) Konopka, A.; Sokalski, T.; Michalska, A.; Lewenstam, A.; Maj-Zurawska, M. *Anal. Chem.* **2004**, *76*, 6410-6418.
(133) Lindner, E.; Gyurcsányi, R. E.; Buck, R. P. *Electroanalysis* **1999**, *11*, 695-702.
(134) Michalska, A.; Dumańska, J.; Maksymiuk, K. *Anal. Chem.* **2003**, *75*, 4964-4974.
(135) Eric, B.; Ernö, P. In *Electroanalytical Chemistry*; CRC Press, 2011, pp 1-74.
(136) Höfler, L.; Bedlechowicz, I.; Vigassy, T.; Gyurcsányi, R. E.; Bakker, E.; Pretsch, E. *Anal. Chem.* **2009**, *81*, 3592-3599.
(137) Sutter, J.; Radu, A.; Peper, S.; Bakker, E.; Pretsch, E. *Anal. Chim. Acta* **2004**, *523*, 53-59.
(138) Chumbimuni-Torres, K. Y.; Rubinova, N.; Radu, A.; Kubota, L. T.; Bakker, E. *Anal. Chem.* **2006**, *78*, 1318-1322.
(139) Mensah, S. T.; Gonzalez, Y.; Calvo-Marzal, P.; Chumbimuni-Torres, K. Y. *Anal. Chem.* **2014**, *86*, 7269-7273.
(140) Ceresa, A.; Bakker, E.; Hattendorf, B.; Günther, D.; Pretsch, E. *Anal. Chem.* **2001**, *73*, 343-351.
(141) Boswell, P. G.; Bühlmann, P. *J. Am. Chem. Soc.* **2005**, *127*, 8958-8959.
(142) Boswell, P. G.; Szíjjártó, C.; Jurisch, M.; Gladysz, J. A.; Rábai, J.; Bühlmann, P. *Anal. Chem.* **2008**, *80*, 2084-2090.
(143) Lai, C.-Z.; Fierke, M. A.; da Costa, R. C.; Gladysz, J. A.; Stein, A.; Bühlmann, P. *Anal. Chem.* **2010**, *82*, 7634-7640.
(144) Chen, L. D.; Lai, C.-Z.; Granda, L. P.; Fierke, M. A.; Mandal, D.; Stein, A.; Gladysz, J. A.; Bühlmann, P. *Anal. Chem.* **2013**, *85*, 7471-7477.
(145) Lai, C.-Z.; Joyer, M. M.; Fierke, M. A.; Petkovich, N. D.; Stein, A.; Bühlmann, P. *J. Solid State Electrochem.* **2009**, *13*, 123-128.
(146) Yu, S.; Li, F.; Qin, W. *Sens. Actuators, B* **2011**, *155*, 919-922.
(147) Guziński, M.; Lisak, G.; Sokalski, T.; Bobacka, J.; Ivaska, A.; Bocheńska, M.; Lewenstam, A. *Anal. Chem.* **2013**, *85*, 1555-1561.
(148) Mendecki, L.; Fayose, T.; Stockmal, K. A.; Wei, J.; Granados-Focil, S.; McGraw, C. M.; Radu, A. *Anal. Chem.* **2015**, *87*, 7515-7518.

(149) E. Gyurcsanyi, R.; Nyback, A.-S.; Ivaska, A.; Toth, K.; Nagy, G. *Analyst* **1998**, *123*, 1339-1344.
(150) Hayashi, K.; Yamanaka, M.; Toko, K.; Yamafuji, K. *Sens. Actuators, B* **1990**, *2*, 205-213.
(151) Lvova, L.; Kim, S. S.; Legin, A.; Vlasov, Y.; Yang, J. S.; Cha, G. S.; Nam, H. *Anal. Chim. Acta* **2002**, *468*, 303-314.
(152) Rius-Ruiz, F. X.; Crespo, G. A.; Bejarano-Nosas, D.; Blondeau, P.; Riu, J.; Rius, F. X. *Anal. Chem.* **2011**, *83*, 8810-8815.
(153) Lan, W.-J.; Zou, X. U.; Hamedi, M. M.; Hu, J.; Parolo, C.; Maxwell, E. J.; Bühlmann, P.; Whitesides, G. M. *Anal. Chem.* **2014**, *86*, 9548-9553.
(154) Novell, M.; Guinovart, T.; Blondeau, P.; Rius, F. X.; Andrade, F. J. *Lab Chip* **2014**, *14*, 1308-1314.
(155) Cui, J.; Lisak, G.; Strzalkowska, S.; Bobacka, J. *Analyst* **2014**, *139*, 2133-2136.
(156) Szűcs, J.; Gyurcsányi, R. E. *Electroanalysis* **2012**, *24*, 146-152.
(157) Walter, B. *Anal. Chem.* **1983**, *55*, 498A-514A.
(158) Novell, M.; Parrilla, M.; Crespo, G. A.; Rius, F. X.; Andrade, F. J. *Anal. Chem.* **2012**, *84*, 4695-4702.
(159) Cuartero, M.; del Río, J. S.; Blondeau, P.; Ortuño, J. A.; Rius, F. X.; Andrade, F. J. *Anal. Chim. Acta* **2014**, *827*, 95-102.
(160) Martinez, A. W.; Phillips, S. T.; Butte, M. J.; Whitesides, G. M. *Angew. Chem., Int. Ed.* **2007**, *46*, 1318-1320.
(161) Lisak, G.; Cui, J.; Bobacka, J. *Sens. Actuators, B* **2015**, *207, Part B*, 933-939.
(162) Cuartero, M.; Crespo, G. A.; Bakker, E. *Anal. Chem.* **2015**, *87*, 1981-1990.
(163) Kofler, J.; Nau, S.; List-Kratochvil, E. J. W. *J. Mater. Chem. B* **2015**, *3*, 5095-5102.
(164) Wang, X.; Qin, Y.; Meyerhoff, M. E. *Chem. Commun.* **2015**, *51*, 15176-15179.
(165) Szűcs, J.; Lindfors, T.; Bobacka, J.; Gyurcsányi, R. E. *Electroanalysis* **2016**, *28*, 778-786.
(166) Boeva, Z. A.; Lindfors, T. *Sens. Actuators, B* **2016**, *224*, 624-631.
(167) Egginger, M.; Bauer, S.; Schwodiauer, R.; Neugebauer, H.; Sariciftci, N. S. *Monatsh. Chem.* **2009**, *140*, 735-750.
(168) Singh, R.; Kumar, J.; Singh, R. K.; Kaur, A.; Sood, K. N.; Rastogi, R. C. *Polymer* **2005**, *46*, 9126-9132.
(169) Veder, J. P.; De Marco, R.; Patel, K.; Si, P.; Grygolowicz-Pawlak, E.; James, M.; Alam, M. T.; Sohail, M.; Lee, J.; Pretsch, E.; Bakker, E. *Anal. Chem.* **2013**, *85*, 10495-10502.
(170) Li, Z.; Jaroniec, M. *J. Am. Chem. Soc.* **2001**, *123*, 9208-9209.
(171) Li, Z.; Jaroniec, M. *Chem. Mater.* **2003**, *15*, 1327-1333.
(172) Mochida, I.; Shimizu, K.; Korai, Y.; Otsuka, H.; Sakai, Y.; Fujiyama, S. *Carbon* **1990**, *28*, 311-319.

(173) Kim, S.-S.; Shah, J.; Pinnavaia, T. J. *Chem. Mater.* **2003**, *15*, 1664-1668.
(174) Li, Z.; Jaroniec, M. *Anal. Chem.* **2004**, *76*, 5479-5485.
(175) Li, Z.; Jaroniec, M.; Lee, Y.-J.; Radovic, L. R. *Chem. Commun.* **2002**, 1346-1347.
(176) Boehm, H. P.; Diehl, E.; Heck, W.; Sappok, R. *Angew. Chem., Int. Ed.* **1964**, *3*, 669-677.
(177) Meier, P. C. *Anal. Chim. Acta* **1982**, *136*, 363-368.
(178) Nishihara, H.; Kyotani, T. *Adv. Mater.* **2012**, *24*, 4473-4498.
(179) Vu, A.; Li, X.; Phillips, J.; Han, A.; Smyrl, W. H.; Bühlmann, P.; Stein, A. *Chem. Mater.* **2013**, *25*, 4137-4148.
(180) Bakker, E.; Pretsch, E. *Angew. Chem., Int. Ed.* **2007**, *46*, 5660-5668.
(181) Payne, R. B.; Buckley, B. M.; Rawson, K. M. *Ann. Clin. Biochem.* **1991**, *28*, 68-72.
(182) D'Orazio, P.; Verghese, D. *Ann. Clin. Biochem.* **1991**, *28*, 628-629.
(183) Mi, Y.; Mathison, S.; Bakker, E. *Electrochem. Solid-State Lett.* **1999**, *2*, 198-200.
(184) Shibata, M.; Sakaida, H.; Kakiuchi, T. *Anal. Chem.* **2011**, *83*, 164-168.
(185) Kisiel, A.; Michalska, A.; Maksymiuk, K.; Hall, E. A. H. *Electroanalysis* **2008**, *20*, 318-323.
(186) Zuliani, C.; Matzeu, G.; Diamond, D. *Talanta* **2014**, *125*, 58-64.
(187) Martinez, A. W.; Phillips, S. T.; Whitesides, G. M.; Carrilho, E. *Anal. Chem.* **2009**, *82*, 3-10.
(188) Maxwell, E. J.; Mazzeo, A. D.; Whitesides, G. M. *MRS Bull.* **2013**, *38*, 309-314.
(189) Cate, D. M.; Adkins, J. A.; Mettakoonpitak, J.; Henry, C. S. *Anal. Chem.* **2014**, *87*, 19-41.
(190) van den Berg, A. M. J.; Smith, P. J.; Perelaer, J.; Schrof, W.; Koltzenburg, S.; Schubert, U. S. *Soft Matter* **2007**, *3*, 238-243.
(191) Carrilho, E.; Martinez, A. W.; Whitesides, G. M. *Anal. Chem.* **2009**, *81*, 7091-7095.
(192) Upreti, P.; Metzger, L. E.; Bühlmann, P. *Talanta* **2004**, *63*, 139-148.
(193) Ma, S. C.; Yang, V. C.; Meyerhoff, M. E. *Anal. Chem.* **1992**, *64*, 694-697.
(194) Chumbimuni-Torres, K. Y.; Dai, Z.; Rubinova, N.; Xiang, Y.; Pretsch, E.; Wang, J.; Bakker, E. *J. Am. Chem. Soc.* **2006**, *128*, 13676-13677.
(195) Liang, R.-N.; Song, D.-A.; Zhang, R.-M.; Qin, W. *Angew. Chem., Int. Ed.* **2010**, *49*, 2556-2559.
(196) Yamada, K.; Henares, T. G.; Suzuki, K.; Citterio, D. *Angew. Chem., Int. Ed.* **2015**, *54*, 5294-5310.
(197) Kumar, A. A.; Hennek, J. W.; Smith, B. S.; Kumar, S.; Beattie, P.; Jain, S.; Rolland, J. P.; Stossel, T. P.; Chunda-Liyoka, C.; Whitesides, G. M. *Angew. Chem., Int. Ed.* **2015**, *54*, 5836-5853.
(198) Dungchai, W.; Chailapakul, O.; Henry, C. S. *Anal. Chem.* **2009**, *81*, 5821-5826.
(199) Pelton, R. *TrAC, Trends Anal. Chem.* **2009**, *28*, 925-942.

(200) Grygolowicz-Pawlak, E.; Crespo, G. A.; Ghahraman Afshar, M.; Mistlberger, G.; Bakker, E. *Anal. Chem.* **2013**, *85*, 6208-6212.
(201) Hu, J.; Stein, A.; Bühlmann, P. *TrAC, Trends Anal. Chem.* **2016**, *76*, 102-114.
(202) Dürselen, L. F. J.; Wegmann, D.; May, K.; Oesch, U.; Simon, W. *Anal. Chem.* **1988**, *60*, 1455-1458.
(203) Scott, M. G.; Heusel, J. W.; LeGrys, V. A.; Siggaard-Andersen, O. In *Tietz Textbook of Clinical Chemistry*, Burtis, C. A.; Ashwood, E. R., Eds.; W. B. Saunders Company: Philadelphia, 1999.
(204) Ogawara, S.; Carey, J. L.; Zou, X. U.; Bühlmann, P. *ACS Sensors* **2016**, *1*, 95-101.
(205) Rumpf, G.; Spichiger-Keller, U.; Bühler, H.; Simon, W. *Anal. Sci.* **1992**, *8*, 553-559.
(206) Oh, J.-M.; Chow, K.-F. *Anal. Methods* **2015**, *7*, 7951-7960.
(207) Mahadeva, S. K.; Walus, K.; Stoeber, B. *ACS Appl. Mater. Interfaces* **2015**, *7*, 8345-8362.
(208) Mettakoonpitak, J.; Boehle, K.; Nantaphol, S.; Teengam, P.; Adkins, J. A.; Srisa-Art, M.; Henry, C. S. *Electroanalysis* **2016**, *28*, 1420-1436.
(209) Yamada, K.; Shibata, H.; Suzuki, K.; Citterio, D. *Lab Chip* **2017**, *17*, 1206-1249.
(210) Yang, Y.; Noviana, E.; Nguyen, M. P.; Geiss, B. J.; Dandy, D. S.; Henry, C. S. *Anal. Chem.* **2017**, *89*, 71-91.
(211) Ding, J.; He, N.; Lisak, G.; Qin, W.; Bobacka, J. *Sens. Actuators, B* **2017**, *243*, 346-352.
(212) Sjöberg, P.; Määttänen, A.; Vanamo, U.; Novell, M.; Ihalainen, P.; Andrade, F. J.; Bobacka, J.; Peltonen, J. *Sens. Actuators, B* **2016**, *224*, 325-332.
(213) Hu, J.; Stein, A.; Bühlmann, P. *Angew. Chem., Int. Ed.* **2016**, *55*, 7544-7547.
(214) Pięk, M.; Piech, R.; Paczosa-Bator, B. *J. Electrochem. Soc.* **2016**, *163*, B573-B579.
(215) Melby, L. R.; Harder, R. J.; Hertler, W. R.; Mahler, W.; Benson, R. E.; Mochel, W. E. *J. Am. Chem. Soc.* **1962**, *84*, 3374-3387.
(216) Ferraris, J.; Cowan, D. O.; Walatka, V.; Perlstein, J. H. *J. Am. Chem. Soc.* **1973**, *95*, 948-949.
(217) Jaeger, C. D.; Bard, A. J. *J. Am. Chem. Soc.* **1979**, *101*, 1690-1699.
(218) Tseng, T.-C.; Urban, C.; Wang, Y.; Otero, R.; Tait, S. L.; Alcamí, M.; Écija, D.; Trelka, M.; Gallego, J. M.; Lin, N.; Konuma, M.; Starke, U.; Nefedov, A.; Langner, A.; Wöll, C.; Herranz, M. Á.; Martín, F.; Martín, N.; Kern, K.; Miranda, R. *Nat. Chem.* **2010**, *2*, 374-379.
(219) Le, T. H.; Nafady, A.; Qu, X.; Bond, A. M.; Martin, L. L. *Anal. Chem.* **2012**, *84*, 2343-2350.
(220) Talin, A. A.; Centrone, A.; Ford, A. C.; Foster, M. E.; Stavila, V.; Haney, P.; Kinney, R. A.; Szalai, V.; El Gabaly, F.; Yoon, H. P.; Léonard, F.; Allendorf, M. D. *Science* **2014**, *343*, 66-69.

(221) Lehmann, M. W.; Evans, D. H. *J. Phys. Chem. B* **1998**, *102*, 9928-9933.
(222) Nafady, A.; Bond, A. M.; Bilyk, A.; Harris, A. R.; Bhatt, A. I.; O'Mullane, A. P.; De Marco, R. *J. Am. Chem. Soc.* **2007**, *129*, 2369-2382.
(223) Bakker, E. *ACS Sensors* **2016**, *1*, 838-841.
(224) Evrard, D.; Lambert, F.; Policar, C.; Balland, V.; Limoges, B. *Chem. - Eur. J.* **2008**, *14*, 9286-9291.
(225) Nakazono, T.; Parent, A. R.; Sakai, K. *Chem. Commun.* **2013**, *49*, 6325-6327.
(226) Cuartero, M.; Acres, R. G.; Bradley, J.; Jarolimova, Z.; Wang, L.; Bakker, E.; Crespo, G. A.; De Marco, R. *Electrochim. Acta* **2017**, *238*, 357-367.
(227) Sapp, S. A.; Elliott, C. M.; Contado, C.; Caramori, S.; Bignozzi, C. A. *J. Am. Chem. Soc.* **2002**, *124*, 11215-11222.
(228) Stein, A.; Wang, Z.; Fierke, M. A. *Adv. Mater.* **2009**, *21*, 265-293.
(229) Liu, Y.-C.; McCreery, R. L. *J. Am. Chem. Soc.* **1995**, *117*, 11254-11259.
(230) Pinson, J.; Podvorica, F. *Chem. Soc. Rev.* **2005**, *34*, 429-439.
(231) Belanger, D.; Pinson, J. *Chem. Soc. Rev.* **2011**, *40*, 3995-4048.
(232) Benedetto, A.; Balog, M.; Viel, P.; Le Derf, F.; Sallé, M.; Palacin, S. *Electrochim. Acta* **2008**, *53*, 7117-7122.
(233) Cline, K. K.; Baxter, L.; Lockwood, D.; Saylor, R.; Stalzer, A. *J. Electroanal. Chem.* **2009**, *633*, 283-290.
(234) Lieber, E.; Rao, C. N. R.; Chao, T. S.; Hoffman, C. W. W. *Anal. Chem.* **1957**, *29*, 916-918.
(235) Landis, E. C.; Hamers, R. J. *Chem. Mater.* **2009**, *21*, 724-730.
(236) Devadoss, A.; Chidsey, C. E. D. *J. Am. Chem. Soc.* **2007**, *129*, 5370-5371.
(237) Stenehjem, E. D.; Ziatdinov, V. R.; Stack, T. D. P.; Chidsey, C. E. D. *J. Am. Chem. Soc.* **2013**, *135*, 1110-1116.
(238) Fierke, M. A.; Olson, E. J.; Bühlmann, P.; Stein, A. *ACS Appl. Mater. Interfaces* **2012**, *4*, 4731-4739.
(239) Yu, S. S. C.; Tan, E. S. Q.; Jane, R. T.; Downard, A. J. *Langmuir* **2007**, *23*, 11074-11082.
(240) D'Souza, F.; Villard, A.; Van Caemelbecke, E.; Franzen, M.; Boschi, T.; Tagliatesta, P.; Kadish, K. M. *Inorg. Chem.* **1993**, *32*, 4042-4048.
(241) Kunishima, M.; Kawachi, C.; Monta, J.; Terao, K.; Iwasaki, F.; Tani, S. *Tetrahedron* **1999**, *55*, 13159-13170.
(242) Aribia, K. B.; Moehl, T.; Zakeeruddin, S. M.; Gratzel, M. *Chem. Sci.* **2013**, *4*, 454-459.
(243) Yao, K. P. C.; Frith, J. T.; Sayed, S. Y.; Bardé, F.; Owen, J. R.; Shao-Horn, Y.; Garcia-Araez, N. *J. Phys. Chem. C* **2016**, *120*, 16290-16297.

(244) Jousselme, B.; Bidan, G.; Billon, M.; Goyer, C.; Kervella, Y.; Guillerez, S.; Hamad, E. A.; Goze-Bac, C.; Mevellec, J.-Y.; Lefrant, S. *J. Electroanal. Chem.* **2008**, *621*, 277-285.
(245) Agnes, C.; Arnault, J.-C.; Omnes, F.; Jousselme, B.; Billon, M.; Bidan, G.; Mailley, P. *Phys. Chem. Chem. Phys.* **2009**, *11*, 11647-11654.
(246) Kabagambe, B.; Izadyar, A.; Amemiya, S. *Anal. Chem.* **2012**, *84*, 7979-7986.
(247) Crespo, G. A.; Cuartero, M.; Bakker, E. *Anal. Chem.* **2015**, *87*, 7729-7737.
(248) Homolka, D.; Hung, L. Q.; Hofmanova, A.; Khalil, M. W.; Koryta, J.; Marecek, V.; Samec, Z.; Sen, S. K.; Vanysek, P.; et al. *Anal. Chem.* **1980**, *52*, 1606-1610.
(249) Kim, Y.; Amemiya, S. *Anal. Chem.* **2008**, *80*, 6056-6065.